Slip behaviour of the Queen Charlotte plate boundary before and after the 2012, M_W 7.8 Haida Gwaii earthquake: evidence from repeating earthquakes

by

Timothy W. Hayward

B.Sc. (Honours Geophysics), University of Manitoba, 2014

A THESIS SUBMITTED IN PARTIAL FULFILLMENT
OF THE REQUIREMENTS FOR THE DEGREE OF

Master of Science

in

THE FACULTY OF GRADUATE AND POSTDOCTORAL STUDIES

(Geophysics)

The University of British Columbia

(Vancouver)

March 2017

Abstract

The Queen Charlotte plate boundary, near Haida Gwaii, B.C., includes the dextral, strike-slip, Queen Charlotte Fault (QCF) and the subduction interface between the downgoing Pacific and overriding North American plates. In this dissertation, we present a comprehensive repeating earthquake catalogue that represents an effective slip meter for both faults in the area. The catalogue comprises 730 individual earthquakes ($0.3 \leq M_W \leq 3.5$) arranged into 224 repeating earthquake families on the basis of waveform similarity. We employ and extend existing relationships for repeating earthquake magnitudes and slips to provide cumulative slip histories for the QCF and subduction interface in 6 adjacent zones within the study area between $52.3°$N and $53.8°$N. We find evidence for creep on both faults; however, the creep rate is significantly less than plate motion rates, which suggests partial locking of both faults. The QCF exhibits the highest degrees of locking south of $52.8°$N, which indicates that the seismic hazard for a major strike-slip earthquake is highest in the southern part of the study area. The October 28, 2012, M_W 7.8 Haida Gwaii thrust earthquake occurred in our study area and had a significant effect on the plate boundary. The QCF is observed to undergo accelerated, right-lateral slip for 1-2 months following the earthquake. The subduction interface exhibits afterslip thrust motion that persists for the duration of the study period (i.e., 3 years and 2 months after the Haida Gwaii earthquake). Afterslip is greatest on the periphery of the main rupture zone of the Haida Gwaii event.

Preface

This dissertation represents original intellectual work of the author, Timothy W. Hayward, and his supervisor, Professor Michael Bostock. Much of the analysis within this dissertation was made possible by software originally developed by Professor Michael Bostock and his research group at the University of British Columbia.

Table of Contents

List of Tables

List of Figures

Acknowledgments

I would first like to acknowledge my supervisor, Professor Michael Bostock, for all his guidance during my time at UBC. This work would not have been possible without his hard work and help along the way.

I'd also like to thank the members of my supervisory committee, Professor Eldad Haber, Professor Mark Jellinek, and Professor Emeritus Ron Clowes for their helpful comments throughout my Master's degree. Additionally, I acknowledge my examination committee, Professor Emeritus Ron Clowes and Professor Felix Herrmann for their comments on my thesis and defence.

The seismogram data used for this project was acquired from the Earthquakes Canada database. Specifically, I'd like to thank Xiuying Jin and Tim Côté for their help in retrieving the data from the repository.

Lastly, I would like to acknowledge the other members of the Laboratory for Earthquake Seismology (LEQS) research group at UBC: Alex Plourde, Geneviève Savard, Lindsay (Yuling) Chuang, Takeshi Akuhara, Xuejun Han, and Yariv Hamiel. Thank you for your encouragement, assistance, and fun times throughout my Master's at UBC.

Chapter 1

Introduction

The Queen Charlotte plate boundary (QCPB) is located off the northwest coast of North America, between the Cascadia subduction zone to the south and the Yakutat collisional zone to the north. The QCPB has hosted Canada's two largest recorded earthquakes: the 1949, M_s 8.1 Queen Charlotte Islands earthquake [Bostwick, 1984; Rogers, 1986; Nishenko and Jacob, 1990], and the 2012, M_W 7.8 Haida Gwaii earthquake [Lay et al., 2013; Cassidy et al., 2014; Kao et al., 2015]. Farther to the north in Alaska, USA, the plate boundary also spawned the M_W 7.5 Craig, Alaska earthquake in 2013 [Aderhold and Abercrombie, 2015; Holtkamp and Ruppert, 2015], as well as other large earthquakes in 1958 and 1972 [Nishenko and Jacob, 1990]. These earthquakes underline the considerable seismic hazard posed by the QCPB.

The QCPB includes the Queen Charlotte Fault (QCF) separating the Pacific and North American plates (Figure 1). The system is relatively simple north of Haida Gwaii, where relative plate motion is almost purely transform and thus a major dextral strike-slip system is present [e.g., Plafker et al., 1978]. However, in the region near Haida Gwaii, the relative plate motions include a significant 15-20° oblique convergent component [e.g., Hyndman and Hamilton, 1993] due to a gradual left-stepping of the QCF. Two possible end-members were originally proposed to explain the mechanism through which this convergence is accommodated: (1) the Pacific plate is obliquely subducting beneath the North American plate [e.g.,
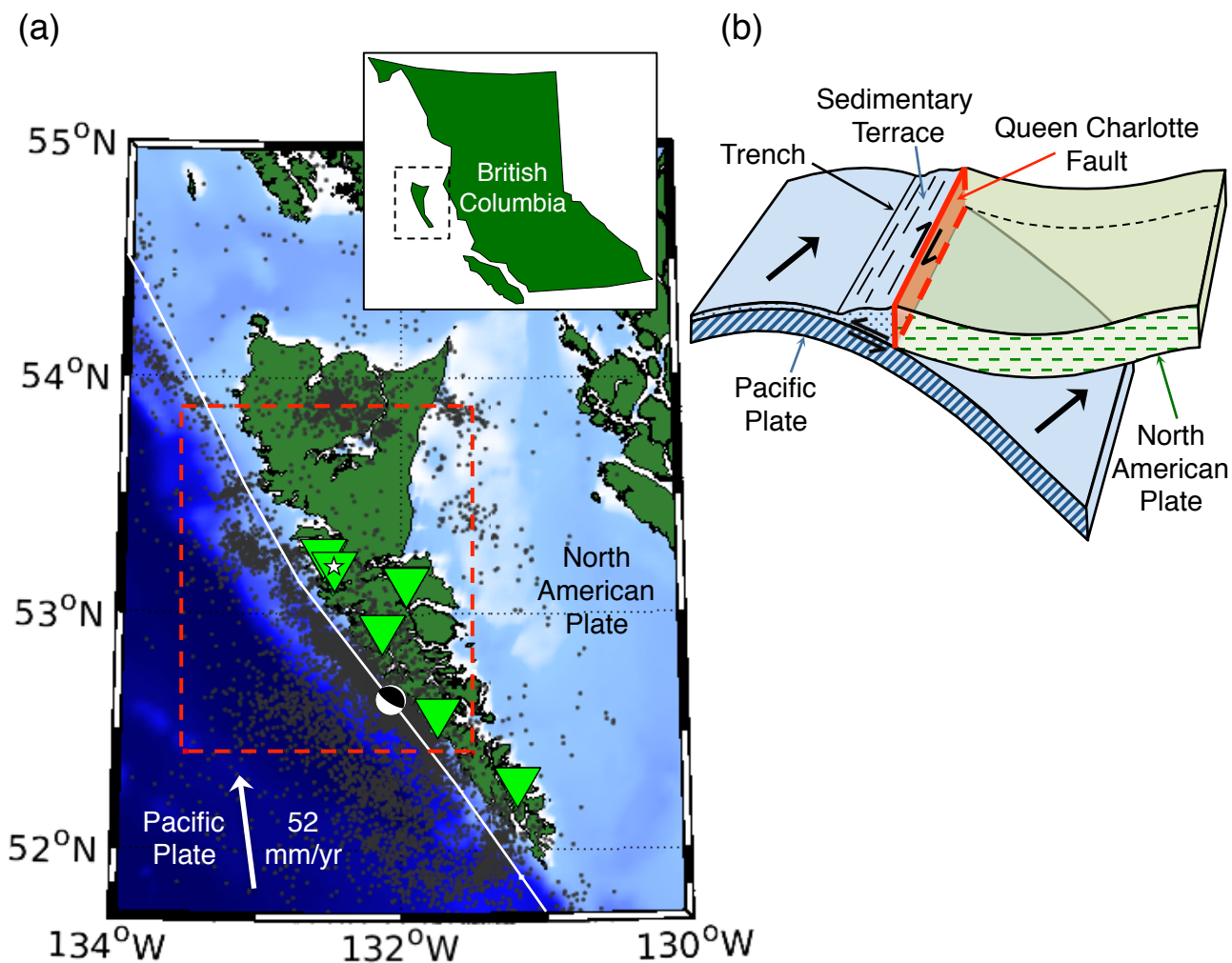
Figure 1: (a) Map of the study area (red, dashed box) including the islands of Haida Gwaii. Also shown are the relative Pacific-North American plate motion [white arrow; Nykolaishen et al., 2015], the Queen Charlotte Fault (white line), background seismicity during the study period (gray dots), the location of the 2012 Haida Gwaii Earthquake (lower hemisphere focal mechanism), and the seismograph stations used in this study. Station DIB is marked by a white star. Bathymetry is coloured from 3 km water depth (dark blue) to 0 (white). Inset map shows the location of Haida Gwaii (dashed rectangle) within the rest of British Columbia, Canada. (b) Schematic illustrating the major elements of the Queen Charlotte plate boundary (*after* Yorath and Hyndman [1983]). Relative plate motions are shown as black arrows. The Pacific Plate obliquely subducts beneath the North American Plate resulting in both right-lateral strike-slip and under-thrust motions.

Hyndman and Ellis, 1981; Hyndman et al., 1982; Mackie et al., 1989; Smith et al., 2003; Bustin et al., 2007], or (2) the convergent component is accounted for by internal deformation and crustal shortening within the two plates [e.g., Dehler and Clowes, 1988; Rohr et al., 2000]. The oblique subduction hypothesis is now widely accepted (Figure 1b) in large part due to the 2012 Haida Gwaii earthquake [e.g., Hyndman, 2015]. This M_W 7.8 earthquake, unlike other large earthquakes along the QCPB, exhibited a thrust mechanism with a sense of motion that is largely margin-perpendicular (Figure 1; Lay et al. 2013; Cassidy et al. 2014). Kao et al. [2015] suggest that the sense of motion may have been closer to parallel with relative plate motions, but nonetheless attribute the event to oblique subduction of the Pacific plate beneath the North American plate. The QCPB, therefore, exhibits slip partitioning, with strike-slip motions taken up along the QCF and convergent motions taken up on the subduction interface [Lay et al., 2013; Hyndman, 2015; Kao et al., 2015]. Although the 2012 earthquake launched a number of geophysical studies of the QCPB, the region remains understudied relative to other major transcurrent plate boundaries such as the San Andreas, Alpine, and Anatolian Faults. Our objective in this study is to supply new constraints on the slip budget of the QCPB through the analysis of repeating earthquakes. Previous studies have analyzed the microseismicity of the QCPB [e.g., Hyndman and Ellis, 1981; Bérubé et al., 1989], but the current work represents the first study to utilize repeating earthquakes in the area.

Repeating earthquakes refer to earthquakes with highly similar locations and rupture characteristics that demonstrate repeated slip of a common fault patch [e.g., Nadeau and Johnson, 1998; Igarashi et al., 2003]. Repeating earthquakes have been observed in a variety of tectonic environments around the world, perhaps most notably along the San Andreas Fault by Nadeau et al. [1995], Nadeau and Johnson [1998], and others. Following the work of Nadeau and Johnson [1998], important empirical and theoretical relations between repeating earthquakes and fault slip/moment have been derived and applied in numerous tectonic environments [e.g., Chen et al., 2007; Kato et al., 2016; Uchida et al., 2016]. In this study, our goal is to create a catalogue of repeating earthquakes along the QCPB and gain new insight into the

slip dynamics and segmentation along the QCPB. Our first step is to cluster earthquakes into repeating earthquake "families" and generate estimates of earthquake moments/slips. Then, following Matsubara et al. [2005] and Uchida et al. [2016], we combine families into proximal groups and analyze the average slip of these groups through time. We consider slip along the QCF and subduction fault segments separately, and pay particular attention to changes in the slip patterns before and after the 2012 Haida Gwaii earthquake.

Chapter 2

Data

2.1   Data Selection

Seismogram data for this study were obtained from the Canadian National Seismograph Network [Earthquakes Canada, 2016] as 24-hour waveform records in the period between January 1, 2005 and December 31, 2015. The seismograph stations and study area are shown in Figure 1a. Six stations on the island of Haida Gwaii are employed for this study; however, due to lower signal-to-noise ratio (SNR) and intermittent coverage at the majority of stations, station DIB proves to be most reliable (data available for 99% of the study period) and is the focus of much of the analysis. The study area ($\sim$22,000 km^2) is centered on DIB and includes all points within $\sim$100 km of DIB, due to the diminishing SNR levels of small earthquakes at greater distances. The hypocenter of the 2012 Haida Gwaii earthquake is located in the southern part of the study area (Figure 1a).

2.2   Assembling the Repeating Earthquake Catalogue

In this study, we use the term repeating earthquake "family" to refer to a set of discrete earthquakes with highly similar location and focal mechanism, and that we infer to represent repeated slip of the same fault patch. Families are identified as sets of waveforms with high correlation coefficients across all events (Figure 2).
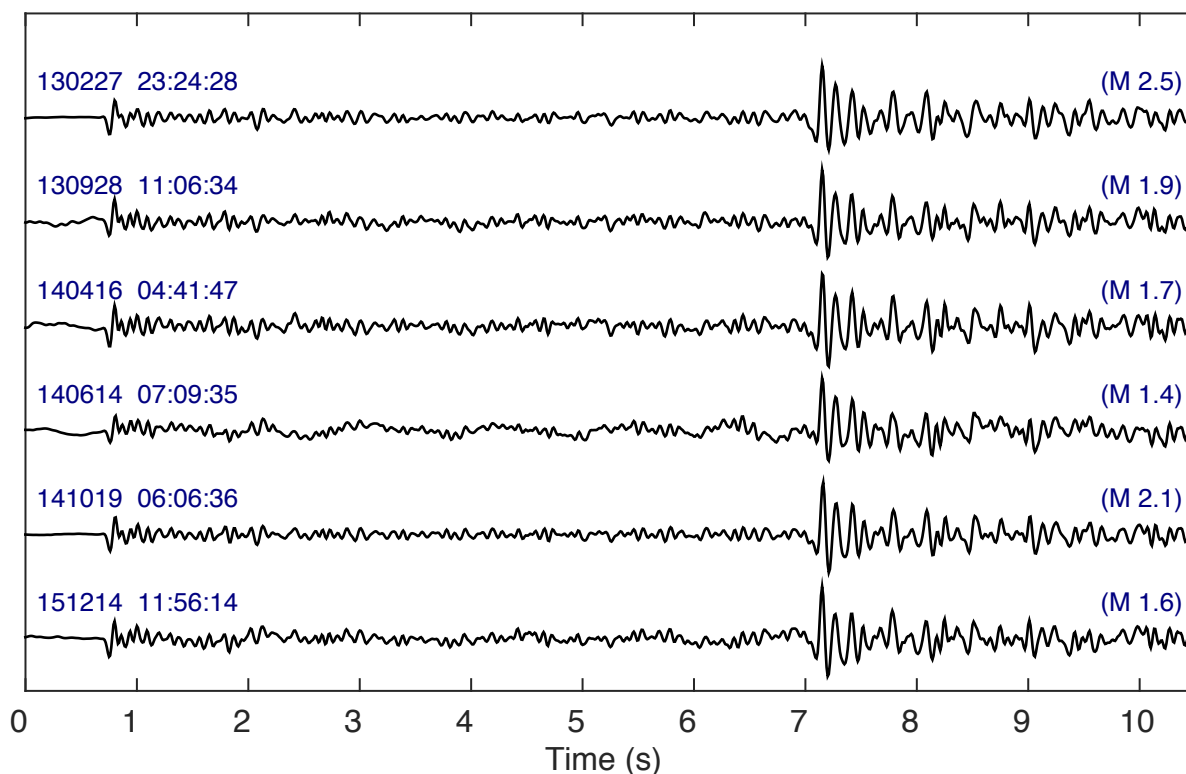
Figure 2: Vertical component waveforms, bandpass filtered between 2-14 Hz, for family 186. Event times are given on left in YYMMDD HH:MM:SS format, moment magnitudes are given on right in parentheses, and the seismograms have been normalized by their maximum amplitudes to enable visual comparison. Both P waves (∼0.75 s) and S waves (∼7 s) display high waveform similarity.

To create a catalogue of repeating earthquake families we start with the Geological Survey of Canada earthquakes list of ∼7300 earthquakes ($M \geq 0$) in the study area recorded during the 2005-2015 study period. Manually selected event windows start immediately prior to the P wave arrival and end when the S wave coda envelope amplitude is 10% that of the maximum amplitude. This window is chosen to ensure that waveform correlations register primarily signal with minimal contamination by noise. The correlation between every pair of earthquake waveforms is then calculated to create a ∼[7300 × 7300] matrix of pairwise correlation coefficients (CC).

Two important aspects of all repeating earthquake studies are the choice of CC threshold and the clustering algorithm used to define families. Changing the threshold or the clustering

algorithm can lead to different family definitions and different numbers of earthquakes iden-
tified as repeats. In addressing the *CC* threshold, we considered a passband of 2-14 Hz for
all our analyses and set the *CC* threshold at 0.90. The pass band is relatively conservative, as
many previous studies have employed a narrower passband of ~1-8 Hz and a *CC* threshold of
~0.95 [e.g., Igarashi et al., 2003; Matsubara et al., 2005]. We choose a low corner of 2 Hz
instead of 1 Hz due to poorer SNR at frequencies near 1 Hz in the vicinity of station DIB. The
high corner of 14 Hz was chosen to compensate for diminished spatial resolution due to lim-
ited station coverage. Because much of our analysis relies on the single (3-component) station
DIB, there are fewer constraints on waveform similarity than in previous studies of repeating
earthquakes where larger numbers of stations are available. The higher frequency waveform
signature provides a more unique "finger-print" for each family than would be achieved using
lower frequencies alone. To assess the effect of this modified frequency passband, we consider
the differences in *CC* when measured at different frequencies. In order to facilitate statistical
analysis, we apply the Fisher Transformation [Fisher, 1921] to all *CC* values to yield the Fisher
correlation coefficient (*FCC*):

$$FCC = \frac{1}{2} \ln \left[\frac{1+CC}{1-CC} \right] . \tag{1}$$

The *FCC* exists on the interval (-∞, ∞) and is more nearly normally distributed than the *CC*,
which is bounded on the interval [-1,1] [Fisher, 1921]. To establish a baseline with previous
studies that employed larger numbers of stations, we compare the *FCC* measured in both the
2-8 Hz and 2-14 Hz passbands. A more ideal comparison would use a 1-8 Hz passband (instead
of 2-8 Hz) as the benchmark, but unfortunately, due to poor SNR for frequencies near 1 Hz,
this proves to be difficult. We compute pairwise *FCC*s measured at both 2-8 Hz and 2-14 Hz,
and fit the data using a total least squares approach (Fig. 3a; Van Huffel and Vandewalle 1991):

$$FCC_{2-14\,\text{Hz}} = (0.8266)FCC_{2-8\,\text{Hz}} - 0.0103 . \tag{2}$$

(a)

(b)
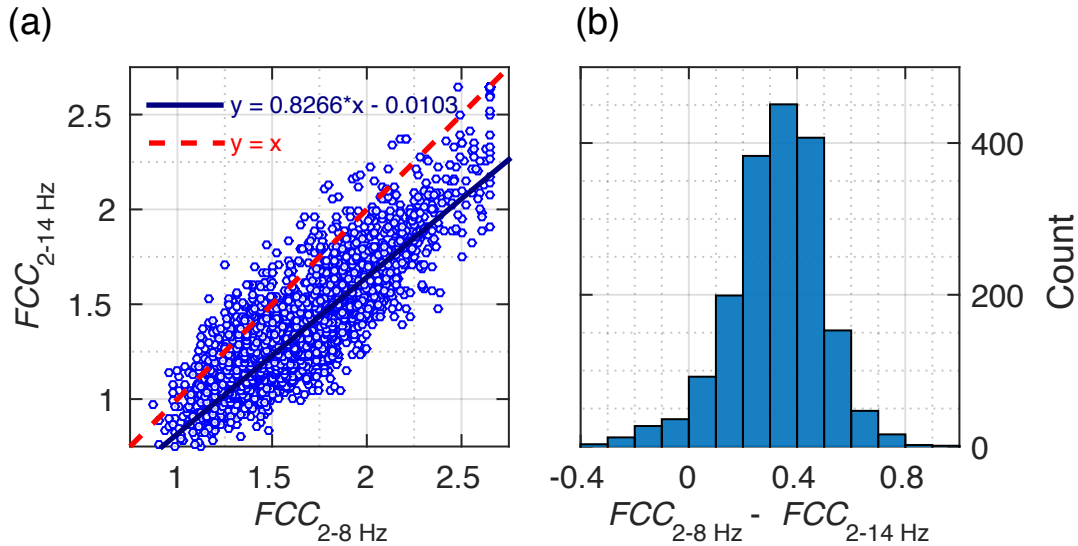
Figure 3: (a) Crossplot of all pairwise Fisher correlation coefficients (FCC) between events at 2-8 Hz and 2-14 Hz. Only points with F$CC_{2-8Hz} > 1.4722$ ($CC_{2-8Hz} > 0.90$) are used to calculate the total least squares best fit line (solid blue line). The 1-to-1 line (dashed red line) is shown for reference. (b) Histogram of the difference between FCC for all pairwise event comparisons in the two passbands of interest. The distribution is approximately normal with a mean of 0.4.

 The errors to the total least squares line are approximately normally distributed in the FCC domain with a mean of 0 and a standard deviation of 0.13. Only points with $FCC_{2-8\,\mathrm{Hz}} > 1.4722$ ($CC_{2-8\,\mathrm{Hz}} > 0.90$) are used to calculate the best-fitting line (2) because we are only interested in the scaling for waveforms exhibiting high correlation. As expected, the FCC is lower in the wider passband of 2-14 Hz than in the narrower 2-8 Hz passband. From (2), a value of $FCC_{2-8\,\mathrm{Hz}} = 1.8318$ ($CC_{2-8\,\mathrm{Hz}} = 0.95$) corresponds to $FCC_{2-14\,\mathrm{Hz}} = 1.5039$ ($CC_{2-14\,\mathrm{Hz}} = 0.9058$). In Figure 3b the difference between $FCC_{2-8\,\mathrm{Hz}}$ and $FCC_{2-14\,\mathrm{Hz}}$ is shown. The distribution is approximately normal with a mean of $\sim$0.4. A difference in FCC of 0.4 corresponds to a difference in CC of $\sim$0.06-0.03 (in the vicinity of CC=[0.90,0.95]). From this analysis, we establish that a threshold of $CC_{2-14\,\mathrm{Hz}} = 0.90$ corresponds approximately to the $CC_{2-8\,\mathrm{Hz}}$ measure of 0.95 that is more typical of previous studies on repeating earthquakes. The CC threshold of 0.90 is the same as that employed by Schmittbuhl et al. [2016], and similar to that of Chen et al. [2008].

    We define the repeating earthquake families by implementing a clustering algorithm

based on the Unweighted Pair Group Method with Arithmetic Mean (UPGMA; Romesburg 2004). Many previous repeating earthquake studies have used "chain-like" methods, wherein if event *A* correlates highly with *B*, and *B* correlates highly with *C*, then it is assumed that *A* and *C* also belong together, regardless of their correlation [e.g., Igarashi et al., 2003; Rubinstein and Ellsworth, 2010; Uchida and Matsuzawa, 2013]. However, in this study, possibly due to the limited station availability, we find that chain-like algorithms lead to large families with events that clearly do not belong in the same repeating earthquake family, and so a more sophisticated clustering algorithm is needed.

The UPGMA algorithm is an agglomerative, hierarchical process, and as such, each event begins as its own cluster, and clusters are subsequently combined until a desired *CC* threshold has been reached. Consider a pairwise *CC* matrix with 5 events labelled *A*, *B*, *C*, *D*, and *E* as in Figure 4. The clustering process performs the following steps: (1) group the two events with the highest *CC* (*A* and *D*) into a new cluster (*AD*), (2) recalculate the *CC* of this new cluster with all other items (*B*,*C*, and *E*) as the average of the *CC*s with the cluster's previously separate members, (3) locate the new highest *CC* in the matrix (whether that be between clusters, individuals, or a combination of the two) and repeat steps 1 and 2 until the desired *CC* threshold is reached. The algorithm is *unweighted* because whenever correlations to a new cluster are calculated, each original *CC* value is weighted equally (i.e., correlations made earlier are weighted equally to those made later). For example, at the first iteration in Figure 4, the new *CC* values are recalculated simply by:

$$CC_{AD\leftrightarrow B} = \frac{CC_{A\leftrightarrow B} + CC_{D\leftrightarrow B}}{2}, \tag{3}$$

where, e.g., $CC_{A\leftrightarrow B}$ is defined as the *CC* between events *A* and *B*. At the third iteration in Figure 4, the new *CC*s must be calculated more carefully to account for the different number of events in the clusters being combined:

$$CC_{ADB\leftrightarrow EC} = \frac{2\,[CC_{AD\leftrightarrow EC}] + 1\,[CC_{B\leftrightarrow EC}]}{3}. \tag{4}$$

(a)

	A	B	C	D	E
A	■	0.96	0.82	(0.98)	0.84
B	0.96	■	0.88	0.94	0.90
C	0.82	0.88	■	0.92	0.96
D	(0.98)	0.94	0.92	■	0.88
E	0.84	0.90	0.96	0.88	■

	AD	B	C	E
AD	■	0.95*	0.87*	0.86*
B	0.95*	■	0.88	0.90
C	0.87*	0.88	■	(0.96)
E	0.86*	0.90	(0.96)	■

	AD	EC	B
AD	■	0.865*	(0.95)
EC	0.865*	■	0.89*
B	(0.95)	0.89*	■

	ADB	EC
ADB	■	0.873*
EC	(0.873*)	■

1st Iteration

2nd Iteration

3rd Iteration

(b)
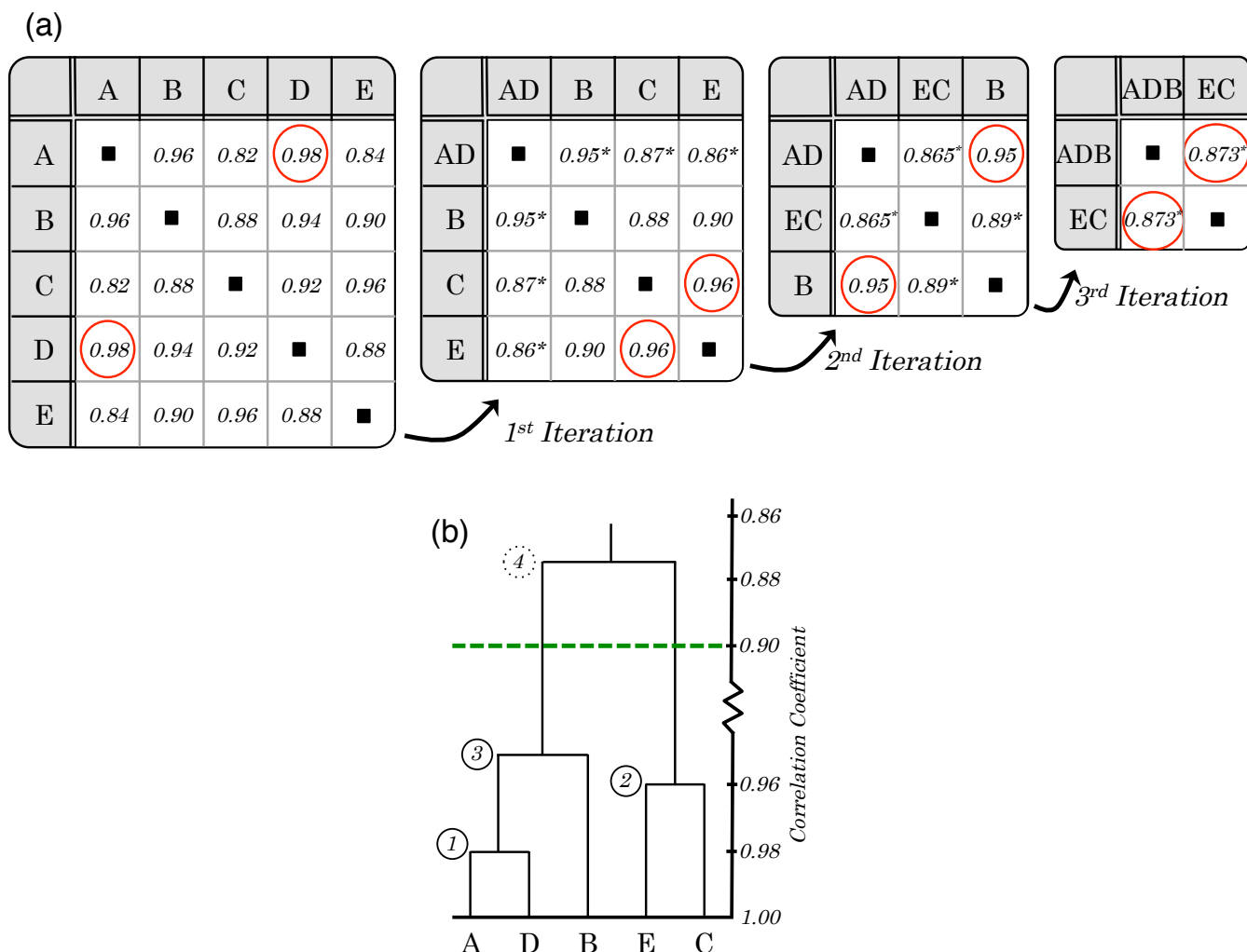
Figure 4: (a) Schematic representation of the UPGMA clustering algorithm employed to define the repeating earthquake families. Events are named A, B,..., E and their pair-wise correlation coefficients are given as matrix entries. The highest correlations in the current matrix are indicated by a red circle and the coefficients that were re-calculated during the previous iteration are marked by an asterisk. Assuming a correlation threshold of 0.90, the algorithm would halt at iteration 3 (due to the highest correlation being less than the threshold) and two earthquake families would be defined (ADB and EC). (b) The same toy problem as in (a), but illustrated as a dendrogram. Iteration numbers are given in circles, with solid circles indicating steps that were completed and dashed circles indicating steps that were not completed due to the correlation threshold (dashed green line) being too low.

This algorithm results in clusters in which the average *CC* of each member event with all other members in the family is greater than the desired *CC* threshold. We run the UPGMA algorithm with a *CC* threshold of 0.90 on the $[7300 \times 7300]$ matrix of all pairwise *CC*s. This defines 224 families comprising at least 2 earthquakes each, for a total of 494 individual

repeating earthquakes that are thought to be associated with the QCPB. The location of each family is defined as the average location of all repeating earthquakes within the family.

2.3   Addressing Catalogue Completeness

As previously mentioned, Haida Gwaii was not consistently instrumented during the study period of 2005-2015. As a consequence, many events, including repeating earthquakes, are likely missing from the Geological Survey of Canada's earthquakes catalogue. To address this issue, we employ a matched filter to search for additional repeating events [Gibbons and Ringdal, 2006]. Each repeating earthquake family is assigned a representative event that has the highest average correlation with other members of the family. This event is then used as a template to search the DIB data set for additional (non-catalogued) events with CC greater than 0.90. In doing so, we supplement the 224 repeating earthquake families with an additional 236 events, bringing the total number of earthquakes in the repeating earthquake catalogue to 730 (Appendix A). These 224 families, and associated 730 earthquakes, are also manually inspected to ensure that the repeating earthquake catalogue is robust. Note that in addition to the 224 families associated directly with the QCPB, 92 other families were also identified in the study area by the UPGMA and matched filter processes. However, through visual inspection of these 92 families' locations and/or polarities inconsistent with expected focal mechanisms, they are inferred to occur on subsidiary structures and thus are rejected from further analysis. All families, both related and unrelated to the QCPB, are shown in Figure 5.
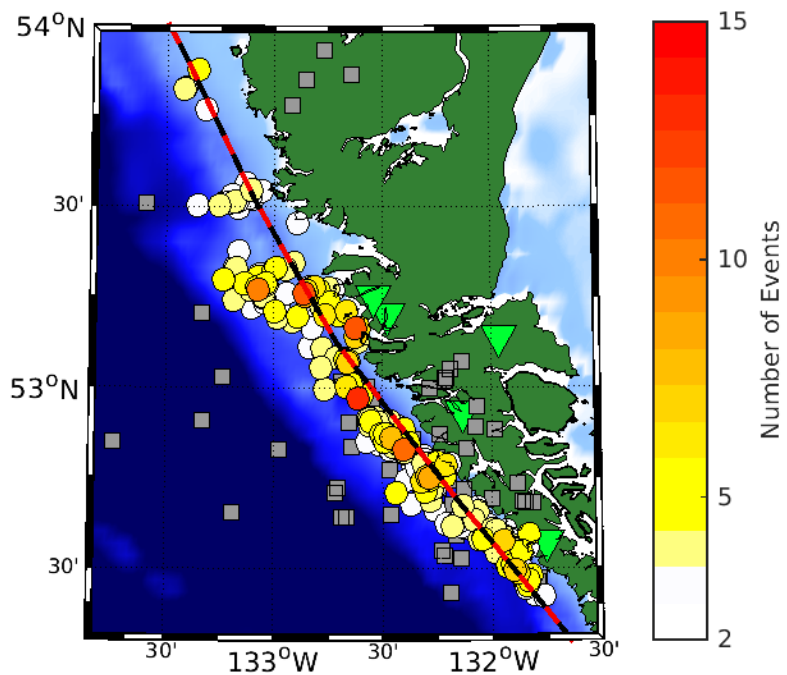
Figure 5: Map of all repeating earthquake families defined in this study, both related (coloured circles) and unrelated (gray squares) to the Queen Charlotte plate boundary. The circles are coloured by the number of events in the family. The red and black dashed line is the QCF, and bathymetry is coloured with the same scale as in Figure 1a.

Chapter 3

Repeating Earthquake Properties

The repeating earthquake catalogue resulting from UPGMA clustering (Section 2.2) and matched filter processing (Section 2.3) affords a comprehensive list of families and events; however, information on magnitudes and focal mechanisms is incomplete. In this Chapter, we calculate moments (M_0), moment magnitudes (M_W), slips, and focal mechanisms for each of the repeating earthquakes in the catalogue, and assemble the repeating earthquake families into groups along the QCPB.

3.1   Magnitude and Moment

3.1.1   Converting Local Magnitude to Moment Magnitude

Due to the low magnitudes of most earthquakes in our catalogue, many were originally calculated using the local magnitude (M_L) scale from which we must estimate M_0 and slip. We first convert the M_L values to M_W using the relation of Shearer et al. [2006], which considers the scaling between M_L, M_W, and M_0. Moment magnitude is defined by [Hanks and Kanamori, 1979]:

$$M_W = \frac{2}{3} \left[\log_{10} M_0 - 9.1 \right],$$
(5)

with M_0 measured in N·m. However, in their study of California earthquakes, Shearer et al. [2006] demonstrate a linear relationship between M_L and $\log_{10} M_0$ with slope 0.96 over the range $1 \leq M_L \leq 3$ (Figure 6a), consistent with the expected slope of ~ 1.0 for earthquakes exhibiting self-similarity [Shearer, 2009]. This observation for M_L deviates from that for M_W, which exhibits a slope of 2/3 as per (5). The larger scaling factor for M_L varies across studies, but is consistently greater than 2/3 [e.g., Bakun, 1984; Abercrombie, 1996; Ben-Zion and Zhu, 2002]. This scaling only applies to M_L values below a certain magnitude threshold, as only magnitudes of small earthquakes will be underestimated by the local magnitude calculation [Figure 6; Shearer et al., 2006]. We adopt the same $M_L = 3.0$ threshold as Shearer et al. [2006], such that for $M_L \geq 3.0$ the M_L and M_W scales are considered equivalent. For $M_L < 3.0$, a scaling factor of 0.96 is applied to calculate M_W (Figure 6b):

$$M_W = \begin{cases} \left[\left(\frac{2}{3} \right) \left(\frac{1}{0.96} \right) \right] M_L + 0.917 & : \quad M_L < 3.0 \\ \\ M_L & : \quad M_L \geq 3.0 \end{cases}. \tag{6}$$

From these estimates of M_W, it is straight-forward to calculate M_0 from (5).

3.1.2 Moments from Singular Value Decomposition

The M_W and M_0 values that we determine from (5, 6) are a good starting point; however, they are not sufficiently accurate to achieve meaningful estimates of fault slip. Due to the limited station coverage and inaccuracies involved in the conversion from M_L to M_W, a better method to estimate earthquake moment is required. Moreover, the earthquakes identified via the matched filter processing (Section 2.3) are without initial magnitude estimates. We follow Rubinstein and Ellsworth [2010] and apply Singular Value Decomposition (SVD) to both estimate the moments of the events detected by the matched filter and better constrain the moments of the earthquakes with magnitude estimates from (6).

The SVD method takes advantages of the waveform similarity within a family to provide better estimates of relative earthquake moments than conventional magnitude estimation

(a)

(b)
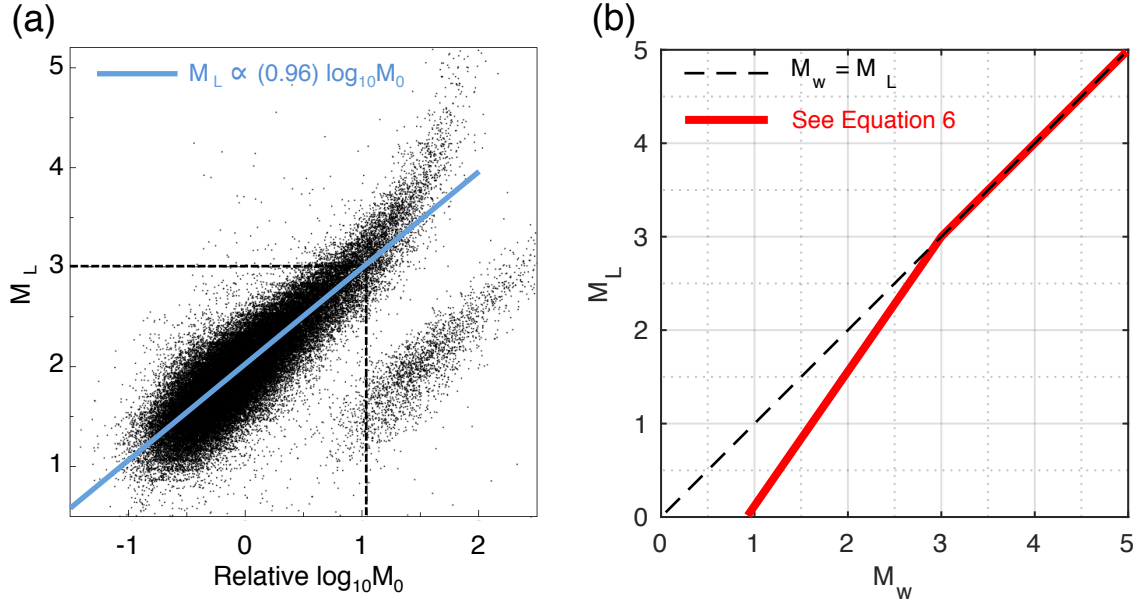
Figure 6: (a) Relationship between M_L and $\log_{10}M_0$ (*after* Shearer et al. [2006]). The best fit line (blue line) has a slope of 0.96, and is valid for $M_L < 3.0$. Above this threshold (black, dashed line), the data do not follow the same linear relationship. The second population of points to the right, with higher $\log_{10}M_0$, results from incorrect recording of network gain, and are not considered. (b) Relationship used in the present study to relate M_W to M_L (red line) based on (a). See text and (6).

techniques. This technique is particularly favourable when dealing with small earthquakes (which exhibit approximately constant durations when recorded at frequencies significantly below their corner frequencies) and when station coverage is limited [Rubinstein and Ellsworth, 2010], and thus is well-suited to our study. For each repeating earthquake family, consider a matrix, **R**, whose rows are composed of the aligned time series of all waveforms constituting that family, station, and component. Using SVD, **R** can be decomposed as

$$\mathbf{R} = \mathbf{U}\mathbf{S}\mathbf{V}^T \tag{7}$$

where **U** and **V** are matrices with columns of input and output basis vectors, respectively, and **S** is a diagonal matrix containing singular values (s_i) along the main diagonal. The importance of individual output basis vectors (columns of **V**, $\mathbf{v}_i$) in describing **R** is expressed by the associated s_i, with higher values of s_i indicating a more important output basis vector. The input basis vectors (columns of **U**, $\mathbf{u}_i$) describe the weights applied to each scaled output vector ($s_i\mathbf{v}_i$) to

reconstruct the rows of the original data matrix, **R**.

In the case of repeating earthquakes, **R** is composed of highly similar rows, so most of the data can be explained by the first output basis vector (i.e., $s_1 \gg s_{2,\dots,n}$; Figure 7). For every earthquake we calculate the ℓ_2-norm of the residual resulting from subtracting the weighted first basis output vector from the original waveform (Figure 7). The average residual, across all earthquakes of all families, has just 20.9% of the energy of the original waveform, which compares well with the value of 18.6% quoted by Rubinstein and Ellsworth [2010]. In considering only the first basis output vector, we assume that all other output basis vectors
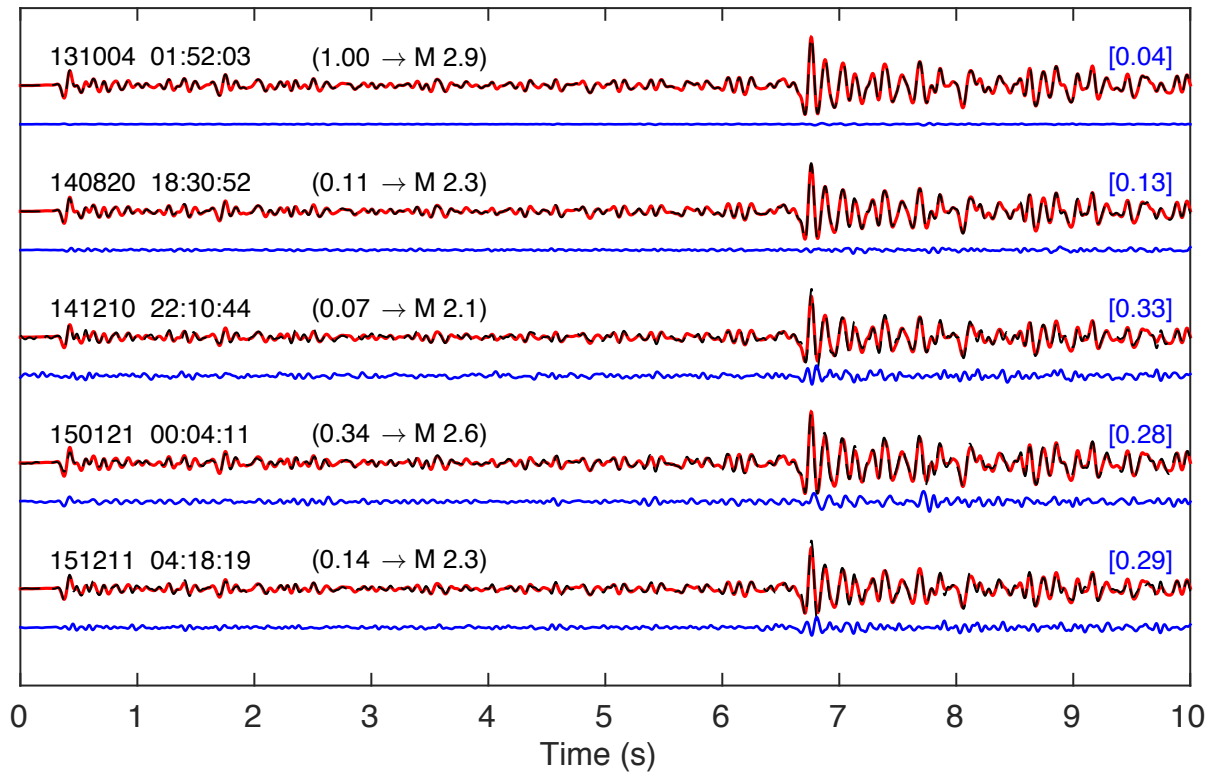
Figure 7: Vertical component waveforms recorded at station DIB (dashed black line) and SVD reconstruction using the weighted first basis output vector (solid red line) for family 183. The original and reconstructed waveforms show nearly perfect overlap and the residual waveforms (i.e., original minus reconstructed; solid blue line) are small. Dates of each event are given on the left in YYMMDD HH:MM:SS format. Moment weights relative to the first event are shown in parentheses with the final magnitude estimate (see text for full explanation). The ℓ_2-norm of the residual relative to the ℓ_2-norm of the original seismogram is shown in square brackets on the right. Plotted amplitudes within one event (original, reconstruction, and residual) are true, but scales vary between the five different events.

represent noise. It is likely that in addition to noise, subtle changes in source properties and/or material properties along the earthquake ray path constitute the lower level output basis vectors. However, following Rubinstein and Ellsworth [2010], we ignore these other vectors due to their relatively small amplitudes and because the first output basis vector effectively constrains the amplitude of the repeating earthquakes. The first column of $\mathbf{U}$ ($\mathbf{u}_{i1}$) thus contains the relative moment weights for all earthquakes in a given repeating earthquake family. This allows for all pairwise comparisons of relative moments to be made within a family, such as

$$M_{0A} - w_{AB}M_{0B} = 0, \tag{8}$$

where M_{0A} and M_{0B} are the absolute moments of event A and event B, respectively, and w_{AB} is the moment ratio of A relative to B. The SVD is performed separately on the three component waveforms from station DIB, and the ratio w_{AB} (8) is taken as the average result across the three components. The way in which we utilize these pairwise M_0 comparisons differs from that of Rubinstein and Ellsworth [2010], as follows. We first consider all pairwise M_0 comparisons for a given family and assemble a matrix equation. For a family with n earthquakes there are $\frac{n(n-1)}{2}$ pairwise comparisons, and thus $\frac{n(n-1)}{2}$ rows in the system. For example, for a family with three earthquakes ($A, B,$ and C), the system can be written as

$$\begin{bmatrix} 1 & -w_{AB} & 0 \\ 1 & 0 & -w_{AC} \\ 0 & 1 & -w_{CB} \end{bmatrix} \begin{bmatrix} M_{0A} \\ M_{0B} \\ M_{0C} \end{bmatrix} = \begin{bmatrix} 0 \\ 0 \\ 0 \end{bmatrix}. \tag{9}$$

However, in (9), the rank of the left-hand matrix is 2, whereas the number of rows is 3 (generally the rank is $(n-1)$ and the number of rows is $\frac{n(n-1)}{2}$). The redundant equations in this system are perfectly consistent because they come from the weighting of a single output basis vector, and thus we may choose the first $(n-1)$ equations (ordered systematically as in (9)) and discard the remaining equations. This corresponds to retaining all comparisons to the first

earthquake, which results in a system of the form

$$
\begin{bmatrix}
1 & -w_{AB} & 0 \\
1 & 0 & -w_{AC}
\end{bmatrix}
\begin{bmatrix}
M_{0A} \\
M_{0B} \\
M_{0C}
\end{bmatrix}
=
\begin{bmatrix}
0 \\
0
\end{bmatrix} .
\tag{10}
$$

In general, for a family with n earthquakes, the system is written as

$$
\begin{bmatrix}
1 & -w_{12} & 0 & 0 & \cdots & 0 \\
1 & 0 & -w_{13} & 0 & \cdots & 0 \\
\vdots & \vdots & \vdots & \vdots & \ddots & \vdots \\
1 & 0 & 0 & 0 & \cdots & -w_{1n}
\end{bmatrix}
\begin{bmatrix}
M_{01} \\
M_{02} \\
M_{03} \\
\vdots \\
M_{0n}
\end{bmatrix}
=
\begin{bmatrix}
0 \\
0 \\
\vdots \\
0
\end{bmatrix} .
\tag{11}
$$

Note that the left-hand matrix in (11) has size $[(n-1) \times n]$ and rank $(n-1)$. The equations in this system enforce precise relative moments between all members of a repeating earthquake family. To constrain absolute moments, we utilize the original M_0 estimates derived from Section 3.1.1. There are numerous options regarding how to employ the original magnitude estimates. A single earthquake (e.g., the one with largest magnitude) could be used, in combination with weights w_{ij} (11), to define M_0 for all other earthquakes within the family. However, to avoid relying on a single measurement and instead take advantage of all available information, we prefer to use a combination of all catalogued absolute moment estimates, which we denote by M_0^{cat}. One simple way to accomplish this is to constrain the sum of M_0 in the solution to be equal to the sum of M_0^{cat}, but this approach is susceptible to errors in magnitude estimates for the largest events. We suggest a more intricate combination of original recorded moments,

which is added as an additional row to (11), producing the system

$$
\begin{bmatrix}
1 & -w_{12} & 0 & 0 & \cdots & 0 \\
1 & 0 & -w_{13} & 0 & \cdots & 0 \\
\vdots & \vdots & \vdots & \vdots & \ddots & \vdots \\
1 & 0 & 0 & 0 & \cdots & -w_{1n} \\
\prod_{j\neq 1} w_{1j} & \prod_{j\neq 2} w_{1j} & \prod_{j\neq 3} w_{1j} & \prod_{j\neq 4} w_{1j} & \cdots & \prod_{j\neq n} w_{1j}
\end{bmatrix}
\begin{bmatrix}
M_{01} \\
M_{02} \\
M_{03} \\
\vdots \\
M_{0n}
\end{bmatrix}
=
\begin{bmatrix}
0 \\
0 \\
\vdots \\
0 \\
\sum_{i}\left(M_{0i}^{cat} \prod_{j\neq i} w_{1j} \right)
\end{bmatrix},
\tag{12}
$$

or, more succinctly,

$$
\mathbf{Gm = d}. \tag{13}
$$

We choose the M_0^{cat} constraint in (12) because it is orthogonal to the rest of the system and so better honours the scaling constraints in (11), which are anticipated to be more accurate and robust than constraints from absolute moments. A full derivation and justification of the final equation in (12) is available in Appendix B. By representing the system in this way, we satisfy all relative M_0 information from the SVD analysis in the first $(n-1)$ rows, and constrain all M_0^{cat} information with a single equation (i.e., the nth row). Recall that in the present study, matched filter detections have no associated M_0^{cat} values. Consequently, the nth row in $\mathbf{G}$ may be missing entries, such that $\prod_{j\neq i} w_{1j}$ is replaced by 0. Importantly, even in the case of missing M_0^{cat} values, $\mathbf{G}$ has size $[n \times n]$ and rank n. These properties of $\mathbf{G}$ allow us to solve (13) for the true moments ($\mathbf{m}$) directly:

$$
\mathbf{m = G^{-1}d}. \tag{14}
$$

In the present study, the condition number of $\mathbf{G}$ for all repeating earthquake families is sufficiently low to use (14) as an accurate and stable solution.

As mentioned previously, this method produces M_0 estimates for earthquakes that had no prior measure of M_0, and also improves the accuracy of M_0 estimates for all repeating earthquakes in our catalogue [Rubinstein and Ellsworth, 2010]. Predictably, larger earthquakes

have greater control on the SVD than smaller earthquakes (Figure 8). We find that, following the SVD and inversion processes, earthquakes with original $M_W > 2.5$ rarely change by more than 0.2 magnitude units, whereas the magnitudes of smaller earthquakes can change by up to $\sim$0.6 (Figure 8). We also note that there appears to be a small gross bias by the procedure to decrease the magnitudes compared to those from the original recorded magnitudes. This is observed as a "fat-tail" on the negative side of the distribution in Figure 8, and may result from significant power of the original waveforms being present in the lower-level basis vectors that are discarded in the SVD analysis. Rubinstein and Ellsworth [2010] report that this effect is weakly magnitude-dependent, whereby smaller earthquakes are more affected than larger earthquakes. This leads to a weak magnitude-dependent bias: smaller earthquakes are more likely to be underestimated by this procedure, and larger earthquakes are more likely to be overestimated. However, our results agree with those of Rubinstein and Ellsworth [2010] in that this magnitude-dependent bias is very weak and can be safely ignored.
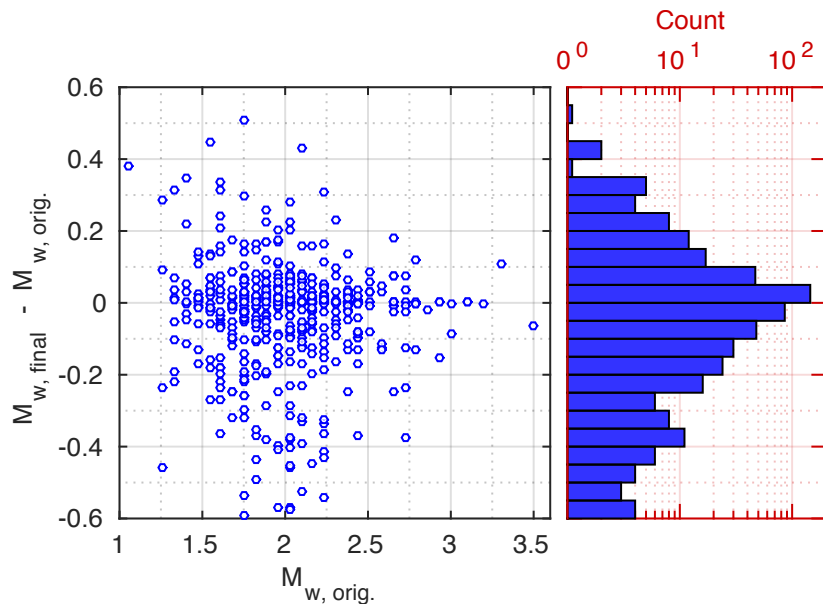
Figure 8: Comparison of M_W estimates before and after SVD analysis and inversion for earthquake moment. Only events that had initial M estimates are shown (494 total events). $M_{w,orig.}$ values are those after correcting from M_L (see Section 3.1.1). The cross-plot shows that changes to smaller events are more extreme than those to larger events because larger magnitude events tend to control the SVD analysis. The histogram to the right (red axes), which uses the same y-axis as the crossplot, shows that there is a slight bias in the analysis to smaller magnitudes.

The final magnitude distribution of the repeating earthquakes is in the range $0.3 \leq M_W \leq 3.5$, and the majority of the events fall near $M_W\,2.0$ (Figure 9). As expected, matched filtering (Section 2.3) identifies a higher proportion of low magnitude earthquakes than the original clustering process (Figure 9), because these low magnitude events are more likely to be missed by standard detection routines. However, note that the matched filtering does contribute a substantial number of higher magnitude events (Figure 9b), and thus contributes significantly to catalogue completeness and our efforts to accurately quantify the slip budgets of the QCPB. The original search for repeating earthquakes was performed over the magnitude range $0.0 \leq M \leq 7.0$, but no large earthquakes in the study area satisfied the waveform similarity criteria described above to be included in repeating earthquake families.
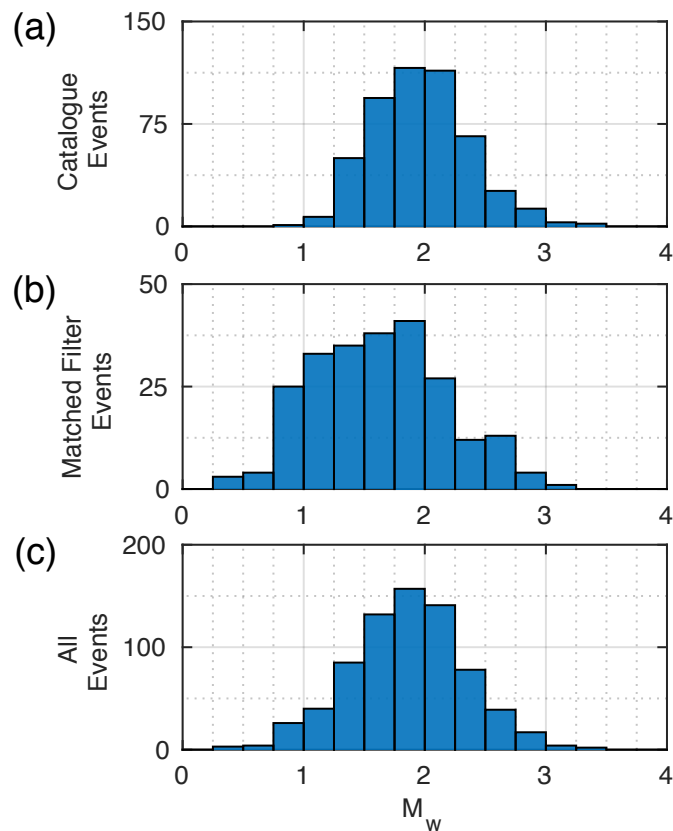
Figure 9: Magnitude histograms for repeating earthquakes (a) from the original GSC earthquake list, (b) added by the matched filter process, and (c) from the combination of the two (i.e., the entire repeating earthquake catalogue of the present study). The matched filter identifies a higher proportion of smaller magnitude events, but still contributes a significant number of larger earthquakes to the repeating earthquake catalogue. Note the different event scales (y-axes) for each of the histograms.

3.2 Fault Slip

The major goal of this study is to gain an understanding of the slip dynamics of the QCPB. Accordingly, the slip for each individual repeating earthquake must be estimated. To do this, we employ a relation relating M_0 to fault slip (d) for repeating earthquakes from Nadeau and Johnson [1998]:

$$\log_{10} d = (0.17) \log_{10} M_0 - 2.36, \tag{15}$$

where d is measured in cm, and M_0 is measured in dyne·cm. This relationship was originally developed by Nadeau and Johnson [1998] for the San Andreas Fault, but has been later shown to apply to repeating earthquakes in numerous tectonic environments, including the northeastern Japan subduction zone [Igarashi et al., 2003] and the Chihshang Fault in Taiwan [Chen et al., 2008]. The relationship between moment and slip (15) has subsequently been applied to repeating earthquakes on both subduction and strike-slip faults world-wide [e.g., Matsubara et al., 2005; Kato et al., 2016; Uchida et al., 2016]. Assuming it is generally valid, we employ (15) for all repeating earthquakes in our study, including both those on the subduction interface and those on the strike-slip QCF.

The slip characteristics of all repeating earthquake families in the present study may be divided into two main groups: "burst"-type, and "steady"-type families. Burst-type families have all their events clustered closely in time and therefore do not generally persist for a significant portion of the study period, however some families exhibit multiple burst episodes (Figure 10). Conversely, steady-type families tend to have more regularly spaced repeating earthquakes over a longer time period (Figure 10). A similar phenomenon has been observed by previous studies in the northeastern Japan subduction zone [Igarashi et al., 2003] and North Anatolian Fault [Schmittbuhl et al., 2016]. Burst-type events are expected to occur during nucleation and after-shock sequences of large earthquakes, whereas the steady-type families are inferred to result from constant tectonic loading on the fault [Igarashi et al., 2003; Schmittbuhl et al., 2016]. Although the slip patterns, and the underlying stress-forcing regimes, may be very different for

(a)

Family 186

(b)

Family 223
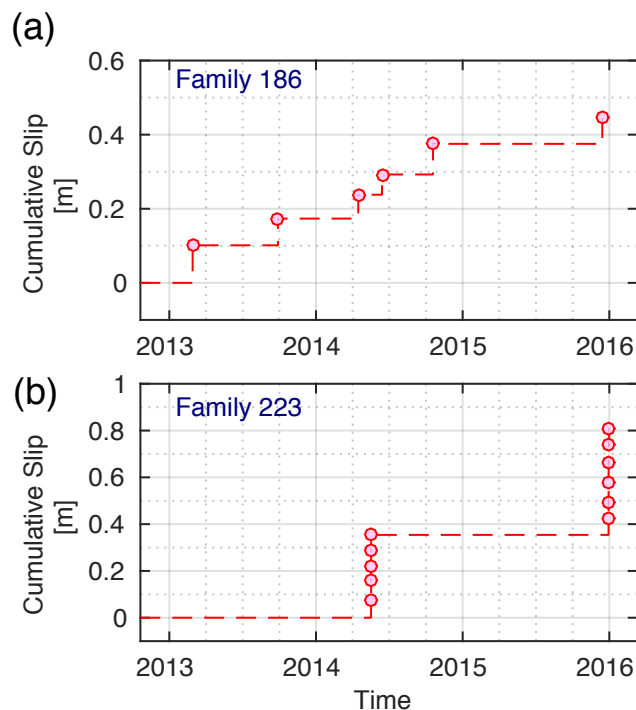
Time

Figure 10: Examples of slip histories for (a) a steady-type repeating earthquake family where isolated earthquakes occur in regular recurrence times, and (b) a burst-type repeating earthquake family where earthquakes are clustered in time. The burst-type family 223 consists of two bursts of activity in mid-2014 and late-2015. Individual earthquakes are shown by pink circles.

these two family types, both types contribute significantly to the overall slip budget of the plate boundary and are thus both important in the analysis.

3.3 Polarity Constraints on Focal Mechanisms

Due to limited station coverage and low magnitudes of the repeating earthquakes in this study, we are unable to solve for reliable focal mechanisms. However, it is important to distinguish, where possible, between repeating earthquakes on the subduction and strike-slip portions of the QCPB (Figure 1b). To accomplish this, we manually inspect the P-wave polarities of all repeating earthquake families and determine if they are consistent with dextral strike-slip motion along the QCF, thrust motion along the subduction interface, or neither (Figure 11). Although repeating earthquakes can be observed along smaller faults, most repeating earthquakes (in particular, steady-type families) occur on major plate boundaries because a

near-constant tectonic force can generate repeated slips of the same fault patch [e.g., Igarashi et al., 2003; Chen et al., 2007]. With this in mind, repeating earthquake families that are classified as subduction-type in this study are those with polarities that are consistent with subduction motion and inconsistent with dextral strike-slip motion for all available event/station recordings. A similar criterion is applied for families that are classified as QCF-type. Examples of this classification process are illustrated in Figure 11.
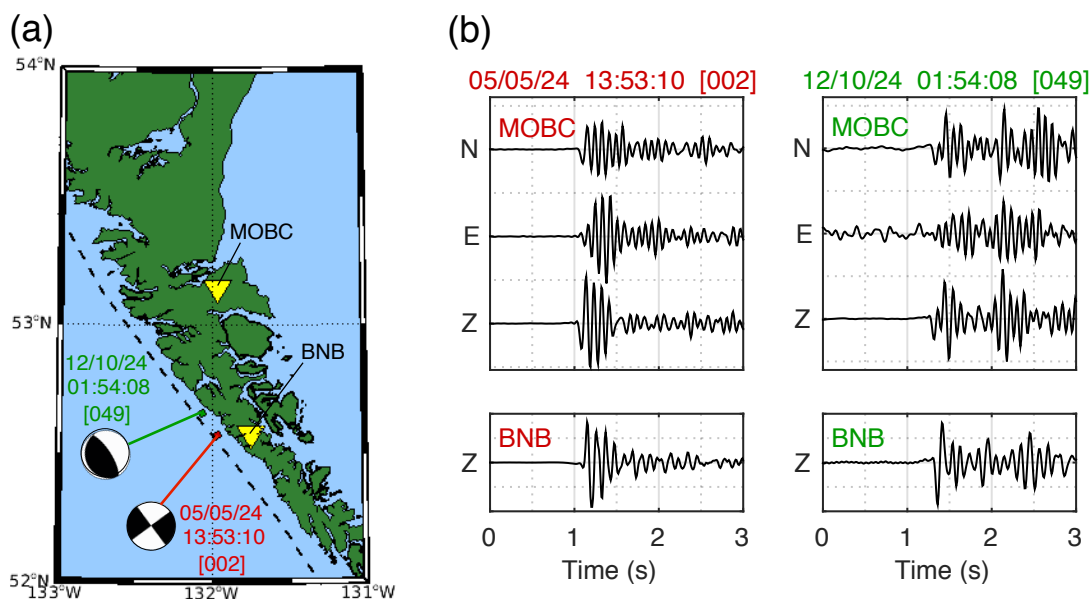
Figure 11: Example of how focal mechanisms are assigned to repeating earthquake families in the present study. (a) Two nearby events and their assumed upper hemisphere focal mechanisms are shown relative to stations MOBC and BNB (yellow triangles) and the QCF (black dashed line). Dates are given in YY/MM/DD HH:MM:SS format with family ID given in brackets. (b) Observed P-waves for the two events recorded at MOBC (top panel) and BNB (bottom panel). Both subduction thrust and dextral strike-slip earthquakes from the given area exhibit negative polarity at MOBC. However, at BNB the strike-slip event (positive polarity) can be distinguished from the subduction event (negative polarity). See text for full explanation of process.

The hypocenter of a family is also considered when classifying it as subduction- or QCF-type. However, the locations are generally used as supporting, rather than defining, evidence because the hypocenters being used are those from the original GSC earthquakes catalogue, and as such may be subject to appreciable errors, especially for smaller earthquakes. For example, many earthquakes in the repeating earthquake catalogue do not possess depth estimates, and so using depth of the earthquake to distinguish between the QCF and subduction interface is not

possible. In general, if multiple earthquakes consistently show that a family's location cannot be attributed to either the QCF or subduction interfaces then the hypocenter information is considered, but in many cases it is the waveform and polarity that is used as the principal line of evidence in defining the focal mechanism of a family.

In some cases, due to station geometry, it is not possible to distinguish between polarities for strike-slip and thrust motions. In these cases, the family is classified as "unclear" and is considered in the slip calculations for both the subduction and QCF interfaces to place lower and upper limits on slip estimates. The distribution of families based on focal mechanism and associated fault interface is shown in Table 1. As mentioned in Section 2.3, the process of inspecting polarities reveals 92 additional families that, when considering polarities and hypocenter locations, are classified neither as subduction nor QCF earthquakes, and thus are rejected from further analysis (Figure 5). The majority of these additional families are composed of only two events and do not contribute significantly to the overall moment budget of the repeating earthquakes in this study.

Table 1: Repeating earthquake families classified by focal mechanism assignment and fault interface. Families in the"unclear" category are those whose polarities cannot be unambiguously attributed to either thrust or strike-slip motions. These unclear families are considered in the slip calculations for both subduction and QCF interfaces to create upper and lower estimates of slip.

Type	Number of Families	Total Number of Repeating Earthquakes	Total Cumulative Moment Release [N·m]
Subduction Thrust	87	320	7.9043×10^{14}
QCF Strike-Slip	76	240	1.2020×10^{15}
Unclear	61	170	2.2586×10^{14}

3.4 Combining Repeating Earthquake Families into Groups

3.4.1 Grouping Methodology

Previous studies have demonstrated that repeating earthquakes are effective slip meters for both the seismic fault patch that ruptures during the earthquake and surrounding areas that slip aseismically. This theory is supported by both observational field studies [e.g., Nadeau and Johnson, 1998; Chen et al., 2007; Kato et al., 2016; Schmittbuhl et al., 2016; Uchida et al., 2016] as well as modelling and lab studies [e.g., Beeler et al., 2001; Chen and Lapusta, 2009]. The measurements of slip resulting from repeating earthquakes differ from those obtained by GPS techniques in that the repeating earthquake method samples slip on the fault surface directly, whereas GPS measures slip at the earth's surface and requires an inverse problem to resolve slip of the fault at depth. With this in mind, our main objective in the present study is to determine the slip characteristics of the entire QCPB using the point measurements of slip that we obtain from each repeating earthquake family. We follow the work of Matsubara et al. [2005] and Uchida et al. [2016] by arranging the repeating earthquake families into groups that are related both spatially and by focal mechanism assignment. That is, we divide all repeating earthquake families that represent dextral strike-slip motion along the QCF into spatially-related groups along the fault. The same is done for the subduction interface. We then average the slip histories for all repeating earthquake families in a given group to recover the average slip on the fault, in that area, through time. In theory all repeating earthquake families in a given group should have nearly identical slip histories because they all represent slip of a similar area of the fault. But, in practice we find that although families in a common group often have related slip histories, there are also discrepancies. The grouping and averaging process allows for the removal of inconsistencies and spurious signals, which is required to investigate the underlying slip signal of the fault interface. To clarify, in the present study, a repeating earthquake "family" is composed of individual earthquakes that represent slip of the same fault patch, whereas a "group" refers to a collection of families that have the same focal

mechanism and are located near each other.

To define groups, we search for families that have similar waveforms and thus similar focal mechanisms. The same UPGMA clustering used to define the repeating earthquake families (Section 2.2) is applied to the first basis output vectors of each family from the SVD analysis (Section 3.1.2). The output basis vectors represent the common elements of each earthquake in a family, and are good approximations of the family's average waveform. Families resulting from the same sense of slip in nearby areas yield similar P and S waves, but different S minus P lag times (Figure 12). Because S waves generally exhibit larger amplitudes than P waves, the *CC* value, and thus the grouping process, is controlled by the similarity of the S waves. Figure 12 illustrates an example of many families in an area exhibiting similar waveforms (and thus representing similar focal mechanisms), despite the fact that they originate from different, but nearby, locations on the fault interface. The example shown in Figure 12 also illustrates that the families in a group (group 5S in Figure 12) typically exhibit common temporal behavior whereby one family is more likely to slip when a nearby family slips. This temporal similarity is not ubiquitous across all families of all groups, but is observed in many cases.

The UPGMA algorithm is used to define initial groups of subduction- and QCF-type groups along the QCPB, and then manual inspection of all families in associated areas is performed to assign all families to groups. Recall from Section 3.3 that in some cases a family cannot be unambiguously assigned to correspond to either dextral strike-slip motion along the QCF or thrust motion on the subduction interface. In these ambiguous cases, the family is classified as having an unclear focal mechanism (Table 1) and is considered in both the nearest subduction- and QCF-type groups, which allows us to place upper and lower limits on group slip.

3.4.2 Final Group Definitions

The final group definitions are shown in Figure 13. Because groups are determined based on observed clustering of the families, there is variation between groups in regards to map area
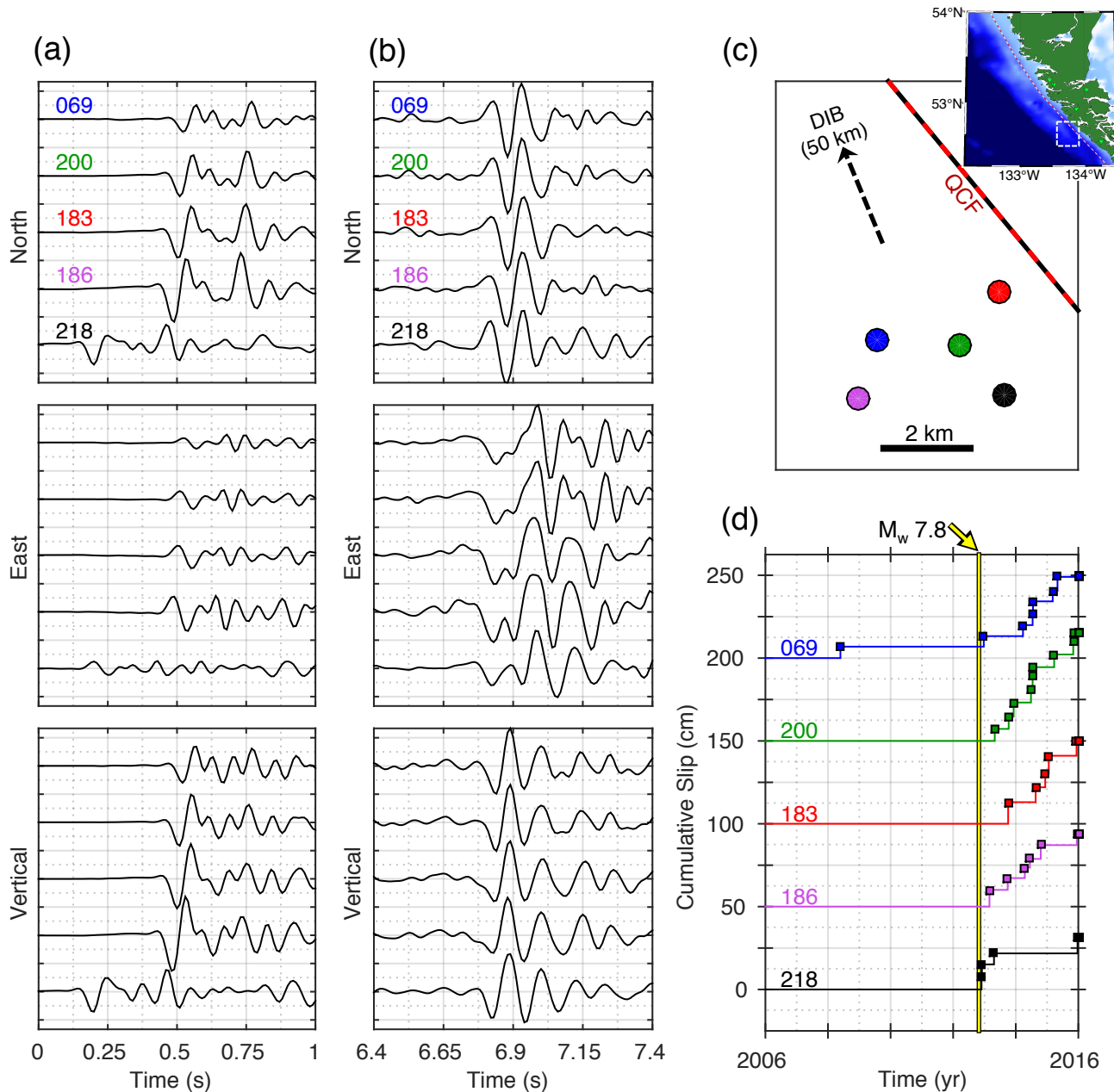
Figure 12: A selection of families from group 5S. (a) P waves and (b) S waves recorded at station DIB. The waveforms are the first output basis vector for the family from the SVD analysis (Section 3.1.2) and represent family average waveforms. P waves have been amplified relative to S waves to facilitate visual comparison. Family labels are given on north component (top panel) and ordering is consistent for other components (middle and bottom panels). Both P waves and S waves show high waveform similarity between families, despite the varying P to S lag times (representing different hypocenter locations). (c) Locations of the families. Map location is shown in inset map (white dashed box). (d) Slip history for the families, showing a temporal connection between families. Individual repeating earthquakes are shown by squares, and the time of the 2012 M_W 7.8 Haida Gwaii earthquake is given as a yellow line.
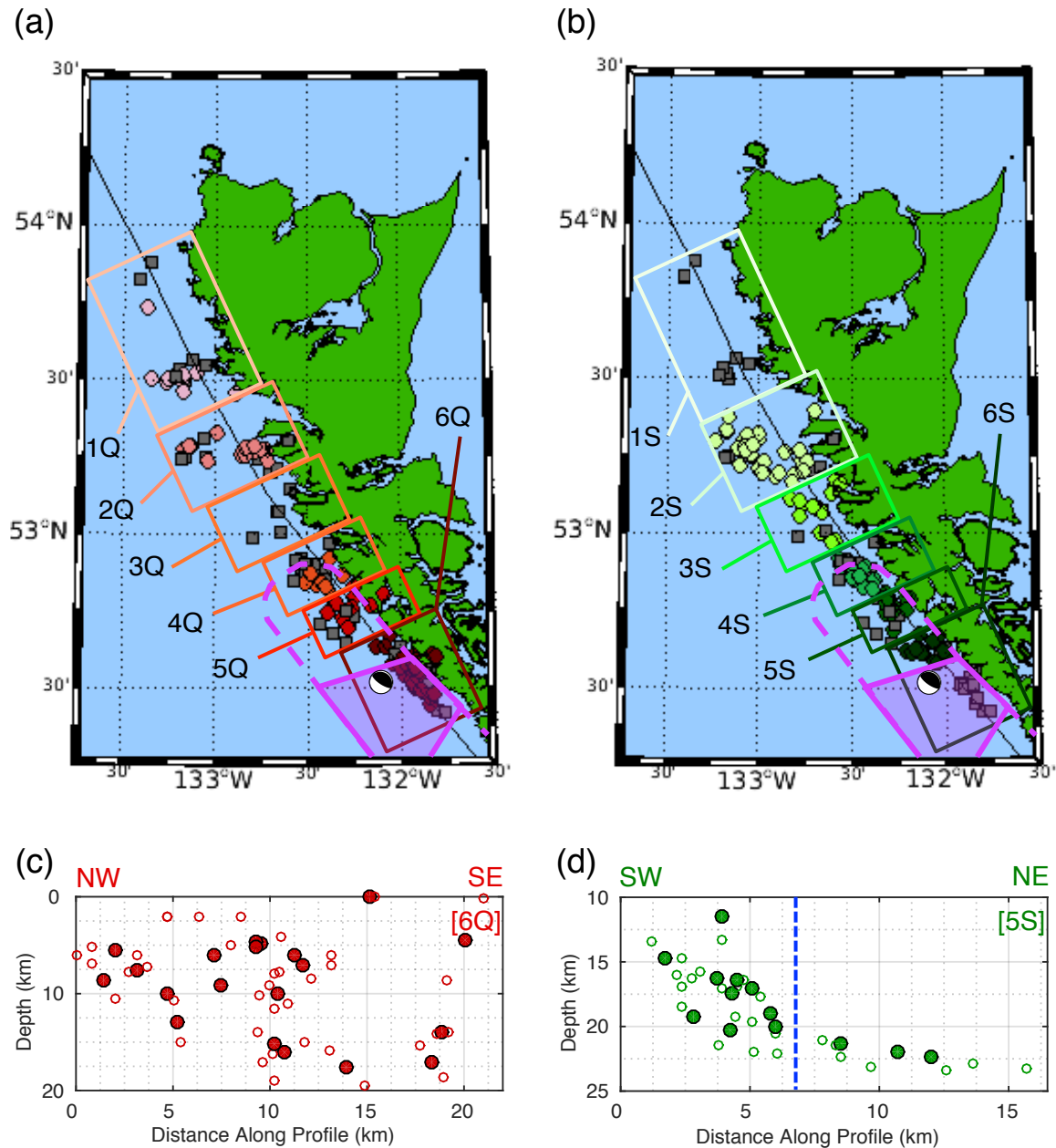
Figure 13: Groupings of (a) QCF strike-slip type and (b) subduction thrust type repeating earthquake families. Individual families (coloured circles) are coloured by group. Families with ambiguous polarities (gray squares) are shown in both (a) and (b). Also shown in (a) and (b) is the hypocenter (lower-hemisphere focal mechanism), rupture zone (dashed, purple line), and area of maximum slip (filled, purple polygon) for the 2012 Haida Gwaii earthquake [Hyndman, 2015; Nykolaishen et al., 2015]. (c) Example of a cross-section of a QCF group (6Q), with profile taken along the strike of the QCF. (d) Example of a cross-section of a subduction group (5S), with profile taken perpendicular to the strike of the QCF (i.e., parallel to plate subduction). The location of the surface trace of the QCF is shown with a blue, dashed line. In cross-sections, filled circles are family average locations, empty circles are individual repeating earthquake locations, and there is a horizontal exaggeration of 2. Note that some families do not have depth estimates, and are absent from the cross-sections. A complete set of cross-sections is provided in Appendix C.

and number of families. Groups represent map areas ranging between 600-1500 km^2 (Figure 13a,b), consist of 9-32 families, and 24-112 individual repeating earthquakes (excluding "unclear" groups). For a full definition of each group, see Appendix C. Groups are labelled as 1Q, 1S, 1U, 2Q, 2S, 2U, etc., where the leading number corresponds to the area of the QCPB and the trailing letter represents the strike-slip QCF ("Q"), the subduction interface ("S"), or unclear ("U") slip-types. Note that groups 1S and 3Q are empty because no families in the corresponding areas exhibit waveforms that are unambiguously due to subduction or strike-slip motions, respectively. However, the unclear families in these areas (i.e., those in groups 1U and 3U) may be due to either sense of slip. Consequently, although there are no well-defined groups 1S and 3Q, upper- and lower-limit slip estimates for these areas are still provided based on the unclear families in the corresponding areas.

Although it is difficult to rely on precise hypocenter information of the repeating earthquakes, due in large part to their small magnitudes and limited station coverage, it is nonetheless insightful to present depth cross-sections of all repeating earthquake groups. Cross-sections for groups 6Q and 5S are shown in Figure 13c,d, and the remainder are provided in Appendix C. Many families are missing catalogue depths and so are omitted from the cross-section analysis. For groups classified as QCF-type, we create profiles parallel to the QCF surface trace. In these groups, families appear uniformly scattered in depth in the range ∼5-20 km (Figure 13c; Appendix C). The distribution of these families' hypocenters is consistent with the inference that they represent strike-slip motion on the vertical QCF. For groups classified as subduction-type, the cross-section profiles are created perpendicular to the QCF so as to be parallel with the dip of the subducting Pacific plate. The locations of families in groups 3S, 4S, 5S, and 6S define a dipping planar feature (Figure 13d; Appendix C), supporting the inference that these repeating earthquake families occur on the plate interface between the subducting Pacific plate and the overriding North American plate. The dip angles measured from groups 3S, 4S, 5S, and 6S are ∼32°, 32°, 31°, and 24° respectively. These dip angles for the subducting plate are consistent with the value of 28 ± 5° estimated from receiver function analysis by Bustin

et al. [2007]. Other studies employing receiver functions and thermal modelling have reported a shallower dip angle of $\sim 20°$ [Smith et al., 2003; Gosselin et al., 2015]. Note that hypocenters for group 2S show too much scatter to permit an accurate measure of dip, and group 1S has no families to analyze (Appendix C).

Chapter 4

Slip History of the Queen Charlotte Plate Boundary

Following the definitions of repeating earthquake groups (Section 3.4; Figure 13), we are able to investigate the slip histories of both the QCF and subduction interface, which together constitute the QCPB. For a given group, we consider the cumulative slip histories of all associated families (e.g., Figures 10 and 12d), and compute the mean to provide the average slip history for the group (Figures 14 and 15).

4.1   Calculating Lower and Upper Limits of Slip

Recall that in addition to the QCF ("Q") and subduction ("S") groups, there are also groups composed of families with ambiguous polarities that are classified as unclear ("U") groups. The unclear families are utilized to provide upper and lower limits for slip estimation. For a given Q- or S-group, every combination of including and excluding unclear families in the calculation of the mean slip history is considered. For example, if an area has three unclear families nearby (U_A, U_B, and U_C), then there are a total of 8 scenarios to consider (Table 2). In the present study, the unclear group with the highest number of families (group 4U) includes 16 families, which leads to 65,536 scenarios to consider when determining the upper and lower
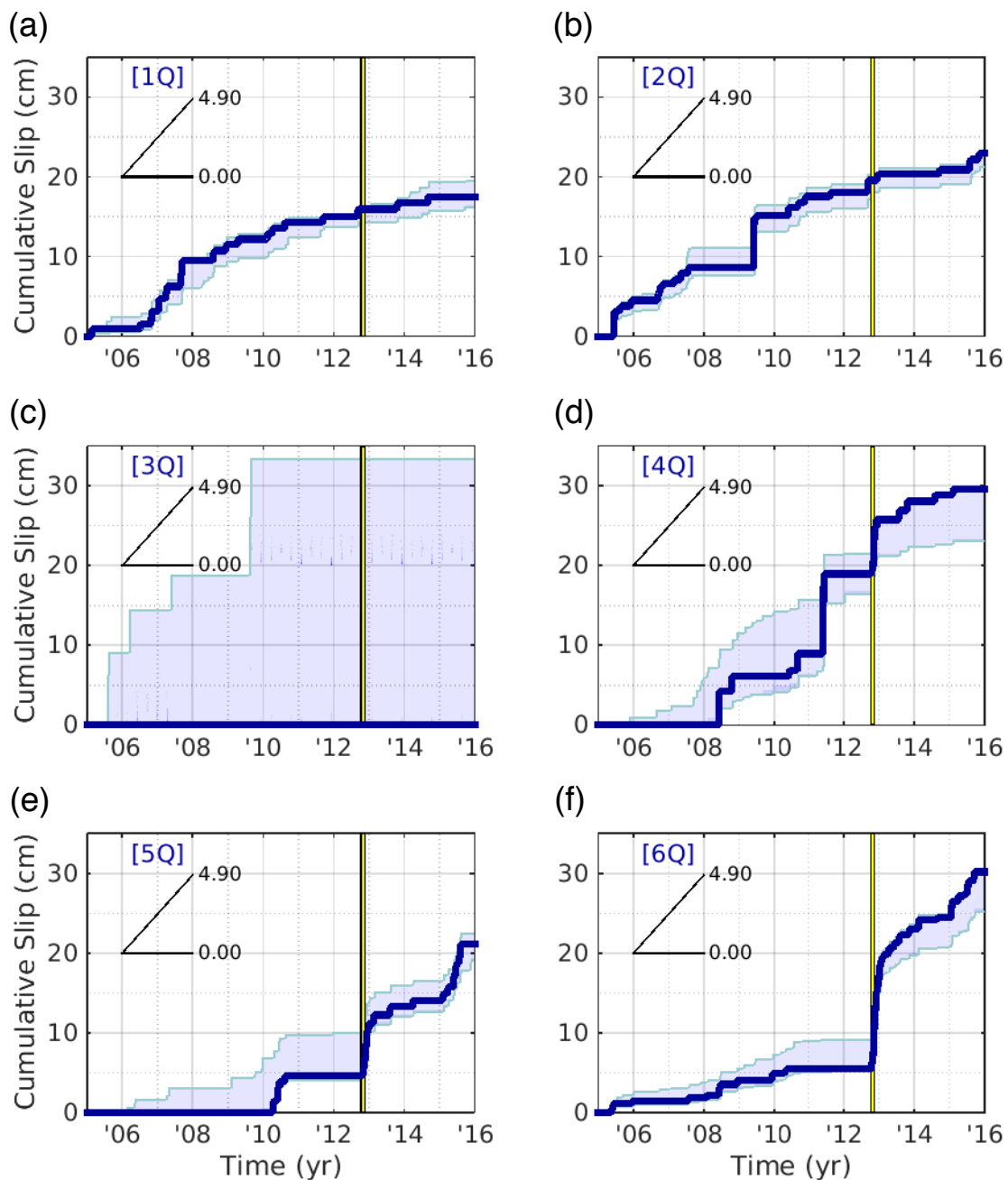
Figure 14: Average cumulative slip histories for all QCF-related repeating earthquake groups. Group IDs are given in brackets in the top left of each plot, and their locations are shown in Figure 13a. Main group estimates (dark blue lines) are calculated as the average cumulative slip for all repeating earthquake families in the group. Lower and upper limits (light blue lines and shaded areas) are calculated through inclusion of families with ambiguous polarities (see text). Group 3Q has no definitive families, and thus has only an upper maximum for slip. The time of the 2012, M_W 7.8 Haida Gwaii earthquake is shown with a vertical yellow line. Also shown is the rate of relative plate motion that acts parallel to the QCF (∼4.90 cm/yr).
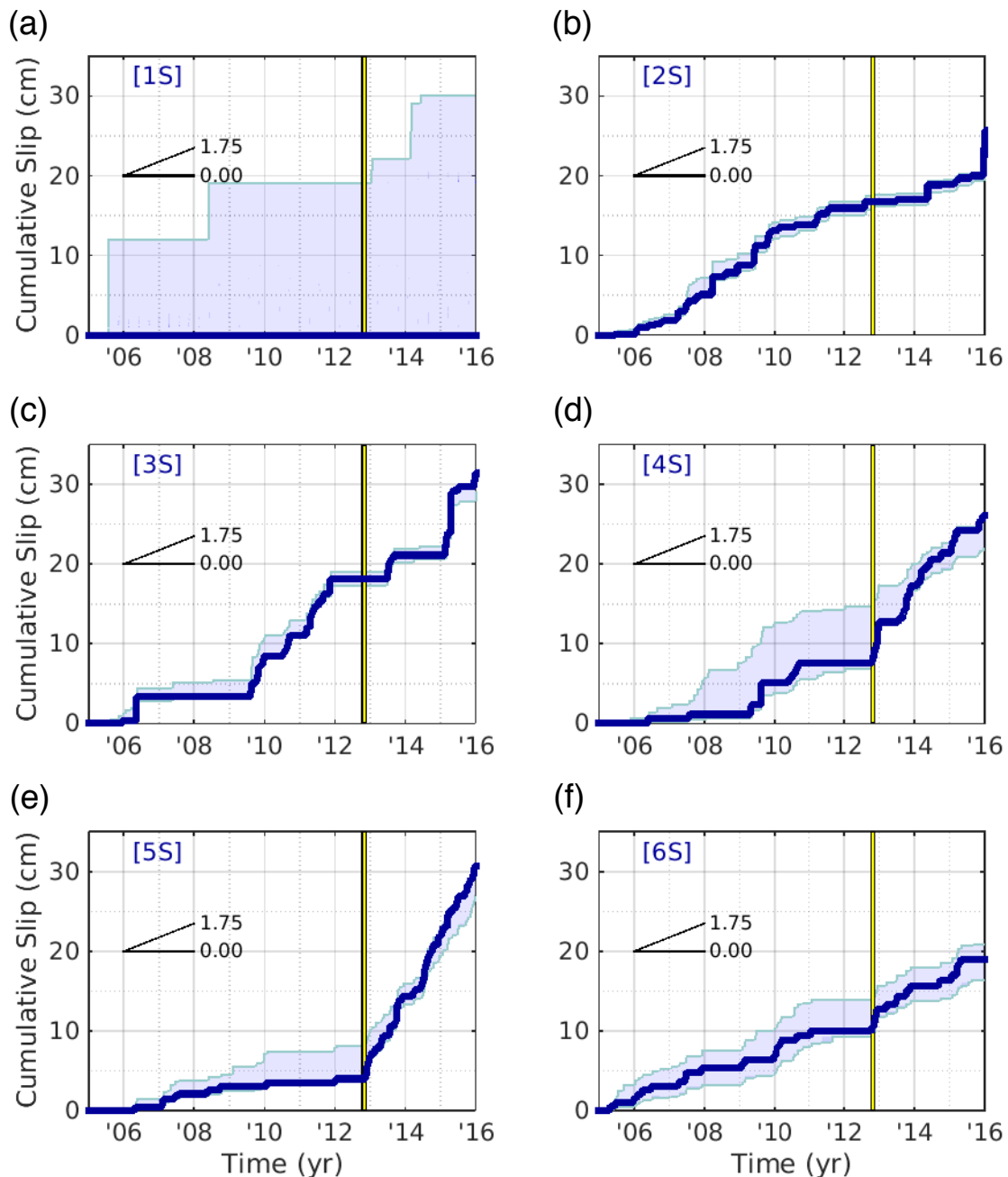
Figure 15: Average cumulative slip histories for all subduction-related repeating earthquake groups. Group IDs are given in brackets in the top left of each plot, and their locations are shown in Figure 13b. Main group estimates (dark blue lines) are calculated as the average cumulative slip for all repeating earthquake families in the group. Lower and upper limits (light blue lines and shaded areas) are calculated through inclusion of families with ambiguous polarities (see text). Group 1S has no definitive families, and thus has only an upper maximum for slip. The time of the 2012, M_W 7.8 Haida Gwaii earthquake is shown with a vertical yellow line. Also shown is the rate of relative plate motion that acts parallel to subduction ($\sim$1.75 cm/yr).

Table 2: Explanation of the different scenarios considered to determine upper and lower estimates of slip for a given group. Every combination of including and excluding "unclear" families is considered, and then maxima and minima are calculated to determine upper and lower limits. In this example there are n families that constitute the main group in question ($M_{1,2,...,n}$), and 3 families in the associated "unclear" group (U_A, U_B, and U_C).

Scenario	Families Considered in Mean Slip Calculation
1	$M_{1,2,...,n}$
2	$M_{1,2,...,n}, U_A$
3	$M_{1,2,...,n}, U_B$
4	$M_{1,2,...,n}, U_C$
5	$M_{1,2,...,n}, U_A, U_B$
6	$M_{1,2,...,n}, U_A, U_C$
7	$M_{1,2,...,n}, U_B, U_C$
8	$M_{1,2,...,n}, U_A, U_B, U_C$

limits of slip. For each scenario, the mean slip history is calculated for all families involved. Then, for every point in time, the minimum and maximum cumulative slip is chosen from the list of all scenarios to yield lower and upper limits on cumulative slip at that point in time.

4.2 Cumulative Slip and Slip Rate Estimates

The final cumulative slip of each group is presented, along with the lower and upper limits as defined above (Section 4.1), in Figure 14 (all QCF-related groups) and Figure 15 (all subduction-related groups). Note that groups 3Q (Figure 14c) and 1S (Figure 15a) are poorly constrained because they possess no definitive families, and thus are characterized solely by an upper limit of slip based on unclear families in their respective areas. Aside from these empty groups, 4Q (Figure 14d) and 4S (Figure 15d) exhibit the most uncertainty because there are more unclear families in that area than anywhere else along the boundary.

Also included in Figures 14 and 15 are the relative plate motion rates between the Pacific and North American plates in the direction that is applicable to the given group. The total slip rate vector between the Pacific and North American plates is ∼5.2 cm/yr, and is characterized by 4.8 - 5.0 cm/yr parallel to the QCF and 1.5 - 2.0 cm/yr perpendicular to the QCF [e.g., Hyndman and Hamilton, 1993; Mazzotti et al., 2003; Hyndman, 2015; Nykolaishen et al.,

2015]. Including these slip rates in Figures 14 and 15 allows us to determine if the observed slip rates, as measured by repeating earthquakes, are lower than, consistent with, or in excess of the expected slip rates from large scale plate motions.

One important issue to address is whether significant changes in the slip behavior of the QCPB occur after the 2012, M_W 7.8 Haida Gwaii subduction earthquake (hereafter HGEQ). For this reason, we employ cumulative slip curves in Figures 14 and 15 to determine slip rates for all repeating earthquake groups both before and after the HGEQ. Note that the cumulative slip measurements in Figure 15 do not include slip directly due to the HGEQ, estimated to be on average 3.3 m and at maximum 7.7 m [Lay et al., 2013], or large aftershocks thereof [Kao et al., 2015]. Unlike the main HGEQ event and its large aftershocks, the repeating earthquakes represent steady slip of the fault interface. We investigate the repeating earthquake groups related to the QCF and subduction interface separately.

4.2.1 Slip Rates of the Queen Charlotte Fault

We first consider the QCF, whose slip history is represented by repeating earthquake groups 1Q, 2Q, ..., 6Q (Figures 13a and 14). The average slip rates for these repeating earthquake groups, both before and after the HGEQ, are shown in Table 3. To determine the "main group" estimates we simply consider the difference in cumulative slip of the main group in

Table 3: Average slip rates for QCF-related groups (see Figure 14) during time periods prior to, and after, the *Mw* 7.8 Haida Gwaii earthquake on Oct. 28, 2012. Note that slip rates following the Haida Gwaii earthquake include (if applicable) accelerated slip immediately following the earthquake. See text for explanation of how slip rates are calculated.

Group	2005/01/01 - 2012/10/28 Slip Rate (cm/yr)			2012/10/28 - 2015/12/31 Slip Rate (cm/yr)		
	Lower Limit	Main Group	Upper Limit	Lower Limit	Main Group	Upper Limit
1Q	1.84	2.04	2.08	0.11	0.49	1.15
2Q	2.31	2.50	2.62	0.55	1.07	1.17
3Q	-	-	4.28	-	-	-
4Q	2.11	2.42	2.75	1.31	3.36	3.36
5Q	0.53	0.59	1.30	4.60	5.20	5.63
6Q	0.68	0.71	1.18	6.21	7.76	7.82

question (Figure 14) during the time period of interest, and divide by the length of the time period. The upper and lower slip rate limits in Table 4 are calculated by using the main group cumulative slip value at the beginning of the time period, and either the upper or lower limit of cumulative slip (Figure 14) at the end of the time period. Note that slip rates in Table 3 incorporate short periods of fast slip for some families (e.g., immediately following the HGEQ; Figure 14d,e,f), and thus may not be representative for the entire duration of the reported time period. Recall that the component of Pacific - North American plate motion acting in the direction parallel to the QCF is ~4.8 - 5.0 cm/yr; this provides a natural comparison for the slip rates determined from repeating earthquakes.

Groups 1Q and 2Q represent the northernmost section of the QCF, which is also the area of the QCF that is farthest from the hypocenter of the HGEQ (Figure 13a). The slip behaviour of these two groups is very similar (Figure 14a,b). Average slip rates of groups 1Q and 2Q prior to the HGEQ are 2.04 and 2.50 cm/yr, respectively, and after the HGEQ these rates decrease to 0.49 and 1.07 cm/yr, respectively (Table 3). However, pre-HGEQ slip rates are inflated due to short periods of fast slip. Group 1Q slips at ~6.9 cm/yr between July, 2006 and September, 2007, and group 2Q exhibits very fast slip in June, 2009. Note that the large transient increase in slip for group 2Q in June, 2009 is not due to a single, large earthquake contaminating the group average; rather, eight separate earthquakes contribute to this increase. If short periods of fast slip are ignored, the slip rates of these two groups remain nearly constant through time, and there appears to be no influence from the HGEQ on slip of the QCF in this region. Overall, the slip rate of these groups is much lower than the large scale plate motion in the direction parallel to the QCF (~4.8 - 5.0 cm/yr).

Group 3Q has no definitive families, and thus only an upper maximum of cumulative slip based on unclear families within its area. However, it is worth noting that the upper limit on slip rate for the time period prior to the HGEQ (4.28 cm/yr; Table 3) is similar to the plate motion rate (~4.8 - 5.0 cm/yr). We cannot establish upper/lower limit slip rate estimates for post-HGEQ times, because there are no repeating earthquakes in groups 3Q or 3U after the

HGEQ.

Group 4Q straddles the northern limit of the rupture area of the HGEQ (Figure 13a), and shows interesting slip behavior. The group exhibits no slip (or very low slip rate if the upper limit is used) between January, 2005 and June, 2008. Between June, 2008 and the HGEQ, the slip rate is 4.3 cm/yr, which is similar to the plate motion rate of $\sim$4.8 - 5.0 cm/yr. The post-HGEQ slip rate is 3.36 cm/yr, and includes a burst of high-slip activity for 1 month following the HGEQ.

Both groups 5Q and 6Q fall within the rupture zone of the HGEQ. Group 5Q is on the periphery of the rupture zone, whereas 6Q is near the zone of maximum slip and contains the epicenter of the event (Figure 13a). The average pre-HGEQ slip rates are similar at 0.59 and 0.71 cm/yr for groups 5Q and 6Q, respectively (Table 3), and both lie well below the plate motion parallel to the QCF ($\sim$4.8 - 5.0 cm/yr). The pre-HGEQ slip rate of group 6Q is more constant through time, whereas all of the slip for group 5Q occurs in 2010 (Figure 14d,e). However, if we consider the upper limit of cumulative slip for 5Q (Figure 14d), the true pre-HGEQ slip of the QCF in the region of 5Q may in fact be more regular. The HGEQ appears to have triggered activity for both groups, with very high slip rates for 2 months following the earthquake. Thereafter, the average slip rates of groups 5Q and 6Q return to values comparable to those prior to the HGEQ. Accelerated slip is again observed for both groups at the beginning of 2015, persisting for $\sim$6-10 months. The post-HGEQ cumulative slip of group 6S is very close to the upper limit of slip (Figure 14f), so if a significant number of unclear families (i.e., those in group 6U) are in fact related to the QCF, the actual slip rate may be slower than currently reported (Table 3).

4.2.2   Slip Rates of the Subduction Interface

Next, we investigate the repeating earthquake groups that represent thrust motions on the subduction interface of the QCPB: 1S, 2S, ..., 6S (Figures 13b and 15). Based on the cumulative slip curves in Figure 15, we calculate main group, lower limit, and upper limit estimates of slip

rate, both before and after the HGEQ (Table 4). These slip rates are determined as in Section 4.2.1, with one exception: the upper limit slip rate for group 1S, for both pre- and post-HGEQ times, is calculated using only the upper limit of cumulative slip from Figure 15a, because there is no main group estimate of slip. In the case of the subduction interface, we are interested in comparing our slip rate values with the component of plate motion that is perpendicular to the QCF (i.e., parallel to subduction). Recall that this margin-perpendicular motion of the Pacific and North American plates is $\sim$1.5 - 2.0 cm/yr.

Table 4: Average slip rates for subduction-related groups (see Figure 15) during time periods prior to, and after, the *Mw* 7.8 Haida Gwaii earthquake on Oct. 28, 2012. Note that slip rates following the Haida Gwaii earthquake include (if applicable) accelerated slip immediately following the earthquake. See text for explanation of how slip rates are calculated.

Group	2005/01/01 - 2012/10/28 Slip Rate (cm/yr)			2012/10/28 - 2015/12/31 Slip Rate (cm/yr)		
	Lower Limit	Main Group	Upper Limit	Lower Limit	Main Group	Upper Limit
1S	-	-	2.44	-	-	3.45
2S	2.07	2.14	2.26	0.83	2.81	1.20
3S	2.22	2.31	2.45	3.48	4.17	4.21
4S	0.90	0.97	1.88	4.56	5.81	5.91
5S	0.48	0.51	1.05	7.24	8.41	8.44
6S	1.25	1.35	1.82	1.85	2.65	3.25

The slip rate of the subduction interface in the vicinity of group 1S (i.e., most northerly section of the study area) is poorly constrained due to the absence of repeating earthquake families in this group (Figure 15a; Appendix C). Nonetheless, we calculate the upper limits of slip rate for the presumed subduction interface in this area to be 2.44 and 3.45 cm/yr for pre- and post-HGEQ times, respectively (Table 4).

Groups 2S and 3S both represent slip along the subduction interface north of the main rupture zone of the HGEQ (Figure 13b). The slip histories of these two groups are very similar (Figure 15b,c), with pre-HGEQ slip rates calculated to be 2.14 and 2.31 cm/yr for 2S and 3S, respectively (Table 4). These pre-HGEQ slip rates are slightly higher than, but comparable to, the estimated convergence rate of the Pacific and North American plates ($\sim$1.5 - 2.0 cm/yr).

The HGEQ does not appear to have had a significant effect on the slip rates of groups 2S and 3S, as no immediate acceleration in slip rate is observed for either group. However, the post-HGEQ average slip rates for these groups are higher than pre-HGEQ rates. The post-HGEQ average slip rates for 2S and 3S are measured to be 2.81 and 4.17 cm/yr, respectively (Table 4). These higher values are due, in large part, to short episodes of fast slip in December, 2015 (Group 2S) and March - April, 2015 (Group 3S).

The slip rates of groups 4S, 5S, and 6S are expected to be more affected by the HGEQ than those of 2S and 3S due to the proximity of these groups to the earthquake. Group 6S is within the main HGEQ rupture zone and contains the hypocenter of the event, 5S is within the northern section of the rupture zone, and 4S straddles the northern limit of rupture (Figure 13b). All three of these groups exhibit slip rates that are lower than the plate motion rate of convergence ($\sim$1.5 - 2.0 cm/yr) for pre-HGEQ times: 0.97 , 0.51, and 1.35 cm/yr for groups 4S, 5S, and 6S, respectively (Table 4). Note that the pre-HGEQ cumulative slip curves for groups 4S and 5S are near the calculated lower limits and far from the upper limits of slip (Figure 15d,e). Accordingly, the actual pre-HGEQ slip rates for groups 4S and 5S may be slightly higher than those reported in Table 4. All of groups 4S, 5S, and 6S experience slip rate increases at the onset of the HGEQ (Figure 15d,e,f). The post-HGEQ slip rates for groups 4S, 5S, and 6S are 5.81, 8.41, and 2.65 cm/yr, respectively (Table 4). All three of these groups exhibit slip rates that are below the plate motion convergence rate prior to the HGEQ, and greater than the plate motion convergence rate after the HGEQ. Importantly, the post-HGEQ increases in slip rates are relatively steady for the time period beginning immediately after the HGEQ through the end of the study period (December, 2015).

Overall, the cumulative slip histories of subduction groups (with the possible exception of group 3S) are better behaved than the corresponding QCF groups. That is, the QCF groups display more intermittent slip rates (Figure 14), whereas the subduction groups tend to slip more steadily (Figure 15). An important example of this difference in slip behavior is the observed effect of the HGEQ on nearby groups. Groups 4S, 5S, and 6S display an abrupt

increase in slip rate at the onset of the HGEQ, and this slip rate is relatively steady until the end of the study period. Conversely, although QCF groups in the same area (i.e., 4Q, 5Q, and 6Q) do exhibit accelerated slip immediately following the HGEQ, it only lasts for a short period of 1 - 2 months (Figure 14d,e,f). The implications of these observations are discussed in Chapter 5.

Chapter 5

Discussion

5.1 Interseismic Slip of the Queen Charlotte Plate Boundary

The repeating earthquake catalogue and the associated cumulative slip curves (Figures 14 and 15) provide insight into the slip dynamics of both the QCF and subduction interface in the study area. In this Section we discuss the implications of our results for the interseismic period (i.e., prior to the HGEQ). Because the HGEQ occurred on the subduction interface and the QCF has not experienced a large earthquake in this area since 1949, the entire study period may be considered to be interseismic with regards to the QCF. Nonetheless, we do observe a response of the QCF to the HGEQ (Section 4.2.1). For simplicity, we will refer to all times prior to the HGEQ as interseismic, and all times after the HGEQ as postseismic, for both the subduction interface and the QCF. Note that the 2013, M_W 7.5 Craig earthquake occurred on the QCF ∼200 km north of our study area [Aderhold and Abercrombie, 2015; Holtkamp and Ruppert, 2015]), but we do not observe any response to this earthquake and thus do not consider it in our analysis.

5.1.1   Interseismic Slip: the Queen Charlotte Fault

The slip rate measurements from our repeating earthquake catalogue indicate that the QCF exhibits interseismic slip throughout the entire study area, and is therefore not completely locked. However, the slip rates that we observe are substantially lower than the plate motion rate parallel to the QCF. Recall that the total plate motion vector is ~5.2 cm/yr, and that 4.8 - 5.0 cm/yr acts parallel to the QCF, whereas the pre-HGEQ slip rates that we measure are between ~0.6 - 2.5 cm/yr (Table 3). The difference in plate motion and actual slip on the fault requires the QCF to be partially locked and stress to be accumulating. This inference is consistent with the results of Mazzotti et al. [2003], who show that the model with the best fit to GPS data in the area is one with a locked QCF between 0 and 14 km depth, steady aseismic slip below 20 km, and a transition between the two zones. Many of the QCF repeating earthquake families are located in the 14-20 km depth range; however, we do also observe shallower families (e.g., Figure 13c), and these shallow families do not exhibit different slip behaviour than deep families. This may indicate some local fault creep in the otherwise locked shallow portion of the QCF, however it may also be due to errors in catalogue depths. Wang et al. [2015] report that the QCF is expected to intersect the subduction interface at 15-20 km depth, which is consistent with both the model of Mazzotti et al. [2003] and the location of the repeating earthquakes in the present study.

The QCF groups' slip rates decrease from north (2.04 and 2.50 cm/yr for groups 1Q and 2Q, respectively) to south (0.59 and 0.71 cm/yr for groups 5Q and 6Q, respectively). This decrease implies a higher degree of locking in the south than in the north. The QCF is closer to parallel with plate motions in the northern part of the study area (Figure 1a) and therefore accommodates a higher proportion of the plate motion, but this difference cannot account for the large difference in slip rates that we observe. This variation in slip rate further suggests that southern regions of the study area (i.e., groups 5Q and 6Q) are more likely to rupture in a major strike-slip earthquake in the future, due to larger stress accumulation. The occurrence of Canada's largest recorded earthquake, the 1949, M_s 8.1 Queen Charlotte Islands earthquake,

provides support for this interpretation. This right-lateral, strike-slip event occurred on the QCF within our study area; its epicenter was located at 53.62°N, 133.27°W [Bostwick, 1984; Rogers, 1986; Nishenko and Jacob, 1990; Earthquakes Canada, 2016]. The extent of the rupture zone is not known precisely. However, slip from the 1949 earthquake was greatest in the northern region of the present study area (the epicenter is in zone 1 of Figure 13a), and decreased to the south with its southern limit near ∼52.5°N [Bostwick, 1984; Rogers, 1986; Nishenko and Jacob, 1990]. The smaller (or, potentially, complete lack of) slip in the south during the 1949 earthquake also suggests that the QCF has higher seismic potential in the southern part of the study area than in the north.

5.1.2   Interseismic Slip: the Subduction Interface

Like the QCF, the subduction interface exhibits non-zero pre-HGEQ slip rates throughout the study area, which suggests that the subduction thrust is not fully locked. Mazzotti et al. [2003] model the subduction interface in the same way they do the QCF: a locked zone between 0 and 14 km depth, a transition zone between 14 and 20 km, and a stable sliding, aseismic zone below 20 km. Our slip rates are generally consistent with the Mazzotti et al. [2003] model, however their model includes annual thrust motions of 0.6 - 1.0 cm/yr, and our pre-HGEQ rates are higher in some places (0.5 - 2.3 cm/yr; Table 3). The depths of repeating earthquakes are consistent with the Mazzotti et al. [2003] model, which requires a locked fault between 0 and 14 km. Nearly all subduction families in the present study occur on a dipping plane, inferred to be the subduction interface (Figure 13d), and are located below 14 km. The only shallower family is family 187 (group 5S; Figure 13d), which is assigned an (average) depth of 11.5 km due to one of its two constituent events being catalogued at 1.0 km depth. Whether the catalogue depth is incorrect or the family should be excluded from the study is not clear. However, the inclusion of this family does not significantly alter the slip rate of group 5S and so we choose to retain it. A non-zero slip rate on the subduction interface is also consistent with Wang et al. [2015], who report that the subduction interface is expected to undergo

fault creep landward of the QCF. Note, however, that our repeating earthquakes include those seaward of, albeit within ∼10 km of, the QCF and so suggest some creep behavior on the fault interface in a region that is modelled by Wang et al. [2015] to be nearly fully locked. We cannot rule out that this discrepancy is due to errors in the locations of the repeating earthquakes.

The northern subduction groups (2S and 3S) exhibit higher rates of pre-HGEQ slip than the southern subduction groups (4S, 5S, and 6S; Table 4). In fact, the slip rates of 2S and 3S (2.14 and 2.31 cm/yr, respectively) are slightly higher than the plate motion convergence rate (1.5 - 2.0 cm/yr), indicating that slip on the fault in the areas of 2S and 3S is keeping up with plate motion with very little accumulated stress. Furthermore, this observation is consistent with the reported northern extent of the HGEQ rupture zone that lies south of groups 2S and 3S (Figure 13b; Hyndman 2015; Nykolaishen et al. 2015). Because these areas did not accumulate significant stress prior to the HGEQ, they would not be expected to experience significant slip during the HGEQ.

In contrast, the pre-HGEQ slip rates of the southern subduction groups 4S, 5S, and 6S (Table 4) are lower than the rate of convergence from plate motions (∼1.5 - 2.0 cm/yr). As for QCF slip rates in these zones (Section 5.1.1), these values indicate loading of the subduction fault and stress accumulation. Note, however, that Mazzotti et al. [2003] report 0.3 - 0.7 cm/yr of shortening within the North American plate, so not all of the ∼1.5 - 2.0 cm/yr of plate motion convergence is necessarily translated into stress accumulation on the subduction thrust. Nonetheless, the location and extent of the rupture zone of the HGEQ (Figure 13b; Hyndman 2015; Nykolaishen et al. 2015) is generally consistent with our results because those zones exhibiting stress accumulation also experienced slip during the HGEQ. However, we note that the pre-HGEQ slip rate of 6S (1.35 cm/yr) is higher than that of 4S and 5S (0.97 and 0.51 cm/yr, respectively). Accordingly, one might expect that 5S accumulated the most stress in the interseismic period and should therefore slip more than 6S during the HGEQ, but this is not the case (Figure 13b). The reason for this inconsistency is not known at this time.

Lastly, there are no definitive subduction families in group 1S, which represents the

most northerly section of the study area. The lack of subduction earthquakes in 1S may be meaningful, because immediately south of this area the strike of the QCF changes and becomes more closely parallel to relative plate motion (Figures 1a and 13b). This change in strike of the QCPB results in less convergence between the Pacific and North American plates, and therefore subduction is likely not expressed in the same way as it is farther south, although underthrusting is nonetheless expected in this area [Hyndman, 2015]. This change in subduction behaviour is consistent with Tréhu et al. [2015], who report an abrupt change in mechanical properties of the QCPB at 53.2°N. Alternatively, earthquake detection thresholds might be higher in this region due to its greater distance from network stations to the south.

5.2 Postseismic Slip of the Queen Charlotte Plate Boundary

The HGEQ is the second largest earthquake ever recorded in Canada and offers an excellent opportunity to study the effects that large earthquakes have on their tectonic environments. This particular earthquake is of interest because it occurred within the subduction component of the very complex QCPB. Thus, it affords insight into the responses of both the strike-slip QCF and the subduction interface to a major subduction earthquake.

5.2.1 Postseismic Slip: the Queen Charlotte Fault

The observed post-HGEQ slip rate responses of the QCF (Figure 14) display variation from north to south across the study area. To the north, groups 1Q and 2Q (Figure 13a) exhibit no change to their slip patterns due to the HGEQ. Whether or not group 3Q falls into this classification as well is difficult to determine because of its large uncertainties. In contrast, the southern part of the study area (i.e., groups 4Q, 5Q, and 6Q) exhibits clear slip acceleration in response to the HGEQ. This effect is strongest in group 6Q, which falls within the zone of maximum rupture for the HGEQ, and decreases to the north for groups 5Q and 4Q. However, these slip accelerations are short-lived (1-2 months following the HGEQ), after which pre-HGEQ slip rates are re-established. At this time, we are unaware of the cause for additional

slip acceleration initiated at the beginning of 2015 for groups 5Q and 6Q (Figure 14e,f). One possible cause is the occurrence of a M_W 6.3 earthquake that occurred at 51.4°N, 131.1°W on April 24, 2015 [Earthquakes Canada, 2016], but whether this magnitude of earthquake could significantly alter the slip of the QCF this far north is unclear. In summary, our results indicate that north of ∼53.0°N the HGEQ did not significantly alter the QCF slip pattern, but that south of ∼53.0°N (to at least ∼52.3°N) the QCF experienced short-term accelerated slip due to the HGEQ and returned to pre-HGEQ slip rates after 1-2 months.

Our results are consistent with the findings from a number of other studies. Hobbs et al. [2015] investigate the Coulomb stress changes due to the HGEQ along the QCF, and report that the Coulomb stress change is strongly positive (i.e., promoting fault slip) in the regions of groups 4Q, 5Q, and 6Q, but is weakly negative (i.e., inhibiting fault slip) in the northern section of our study area. From a conceptual standpoint, Hobbs et al. [2015] explain that enhanced slip of the QCF near the HGEQ rupture zone occurs because movement of the hanging wall during the thrust event acts to locally unclamp the QCF and promote movement. Additionally, Nykolaishen et al. [2015] report that GPS motions near ∼52.5°N, 131.8°W (i.e., within group 6Q of the present study; Figure 13a) are consistent with induced, deep, aseismic slip along the QCF for up to 1 year following the HGEQ. Lastly, the aftershock sequence of the HGEQ has been studied by Farahbod and Kao [2015] and Kao et al. [2015]. Although the majority of aftershocks represent normal faulting, due mainly to extension of the downgoing plate updip of the rupture zone, there are also right-lateral strike-slip events observed. Between 52.5°N and 53°N these strike-slip events are located near the trace of the QCF and are interpreted to represent motion of QCF related to the HGEQ [Farahbod and Kao, 2015; Kao et al., 2015]. Our results from repeating earthquakes, in conjunction with the studies mentioned above, suggest that the QCF participated in the HGEQ sequence south of ∼53°N, but was unaffected to the north of this region. It is important to note that although some elastic strain along the QCF was released during the HGEQ, the QCF remains partially locked, and thus the risk of future large strike-slip earthquakes in the area (especially south of ∼53°N) remains high [e.g., Hobbs et al.,

2015; Kao et al., 2015].

5.2.2 Postseismic Slip: the Subduction Interface

The subduction interface, like the QCF, exhibits post-HGEQ slip rates that vary from north to south. North of ∼53°N, groups 2S and 3S show no observable change in slip rate due to the HGEQ (Figures 13b and 15b,c). Matsubara et al. [2005] make a similar observation for the 2003 Off-Tokachi subduction earthquake in Japan, where repeating earthquake slip rates away from the main rupture zone do not significantly change. However, south of ∼53°N, groups 4S, 5S, and 6S all exhibit accelerated slip immediately following the HGEQ, and these slip rates exceed the convergence rate between the Pacific and North American plates (Figure 15d,e,f). Importantly, this accelerated slip persists until the end of the study period (December, 2015), 3 years and 2 months after the HGEQ. Recall that the QCF also exhibits accelerated slip due to the HGEQ, but that this effect only lasted for 1-2 months. The accelerated subduction slip is strongest for groups 5S (post-HGEQ slip rate of 8.41 cm/yr) and 4S (5.81 cm/yr), and weaker for group 6S (2.65 cm/yr; Table 4).

This slip on the subduction thrust represents afterslip to the HGEQ. Note that, consistent with the afterslip model of Wang et al. [2012], afterslip is strongest in areas surrounding the main rupture zone of the HGEQ (i.e., groups 4S and 5S), and weaker within the zone of maximum slip (i.e., group 6S; Figure 13b). In fact, the locations of repeating earthquake families within group 6S all lie outside the zone of largest slip from the HGEQ (Figure 13b). Similar results are reported by Igarashi et al. [2003], who find that repeating earthquakes tend to be located near, but not within, zones of maximum rupture from large subduction earthquakes because these regions exhibit the highest degrees of aseismic slip.

Wang et al. [2012] model the duration of afterslip for M_W 8.0-8.4 subduction earthquakes, and demonstrate that afterslip may persist for 3-7 years. The HGEQ is a slightly smaller event (M_W 7.8) and thus afterslip would be expected to occur over a shorter time period. However, other factors, including convergence rate and plate geometry, also affect the

duration of afterslip [Wang et al., 2012]. Our results indicate that afterslip is present until at least the end of the study period (December, 2015), approximately 3 years and 2 months after the HGEQ. Slip histories for groups 4S and 6S indicate that the rate of afterslip may be decreasing, consistent with Matsubara et al. [2005] and Wang et al. [2012]; however, this trend is not observed for group 5S. Afterslip estimates made here are also generally consistent with GPS measurements of Nykolaishen et al. [2015], which indicate that the northern periphery of the rupture zone (i.e., groups 4S and 5S) exhibited postseismic thrust motion for the duration of their study period (October 28, 2012 - December 31, 2013). Note that afterslip has also been observed using repeating earthquakes in other subduction zones around the world (e.g., the northeastern Japan subduction zone by Igarashi et al. [2003] and Matsubara et al. [2005]).

Chapter 6

Conclusions

We have demonstrated the utility of repeating earthquakes to study the slip dynamics of the Queen Charlotte plate boundary (QCPB), which includes both the strike-slip Queen Charlotte Fault (QCF) and the subduction interface between the Pacific and North American plates. Repeating earthquake families are identified through a combination of cluster analysis and matched filtering, both based on waveform similarity. The repeating earthquake catalogue that we present here includes 224 families, with 730 individual earthquakes. The subduction interface is represented by 87 families (320 earthquakes) and the QCF by 76 families (240 earthquakes). There are also 61 families (170 earthquakes) whose polarities preclude assignment of a fault of origin. These ambiguous families are incorporated within our analysis to set maximum and minimum bounds on slip for both fault structures.

We extend the algorithm of Rubinstein and Ellsworth [2010] that employs Singular Value Decomposition (SVD) and absolute moment estimates, to determine accurate magnitude estimates for repeating earthquakes. This process exploits the inherent waveform similarity observed for repeating earthquakes to provide better magnitude estimates than conventional methods.

The repeating earthquake families are arranged into three sets: those consistent with an origin on the QCF, those consistent with an origin on the subduction thrust, and those with an

unclear origin. These sets are each further divided based on location into 6 adjacent groups along the QCPB. The average cumulative slip history for both the QCF and subduction interface is then determined for each of the 6 zones.

We find evidence of fault creep on both the QCF and the subduction interface throughout the study area. However, with the exception of the northernmost subduction interface, all creep rates are less than the relative plate motion rates between the Pacific and North American plates, indicating partial locking of both the QCF and subduction thrust. The QCF exhibits higher degrees of locking and stress-loading in the southern region of the study area ($\sim$52.3°N - 52.8°N) than in the north ($\sim$52.8°N - 53.8°N), which supports the notion that the seismic hazard along the QCF is highest in the south.

The 2012, M_W 7.8 Haida Gwaii earthquake (HGEQ) produced changes in slip behaviour along both the QCF and subduction interface. Near the main rupture, the QCF exhibits short-term (1-2 month) accelerated slip in a right-lateral strike-slip sense following the HGEQ. However, most of the QCF elastic-strain was not released during the HGEQ and the seismic risk in this region remains high. In contrast, the subduction thrust has undergone prolonged aseismic afterslip for at least 3 years following the HGEQ. This afterslip is greatest on the periphery of the main HGEQ rupture.

References

Abercrombie, R. (1996). The magnitude-frequency distribution of earthquakes recorded with deep seismometers at Cajon Pass, southern California. *Tectonophysics*, 261:1–7.

Aderhold, K. and Abercrombie, R. (2015). Seismic rupture on an oceanic-continental plate boundary: strike-slip earthquakes along the Queen Charlotte-Fairweather Fault. *Bulletin of the Seismological Society of America*, 105(2B):1129–1142.

Bakun, W. (1984). Seismic moments, local magnitudes, and coda-duration magnitudes for earthquakes in central California. *Bulletin of the Seismological Society of America*, 74(2):439–458.

Beeler, N., Lockner, D., and Hickman, S. (2001). A simple stick-slip and creep-slip model for repeating earthquakes and its implication for microearthquakes at Parkfield. *Bulletin of the Seismological Society of America*, 91(6):1797–1804.

Ben-Zion, Y. and Zhu, L. (2002). Potency-magnitude scaling relations for souther California earthquakes with $1.0 < m_L < 7.0$. *Geophysics Journal International*, 148:F1–F5.

Bérubé, J., Rogers, G., Ellis, R., and Hasselgren, F. (1989). A microseismicity survey of the Queen Charlotte Islands region. *Canadian Journal of Earth Science*, 26:2556–2566.

Bostwick, T. (1984). A re-examination of the August 22, 1949 Queen Charlotte earthquake. Master's thesis, University of British Columbia, Vancouver, Canada.

Bustin, A., Hyndman, R., Kao, H., and Cassidy, J. (2007). Evidence for underthrusting beneath the Queen Charlotte Margin, British Columbia, from teleseismic receiver function analysis. *Geophysics Journal International*, 171(3):1198–1211.

Cassidy, J., Rogers, G., and Hyndman, R. (2014). An overview of the 28 October 2012 M_w 7.7 earthquake in Haida Gwaii, Canada: a tsunamigenic thrust event along a predominantly strike-slip margin. *Pure and Applied Geophysics*, 171:3457–3465. doi: 10.1007/s00024-014-0775-1.

Chen, K., Nadeau, R., and Rau, R. (2007). Towards a universal rule on the recurrence interval scaling of repeating earthquakes? *Geophysical Research Letters*, 34. doi: 10.1029/2007GL030554.

Chen, K., Nadeau, R., and Rau, R. (2008). Characteristic repeating earthquakes in an arc-continent collision boundary zone: The Chihshang fault of eastern Taiwan. *Earth and Planetary Science Letters*, 276:262–272.

Chen, T. and Lapusta, N. (2009). Scaling of small repeating earthquakes explained by interaction of seismic and aseismic slip in a rate and state fault model. *Journal of Geophysical Research*, 114. doi: 10.1029/2008JB005749.

Dehler, S. and Clowes, R. (1988). The Queen Charlotte Islands refraction project. Part I. The Queen Charlotte Fault Zone. *Canadian Journal of Earth Science*, 25:1857–1870.

Earthquakes Canada (2016). Continuous waveform achive. *Natural Resources Canada - Geological Survey of Canada*, AutoDRM@seismo.NRCan.gc.ca.

Farahbod, A. and Kao, H. (2015). Spatiotemporal distribution of event during the first week of the 2012 Haida Gwaii aftershock sequence. *Bulletin of the Seismological Society of America*, 105(2B):1231–1240.

Fisher, R. (1921). On the probable error of a coefficient of correlation deduced from a small sample. *Metron*, 1:3–32.

Gibbons, S. and Ringdal, F. (2006). The detection of low magnitude seismic events using array-based waveform correlation. *Geophysics Journal International*, 165:149–166.

Gosselin, J., Cassidy, J., and Dosso, S. (2015). Shear-wave velocity structure in the vicinity of the 2012 M_w 7.8 Haida Gwaii earthquake from receiver function inversion. *Bulletin of the Seismological Society of America*, 105(2B):1106–1113.

Hanks, T. and Kanamori, H. (1979). A moment magnitude scale. *Journal of Geophysical Research*, 84(B5):2348–2350.

Hobbs, T., Cassidy, J., Dosso, S., and Brillon, C. (2015). Coulomb stress changes following the M_w 7.8 Haida Gwaii, Canada, earthquake: Implications for seismic hazard. *Bulletin of the Seismological Society of America*, 105(2B):1253–1264.

Holtkamp, S. and Ruppert, N. (2015). A high resolution aftershock catalog of the magnitude 7.5 Craig, Alaska, earthquake on 5 January 2013. *Bulletin of the Seismological Society of America*, 105(2B):1143–1152.

Hyndman, R. (2015). Tectonics and structure of the Queen Charlotte Fault Zone, Haida Gwaii, and large thrust earthquakes. *Bulletin of the Seismological Society of America*, 105(2B):1058–1075.

Hyndman, R. and Ellis, R. (1981). Queen Charlotte fault zone: microearthquakes from a temporary array of land stations and ocean bottom seismographs. *Canadian Journal of Earth Science*, 18:776–788.

Hyndman, R. and Hamilton, T. (1993). Queen Charlotte area Cenozoic tectonics and volcanism and their association with relative plate motions along the northeastern Pacific margin. *Journal of Geophysical Research*, 98(B8):14257–14277.

Hyndman, R., Lewis, T., J.A., W., Burgess, M., Chapman, D., and Yamano, M. (1982). Queen Charlotte fault zone: heat flow measurements. *Canadian Journal of Earth Science*, 19:1657–1669.

Igarashi, T., Matsuzawa, T., and Hasegawa, A. (2003). Repeating earthquakes and interplate aseismic slip in the northeastern Japan subduction zone. *Journal of Geophysical Research*, 108(B5):2249. doi: 10.1029/2002JB001920.

Kao, H., Shan, S., and Farahbod, A. (2015). Source characteristics of the 2012 Haida Gwaii earthquake sequence. *Bulletin of the Seismological Society of America*, 105(2B):1206–1218.

Kato, A., Fukuda, J., T., K., and S., N. (2016). Accelerated nucleation of the 2014 Iquique, Chile M_w earthquake. *Scientific Reports*, 6. doi: 10.1038/srep24792.

Lay, T., Ye, L., Kanamori, H., Yamazaki, Y., Cheung, K., Kwong, K., and Koper, K. (2013). The October 28, 2012 M_w7.8 Haida Gwaii underthrusting earthquake and tsunami: slip partioning along the Queen Charlotte Fault transpressional plate boundary. *Earth and Planetary Science Letters*, 375:57–70.

Mackie, D., Clowes, R., Dehler, S., Ellis, R., and Morel-À-l'Huissier, P. (1989). The Queen Charlotte Islands refraction project. Part II. Structural model for transition from Pacific plate to North American plate. *Canadian Journal of Earth Sciences*, 26(9):1713–1725.

Matsubara, M., Yagi, Y., and Obara, K. (2005). Plate boundary slip associated with the 2003 Off-Tokachi earthquake based on small repeating earthquake data. *Geophysical Research Letters*, 32. doi: 10.1029/2004GL022310.

Mazzotti, S., Hyndman, R., Fluck, P., Smith, A., and Schmidt, M. (2003). Distribution of the Pacific/North America motion in the Queen Charlotte Islands - S. Alaska plate boundary zone. *Geophysical Research Letters*, 30. doi: 10.1029/2003GL017586.

Nadeau, R., Foxall, W., and McEvilly, T. (1995). Clustering and periodic recurrence of microearthquakes on the San Andreas fault and Parkfield, California. *Science*, 267:503–507.

Nadeau, R. and Johnson, L. (1998). Seismological studies at Parkfield VI: moment release rates and estimates of course parameters for small repeating earthquakes. *Bulletin of the Seismological Society of America*, 88(3):790–814.

Nishenko, S. and Jacob, K. (1990). Seismic potential of the Queen Charlotte-Alaska-Aleutian seismic zone. *Journal of Geophysical Research*, 95(B3):2511–2532.

Nykolaishen, L., Dragert, H., Wang, K., James, T., and Schmidt, M. (2015). Gps observations of crustal deformation associated with the 2012 M_w 7.8 Haida Gwaii earthquake. *Bulletin of the Seismological Society of America*, 105(2B):1241–1252.

Plafker, G., Hudson, T., and Bruns, T. (1978). Late Quaternary offsets along the Fairweather fault and crustal plate interactions in southern Alaska. *Canadian Journal of Earth Science*, 15:805–816.

Rogers, G. (1986). Seismic gaps along the Queen Charlotte Fault. *Earthquake Prediction Research*, 4:1–11.

Rohr, K., Scheidhauer, M., and Tréhu, A. (2000). Transpression between two warm mafic plates: the Queen Charlotte Fault revisited. *Journal of Geophysical Research*, 105(B4):8147–8172.

Romesburg, H. (2004). *Cluster Analysis for Researchers*. Lulu Press, North Carolina, USA.

Rubinstein, J. and Ellsworth, W. (2010). Precise estimation of repeating earthquake moment: example from Parkfield, California. *Bulletin of the Seismological Society of America*, 100(5A):1952–1961.

Schmittbuhl, J., Karabulut, H., O., L., and Bouchon, M. (2016). Long-lasting seismic repeaters in the Central Basin of the Main Marmara Fault. *Geophysical Research Letters*, 43(18):9527–9534.

Shearer, P. (2009). *Introduction to Seismology, 2nd Edition*. Cambridge University Press, New York, USA.

Shearer, P., Prieto, G., and Hauksson, E. (2006). Comprehensive analysis of earthquake source spectra in southern California. *Journal of Geophysical Research*, 111. doi: 10.1029/2005JB003979.

Smith, A., R.D., H., Cassidy, J., and Wang, K. (2003). Stucture, seismicity, and thermal regime of the Queen Charlotte Transform Margin. *Journal of Geophysical Research*, 108(B11):2156–2202.

Tréhu, A., Scheidhauer, M., Rohr, K., Tikoff, B., Walton, M., Gulick, S., and Roland, E. (2015). An abrupt transition in the mechanical response of the upper crust to transpression along the Queen Charlotte Fault. *Bulletin of the Seismological Society of America*, 105(2B):1114–1128.

Uchida, N., Iinuma, T., Nadeau, R., Bürgmann, R., and Hino, R. (2016). Periodic slow slip triggers megathrust zone earthquakes in northeastern Japan. *Science*, 351(6272):488–492.

Uchida, N. and Matsuzawa, T. (2013). Pre- and postseismic slow slip surrounding the 2011 Tohoku-oki earthquake rupture. *Earth and Planetary Science Letters*, 374:81–91.

Van Huffel, S. and Vandewalle, J. (1991). *The total least squares problem: computational aspects and analysis*. Society for Industrial and Applied Mathematics, Philadelphia, USA.

Wang, K., He, J., Schulzeck, F., Hyndman, R., and Riedel, M. (2015). Thermal condition of the 27 October 2012 M_w 7.8 Haida Gwaii subduction earthquake at the obliquely convergent Queen Charlotte Margin. *Bulletin of the Seismological Society of America*, 105(2B):1290–1300.

Wang, K., Hu, Y., and He, J. (2012). Deformation cycles of the subduction earthquakes in a viscoelastic Earth. *Nature*, 484:327–332.

Yorath, C. and Hyndman, R. (1983). Subsidence and thermal history of Queen Charlotte Basin. *Canadian Journal of Earth Science*, 20:135–159.

Appendix A

Definition of all Repeating Earthquake Families

In Chapter 2 we explain how the repeating earthquake catalogue is created, and how individual earthquakes are clustered into families. The repeating earthquakes within a given family represent slip of the same fault patch, and are identified on the basis high waveform similarity. Table 5 provides a definition for each of the 224 families identified in this study.

Table 5: Details of the repeating earthquake families used in the present study. Family IDs are arbitrarily assigned, but consistent throughout the study. Times are given as seconds into the day (i.e., seconds after midnight). Reported magnitudes are those after the SVD analysis (see Section 3.1.2). Events with detection method noted as "GSC" originated from the GSC earthquakes list, whereas those noted as "MF" were identified with the matched filter processing (see Section 2.3). Events from the matched filter processing do not have reported latitudes, longitudes, or depths, and only a small selection of GSC events have reported depths.

Family ID	Date (YY/MM/DD)	Time (seconds)	Magnitude (M_w)	Slip (cm)	Latitude (dec. deg.)	Longitude (dec. deg.)	Depth (km)	Detection Method
001	05/02/21	33489.000	2.512	10.41	53.705	-133.422	-	GSC
	12/09/11	44831.000	2.456	10.08	53.768	-133.321	-	GSC

Table 5: (continued)

Family ID	Date (YY/MM/DD)	Time (seconds)	Magnitude (M_w)	Slip (cm)	Latitude (dec. deg.)	Longitude (dec. deg.)	Depth (km)	Detection Method
002	05/05/24	49059.000	1.740	6.62	52.570	-132.044	-	GSC
	05/05/24	49990.000	1.695	6.45	52.571	-131.969	-	GSC
	05/06/13	77741.550	1.107	4.56	-	-	-	MF
003	05/06/04	19565.000	1.483	5.69	52.426	-131.806	-	GSC
	05/06/04	20172.000	1.678	6.38	52.426	-131.810	-	GSC
004	05/06/07	58977.000	1.831	6.98	52.603	-131.972	-	GSC
	05/06/09	34844.000	2.311	9.26	52.589	-132.041	-	GSC
005	05/06/19	17467.000	1.591	6.06	53.276	-133.171	-	GSC
	05/06/19	19124.000	1.566	5.97	53.272	-133.176	-	GSC
	15/08/06	5687.000	2.444	10.01	53.307	-133.075	27.6	GSC
	15/08/06	7143.150	1.403	5.43	-	-	-	MF
006	05/06/19	52179.000	1.666	6.34	53.288	-133.137	-	GSC
	05/06/19	57809.000	1.572	5.99	53.288	-133.138	-	GSC
	15/11/08	70518.650	2.066	8.01	-	-	-	MF
	15/11/08	71272.850	1.645	6.26	-	-	-	MF
007	05/06/19	59638.000	1.559	5.95	53.288	-133.136	-	GSC
	05/06/19	70764.000	2.236	8.85	53.288	-133.142	-	GSC
008	05/06/19	24362.000	1.522	5.82	53.269	-133.173	-	GSC
	05/06/19	62948.000	1.498	5.74	53.275	-133.168	-	GSC
009	05/07/13	22392.000	1.685	6.41	52.535	-131.871	-	GSC
	05/07/13	22965.000	1.695	6.45	52.537	-131.873	-	GSC
010	05/05/09	42773.000	1.402	5.43	53.224	-132.810	-	GSC
	05/07/13	79083.000	2.166	8.5	53.269	-132.731	-	GSC

Table 5: (continued)

Family ID	Date (YY/MM/DD)	Time (seconds)	Magnitude (M_w)	Slip (cm)	Latitude (dec. deg.)	Longitude (dec. deg.)	Depth (km)	Detection Method
011	05/07/18	19061.000	1.577	6.02	53.496	-133.170	-	GSC
	05/07/18	21424.000	1.579	6.02	53.497	-133.166	-	GSC
012	05/08/31	27136.000	2.399	9.74	53.842	-133.448	-	GSC
	08/05/23	24048.000	2.364	9.55	53.827	-133.399	-	GSC
	14/02/23	37344.000	2.436	9.96	53.806	-133.415	14.7	GSC
013	05/09/13	22775.000	1.733	6.59	52.519	-131.907	-	GSC
	05/09/13	26703.000	1.703	6.48	52.517	-131.923	-	GSC
014	05/11/07	26402.000	1.622	6.18	53.264	-133.135	-	GSC
	15/08/10	3752.000	1.861	7.1	53.235	-133.190	10.1	GSC
015	05/11/22	83229.000	2.444	10.01	52.880	-132.418	-	GSC
	11/04/26	74573.000	1.958	2	52.868	-132.442	-	GSC
016	05/12/15	67295.000	1.373	5.33	53.095	-132.788	-	GSC
	11/07/19	3861.000	1.368	5.32	53.096	-132.759	-	GSC
	11/07/19	4016.875	0.330	2.89	-	-	-	MF
017	05/12/16	15753.000	1.829	6.97	53.268	-132.740	-	GSC
	05/12/16	16274.000	1.551	5.92	53.276	-132.713	-	GSC
018	05/12/27	63683.000	1.981	7.62	52.629	-132.130	-	GSC
	09/12/15	83606.000	1.704	6.48	52.640	-132.139	-	GSC
019	06/01/03	46357.000	1.603	6.11	52.631	-132.319	-	GSC
	11/05/14	22033.000	1.213	4.86	52.663	-132.263	-	GSC
020	06/01/04	67679.000	1.915	7.33	52.620	-132.200	-	GSC
	10/09/02	28750.000	1.935	7.42	52.625	-132.219	-	GSC

Table 5: (continued)

Family ID	Date (YY/MM/DD)	Time (seconds)	Magnitude (M$_w$)	Slip (cm)	Latitude (dec. deg.)	Longitude (dec. deg.)	Depth (km)	Detection Method
021	06/01/17	4119.000	2.028	7.84	53.068	-132.682	-	GSC
	08/07/13	24070.750	1.388	5.38	-	-	-	MF
	13/07/20	78373.950	1.043	4.4	-	-	-	MF
	15/02/21	16249.000	1.125	2.34	53.084	-132.658	23.5	GSC
022	06/01/26	56308.000	1.661	6.32	53.229	-133.095	-	GSC
	06/01/26	83409.000	2.029	7.84	53.212	-133.115	-	GSC
023	06/01/29	66298.000	1.434	5.53	53.236	-132.764	-	GSC
	06/02/15	46384.000	1.232	4.91	53.225	-132.772	-	GSC
024	05/08/01	13529.525	0.718	3.63	-	-	-	MF
	05/08/07	14801.000	1.406	5.44	53.076	-132.643	-	GSC
	06/03/13	413.000	1.399	5.42	53.070	-132.671	-	GSC
	13/07/20	78245.850	1.172	4.74	-	-	-	MF
025	06/03/29	57036.000	1.988	7.65	52.613	-132.154	-	GSC
	10/01/29	51543.000	2.040	7.89	52.625	-132.109	-	GSC
026	06/04/01	55540.000	1.347	5.26	53.255	-133.155	-	GSC
	06/04/02	32335.000	1.466	5.63	53.231	-133.217	-	GSC
	15/09/25	63610.250	1.236	4.92	-	-	-	MF
027	06/05/11	66846.000	1.771	6.74	52.982	-132.595	-	GSC
	06/05/11	69930.000	1.610	6.13	52.978	-132.597	-	GSC
	06/05/11	70071.000	1.840	7.02	52.979	-132.592	-	GSC
028	06/05/11	71118.525	0.988	4.26	-	-	-	MF
	06/05/11	72474.000	1.767	6.72	52.977	-132.594	-	GSC
	06/05/12	5728.000	1.729	6.57	52.979	-132.593	-	GSC
	06/05/12	8904.300	0.928	4.11	-	-	-	MF

Table 5: (continued)

Family ID	Date (YY/MM/DD)	Time (seconds)	Magnitude (M_w)	Slip (cm)	Latitude (dec. deg.)	Longitude (dec. deg.)	Depth (km)	Detection Method
029	06/05/10	45051.000	1.528	5.84	52.672	-132.378	-	GSC
	06/05/12	38244.000	1.619	6.16	52.681	-132.357	-	GSC
030	06/06/03	57696.000	2.382	9.65	53.188	-132.873	-	GSC
	13/07/02	73224.600	1.972	7.58	-	-	-	MF
	15/08/12	86233.000	2.129	8.32	53.178	-132.951	4.9	GSC
031	06/08/21	67004.000	1.551	5.92	52.921	-132.542	-	GSC
	06/08/21	67209.000	1.281	5.06	52.904	-132.542	-	GSC
	10/10/20	63790.000	1.434	5.53	52.932	-132.534	-	GSC
032	06/09/20	22644.000	1.969	7.57	53.278	-132.817	-	GSC
	06/09/20	24230.000	1.946	7.47	53.276	-132.821	-	GSC
	07/02/24	19573.550	0.842	3.91	-	-	-	MF
033	06/09/26	34078.000	1.540	5.88	52.510	-131.927	-	GSC
	06/09/26	41210.000	1.475	5.66	52.511	-131.917	-	GSC
034	06/10/08	73108.450	0.871	3.97	-	-	-	MF
	06/10/09	3878.000	1.766	6.72	53.275	-132.811	-	GSC
	06/10/10	31052.000	1.460	5.62	53.280	-132.813	-	GSC
	07/05/08	85939.000	1.747	6.65	53.278	-132.810	-	GSC
	07/05/09	3607.525	1.059	4.44	-	-	-	MF
	07/05/09	19777.975	0.816	3.85	-	-	-	MF
035	06/11/02	45038.000	2.334	9.38	53.511	-133.209	-	GSC
	06/11/03	4864.000	1.821	6.94	53.478	-133.322	-	GSC
036	06/10/08	73826.000	2.182	8.58	53.213	-132.993	-	GSC
	06/11/03	85387.000	1.786	6.8	53.208	-132.973	-	GSC

Table 5: (continued)

Family ID	Date (YY/MM/DD)	Time (seconds)	Magnitude (M$_w$)	Slip (cm)	Latitude (dec. deg.)	Longitude (dec. deg.)	Depth (km)	Detection Method
037	05/08/14	50529.000	1.765	6.72	53.284	-132.807	-	GSC
	05/08/27	75644.575	0.999	4.28	-	-	-	MF
	06/11/08	19678.000	1.385	5.37	53.255	-132.770	-	GSC
	07/03/05	30784.450	1.249	4.96	-	-	-	MF
038	07/01/23	389.000	1.629	6.2	52.557	-131.845	-	GSC
	07/01/23	13061.000	1.438	5.54	52.556	-131.840	-	GSC
039	07/01/23	20503.000	2.282	9.1	53.501	-133.351	-	GSC
	07/01/23	22133.000	2.141	8.38	53.505	-133.358	-	GSC
040	07/02/14	9702.000	2.069	8.03	52.763	-132.288	-	GSC
	07/02/14	11263.000	1.606	6.12	52.765	-132.294	-	GSC
041	07/03/31	42445.000	1.433	5.53	53.278	-132.764	-	GSC
	07/06/28	74874.000	1.579	6.02	53.265	-132.803	-	GSC
042	07/04/03	76763.000	1.589	6.06	53.190	-132.886	-	GSC
	07/04/03	77816.000	1.674	6.36	53.200	-132.876	-	GSC
	07/04/04	1301.750	1.003	4.29	-	-	-	MF
	07/04/04	4376.000	1.483	5.69	53.196	-132.902	-	GSC
043	07/04/01	82444.000	2.379	9.63	53.512	-133.192	-	GSC
	07/04/12	55566.000	1.712	6.51	53.526	-133.166	-	GSC
044	05/04/30	84401.550	1.915	7.33	-	-	-	MF
	07/04/13	70167.000	1.853	7.07	52.614	-132.195	-	GSC
	09/12/21	52220.000	1.602	6.1	52.619	-132.175	-	GSC
045	07/04/30	38616.000	2.143	8.38	52.781	-132.364	-	GSC
	07/04/30	39401.000	2.126	8.3	52.804	-132.366	-	GSC

Table 5: (continued)

Family ID	Date (YY/MM/DD)	Time (seconds)	Magnitude (M_w)	Slip (cm)	Latitude (dec. deg.)	Longitude (dec. deg.)	Depth (km)	Detection Method
046	07/05/21	2307.700	1.366	5.31	-	-	-	MF
	07/05/21	23855.000	1.838	7.01	52.996	-132.764	-	GSC
	07/05/21	24097.000	1.710	6.5	52.981	-132.822	-	GSC
047	07/06/14	8133.000	1.831	6.98	53.332	-133.165	-	GSC
	07/06/14	12019.000	1.962	7.54	53.326	-133.181	-	GSC
	15/04/02	40944.350	2.042	7.9	-	-	-	MF
048	07/06/15	16275.000	1.820	6.94	52.809	-132.323	-	GSC
	07/08/01	72479.000	0.806	3.82	52.811	-132.309	-	GSC
049	07/06/27	32518.000	1.953	7.5	52.682	-132.017	-	GSC
	07/12/04	11290.000	1.833	6.99	52.657	-132.064	-	GSC
	12/10/24	6848.175	1.756	6.68	-	-	-	MF
050	07/07/03	6462.000	1.635	6.22	53.208	-132.686	-	GSC
	07/07/03	22257.000	1.739	6.61	53.195	-132.706	-	GSC
	07/07/03	54475.975	1.699	6.46	-	-	-	MF
	07/07/03	81962.550	1.154	4.69	-	-	-	MF
051	07/07/03	12735.000	2.238	8.87	53.189	-132.722	-	GSC
	07/07/03	12826.000	1.458	5.61	53.207	-132.708	-	GSC
	07/07/03	13301.000	1.429	5.51	53.209	-132.676	-	GSC
	07/07/03	41951.725	1.346	5.25	-	-	-	MF

Table 5: (continued)

Family ID	Date (YY/MM/DD)	Time (seconds)	Magnitude (M_w)	Slip (cm)	Latitude (dec. deg.)	Longitude (dec. deg.)	Depth (km)	Detection Method
052	07/07/13	60027.075	0.775	3.76	-	-	-	MF
	07/07/13	68073.850	0.932	4.12	-	-	-	MF
	07/07/13	71479.000	1.028	4.36	53.215	-132.641	-	GSC
	07/07/14	2447.775	0.802	3.82	-	-	-	MF
	07/07/14	13916.000	1.488	5.71	53.208	-132.691	-	GSC
	07/07/15	27368.100	0.323	2.88	-	-	-	MF
053	07/07/21	24643.000	1.456	5.6	53.240	-132.721	-	GSC
	07/07/21	26172.000	1.414	5.47	53.229	-132.765	-	GSC
	07/07/21	26458.000	0.592	3.37	-	-	-	MF
	11/08/03	66792.325	0.780	3.77	-	-	-	MF
054	07/07/26	44113.000	1.614	6.15	53.275	-132.745	-	GSC
	07/07/26	79981.700	1.364	5.31	-	-	-	MF
	14/09/23	85395.000	2.375	9.61	53.273	-132.748	19.9	GSC
055	07/07/31	31990.000	1.754	6.67	52.600	-131.961	-	GSC
	07/07/31	46190.000	1.112	4.58	52.609	-131.918	-	GSC
056	07/08/28	3057.000	1.804	6.87	53.310	-133.064	-	GSC
	07/08/28	84168.000	2.031	7.85	53.308	-133.069	-	GSC
057	07/09/09	32695.000	2.048	7.93	53.506	-133.245	-	GSC
	07/09/09	55924.000	1.510	5.78	53.520	-133.207	-	GSC
058	07/01/25	27047.000	2.107	8.21	52.907	-132.416	-	GSC
	07/09/12	36824.000	1.614	6.15	52.904	-132.520	-	GSC
	07/09/12	40335.775	1.321	5.18	-	-	-	MF
059	07/10/03	79203.000	1.977	7.6	53.188	-132.814	-	GSC
	07/10/03	84601.000	2.100	8.17	53.186	-132.811	-	GSC

Table 5: (continued)

Family ID	Date (YY/MM/DD)	Time (seconds)	Magnitude (M_w)	Slip (cm)	Latitude (dec. deg.)	Longitude (dec. deg.)	Depth (km)	Detection Method
060	07/10/12	46652.000	2.036	7.87	52.877	-132.511	-	GSC
	07/10/12	49593.000	1.798	6.85	52.877	-132.497	-	GSC
061	07/03/16	76059.000	2.008	7.74	53.448	-132.485	-	GSC
	07/06/26	75615.450	2.010	7.75	-	-	-	MF
	07/11/21	11859.000	2.213	8.74	53.347	-132.911	-	GSC
062	07/11/23	49075.000	1.933	7.41	52.610	-132.024	-	GSC
	07/12/02	72645.000	2.025	7.82	52.658	-131.978	-	GSC
063	07/11/20	3011.000	1.452	5.59	52.907	-132.558	-	GSC
	07/11/29	84765.775	1.519	5.81	-	-	-	MF
	07/11/29	85293.000	2.041	7.9	52.907	-132.557	-	GSC
	07/12/24	83691.450	2.042	7.9	-	-	-	MF
064	08/01/23	66075.000	1.858	7.09	52.895	-132.534	-	GSC
	08/02/06	22917.000	2.162	8.48	52.910	-132.483	-	GSC
065	08/02/07	25474.000	2.126	8.3	52.892	-132.524	-	GSC
	08/02/07	26150.000	1.874	7.16	52.891	-132.541	-	GSC
066	08/03/22	33482.000	2.756	12.02	53.269	-133.102	-	GSC
	08/03/22	33571.000	2.844	12.66	53.286	-133.061	-	GSC
067	08/03/22	78527.000	2.545	10.61	53.276	-133.095	-	GSC
	08/03/23	23121.000	2.077	8.07	53.300	-133.056	-	GSC
068	08/03/22	78407.000	2.642	11.24	53.282	-133.074	-	GSC
	08/03/22	85185.250	1.958	7.52	-	-	-	MF
	08/03/23	10399.000	2.481	10.22	53.327	-132.943	-	GSC

Table 5: (continued)

Family ID	Date (YY/MM/DD)	Time (seconds)	Magnitude (M_w)	Slip (cm)	Latitude (dec. deg.)	Longitude (dec. deg.)	Depth (km)	Detection Method
069	08/05/25	31228.000	1.813	6.91	52.748	-132.346	-	GSC
	12/12/23	16072.550	1.668	6.34	-	-	-	MF
	14/03/26	25087.575	1.754	6.67	-	-	-	MF
	14/07/16	36462.750	1.801	6.86	-	-	-	MF
	14/07/21	30693.975	1.943	7.46	-	-	-	MF
	15/03/07	67589.000	1.692	6.43	52.754	-132.296	17.0	GSC
	15/05/02	72061.000	2.133	8.34	52.752	-132.297	21.5	GSC
070	08/06/08	40003.000	2.315	9.28	52.841	-132.454	-	GSC
	08/06/08	78082.000	2.041	7.9	52.839	-132.465	-	GSC
071	08/06/08	50009.775	1.333	5.21	-	-	-	MF
	08/06/09	21321.000	1.511	5.79	52.842	-132.445	-	GSC
	08/06/09	24221.000	2.375	9.61	52.833	-132.454	13.0	GSC
072	08/06/17	1104.000	1.919	7.35	52.584	-132.015	-	GSC
	08/06/17	1333.000	1.813	6.91	52.577	-132.065	-	GSC
	08/06/17	44056.000	2.233	8.84	52.575	-132.048	-	GSC
	08/06/17	57264.450	1.919	7.35	-	-	-	MF
	08/06/17	57493.150	1.813	6.91	-	-	-	MF
073	08/08/10	4216.000	1.840	7.02	53.526	-133.092	-	GSC
	08/08/10	4646.000	1.702	6.47	53.521	-133.108	-	GSC
074	08/08/09	35194.000	2.167	8.5	53.241	-133.070	-	GSC
	08/08/10	24340.000	1.680	6.39	53.259	-133.015	-	GSC
075	06/04/29	56404.000	1.925	7.38	52.686	-132.277	-	GSC
	08/10/03	60290.000	2.002	7.72	52.689	-132.288	-	GSC
	12/01/12	83021.375	1.882	7.19	-	-	-	MF

Table 5: (continued)

Family ID	Date (YY/MM/DD)	Time (seconds)	Magnitude (M_w)	Slip (cm)	Latitude (dec. deg.)	Longitude (dec. deg.)	Depth (km)	Detection Method
076	08/06/07	59154.000	1.964	7.55	53.509	-133.180	-	GSC
	08/11/05	38913.000	2.026	7.83	53.508	-133.190	-	GSC
	15/10/06	33374.000	1.850	7.06	53.529	-133.178	14.3	GSC
077	08/12/08	1985.000	1.854	7.08	52.674	-132.062	-	GSC
	08/12/08	9067.000	1.975	7.6	52.664	-132.075	-	GSC
078	08/12/08	76707.000	2.185	8.6	53.205	-133.016	-	GSC
	08/12/09	1184.000	1.624	6.18	53.214	-132.983	-	GSC
	08/12/09	76364.000	1.624	6.18	-	-	-	MF
	08/12/09	78338.000	1.624	6.18	-	-	-	MF
079	08/12/05	71382.050	1.673	6.36	-	-	-	MF
	08/12/10	32837.000	2.398	9.74	52.907	-132.536	-	GSC
	08/12/10	34487.000	2.102	8.19	52.906	-132.561	-	GSC
080	07/09/09	32923.000	1.457	5.61	53.498	-133.271	-	GSC
	07/09/09	34017.000	1.562	5.96	53.505	-133.263	-	GSC
	08/12/19	48991.000	2.251	8.93	53.505	-133.234	-	GSC
081	06/02/09	62221.000	1.645	6.26	52.609	-132.116	-	GSC
	09/01/23	6258.000	1.844	7.04	52.618	-132.128	-	GSC
082	07/04/04	6847.000	1.934	7.41	52.721	-132.272	-	GSC
	09/01/31	25687.000	2.302	9.21	52.714	-132.278	-	GSC
	09/01/31	59707.000	2.302	9.21	-	-	-	MF
083	09/02/19	34291.000	2.653	11.31	52.500	-131.910	-	GSC
	09/02/19	39480.000	2.172	8.53	52.492	-131.895	-	GSC
084	06/07/05	42259.000	1.680	6.39	52.686	-132.000	-	GSC
	09/02/23	65293.000	1.764	6.71	52.608	-132.135	-	GSC

Table 5: (continued)

Family ID	Date (YY/MM/DD)	Time (seconds)	Magnitude (M_w)	Slip (cm)	Latitude (dec. deg.)	Longitude (dec. deg.)	Depth (km)	Detection Method
085	09/03/02	6919.000	1.900	7.27	52.904	-132.554	-	GSC
	09/03/02	7282.900	1.320	5.17	-	-	-	MF
	09/03/02	9880.000	2.237	8.86	52.902	-132.548	-	GSC
086	09/05/04	8609.000	1.948	7.48	52.905	-132.543	-	GSC
	09/05/04	10613.000	1.786	6.8	52.910	-132.558	-	GSC
	10/07/16	77187.000	1.967	7.56	52.899	-132.531	-	GSC
087	09/04/27	31617.000	1.893	7.24	52.884	-132.400	-	GSC
	09/05/02	14346.000	1.902	7.28	52.885	-132.407	-	GSC
	09/05/12	62395.000	2.006	7.74	52.883	-132.406	-	GSC
	09/06/25	75719.775	1.649	6.27	-	-	-	MF
088	09/06/05	1112.000	2.173	8.53	53.241	-132.893	-	GSC
	09/06/05	2301.625	1.054	4.42	-	-	-	MF
	09/06/05	2984.800	1.148	4.67	-	-	-	MF
	09/06/05	3108.000	1.563	5.96	53.278	-132.823	-	GSC
	09/06/05	33198.050	1.084	4.5	-	-	-	MF
	09/06/05	34000.700	1.153	4.69	-	-	-	MF
	09/06/05	40213.000	1.546	5.91	53.262	-132.876	-	GSC
	09/06/05	60212.775	2.173	8.53	-	-	-	MF
	09/06/05	61401.625	1.054	4.42	-	-	-	MF
	09/06/05	62084.800	1.148	4.67	-	-	-	MF
	09/06/05	62208.000	1.563	5.96	-	-	-	MF
	09/06/07	67768.375	1.285	5.07	-	-	-	MF
	09/06/10	8441.900	0.892	4.02	-	-	-	MF

Table 5: (continued)

Family ID	Date (YY/MM/DD)	Time (seconds)	Magnitude (M_w)	Slip (cm)	Latitude (dec. deg.)	Longitude (dec. deg.)	Depth (km)	Detection Method
089	09/06/05	1545.100	1.623	6.18	-	-	-	MF
	09/06/05	1685.050	1.752	6.66	-	-	-	MF
	09/06/05	1963.000	2.023	7.81	53.240	-132.869	-	GSC
	09/06/05	3668.800	1.512	5.79	-	-	-	MF
	09/06/05	29664.000	1.839	7.01	53.268	-132.844	-	GSC
	09/06/05	60645.100	1.623	6.18	-	-	-	MF
	09/06/05	60785.050	1.752	6.66	-	-	-	MF
	09/06/05	61063.100	2.023	7.81	-	-	-	MF
	09/06/05	62768.800	1.512	5.79	-	-	-	MF
090	09/06/05	32781.000	1.648	6.27	53.264	-132.856	-	GSC
	09/06/05	32990.000	1.958	7.52	53.273	-132.846	-	GSC
	09/06/05	35207.000	1.709	6.5	53.262	-132.865	-	GSC
	09/06/05	50350.825	1.346	5.25	-	-	-	MF
	09/06/05	55881.000	1.950	7.49	53.279	-132.832	-	GSC
	09/07/02	38491.975	1.281	5.05	-	-	-	MF
091	09/06/05	47374.000	1.809	6.89	53.280	-132.819	-	GSC
	09/06/05	47784.000	1.326	5.19	53.263	-132.864	-	GSC
	09/06/05	53158.000	1.753	6.67	53.221	-132.843	-	GSC
092	09/06/12	33929.000	1.769	6.73	52.452	-131.849	-	GSC
	09/06/12	34120.000	2.096	8.16	52.437	-131.874	-	GSC
	09/06/12	34762.000	1.821	6.94	52.458	-131.835	-	GSC
	09/06/12	35769.000	2.373	9.6	52.459	-131.818	-	GSC

Table 5: (continued)

Family ID	Date (YY/MM/DD)	Time (seconds)	Magnitude (M_w)	Slip (cm)	Latitude (dec. deg.)	Longitude (dec. deg.)	Depth (km)	Detection Method
093	09/08/13	44465.000	1.249	4.96	52.898	-132.548	-	GSC
	09/08/13	60729.000	2.307	9.23	52.892	-132.571	-	GSC
	09/08/13	61188.000	1.724	6.56	52.896	-132.557	-	GSC
094	09/08/13	60902.000	1.584	6.04	52.900	-132.544	-	GSC
	09/08/13	64371.000	1.574	6	52.907	-132.535	-	GSC
095	09/08/11	60241.000	1.357	5.28	53.158	-132.523	-	GSC
	09/08/11	67960.550	0.574	3.34	-	-	-	MF
	09/08/14	47621.075	0.869	3.97	-	-	-	MF
	09/08/15	54617.000	1.715	6.52	53.132	-132.598	-	GSC
	09/08/15	74186.000	1.355	5.28	53.122	-132.631	-	GSC
	09/08/16	44799.350	0.482	3.16	-	-	-	MF
	09/08/19	62491.000	1.390	5.39	53.163	-132.643	-	GSC
096	09/02/05	52777.000	2.165	8.49	52.861	-132.419	-	GSC
	09/09/02	11035.000	2.045	7.91	52.847	-132.389	-	GSC
	09/09/02	39239.425	1.627	6.19	-	-	-	MF
097	09/10/08	30262.000	2.179	8.56	53.300	-133.085	-	GSC
	09/10/08	34186.000	1.455	5.6	53.298	-133.084	-	GSC
098	09/10/09	68423.000	2.017	7.79	52.709	-132.265	-	GSC
	09/10/09	72093.000	1.801	6.86	52.706	-132.282	-	GSC

Table 5: (continued)

Family ID	Date (YY/MM/DD)	Time (seconds)	Magnitude (M$_w$)	Slip (cm)	Latitude (dec. deg.)	Longitude (dec. deg.)	Depth (km)	Detection Method
099	09/10/27	14905.000	1.970	7.57	53.008	-132.657	-	GSC
	09/10/30	1873.000	2.106	8.2	52.996	-132.667	-	GSC
	09/11/02	62097.000	1.450	5.58	53.005	-132.676	-	GSC
	13/07/25	8826.600	1.153	4.69	-	-	-	MF
	15/03/01	31491.250	1.374	5.34	-	-	-	MF
	15/03/02	43975.850	1.390	5.39	-	-	-	MF
100	09/11/01	50063.375	1.822	6.94	-	-	-	MF
	09/11/01	50186.000	2.132	8.33	53.302	-133.211	-	GSC
	09/11/01	50705.100	1.658	6.31	-	-	-	MF
	09/11/01	53558.000	1.909	7.31	53.297	-133.260	-	GSC
	09/11/01	55626.050	1.849	7.05	-	-	-	MF
101	05/11/04	13185.000	1.594	6.07	53.008	-132.648	-	GSC
	09/12/06	59539.000	2.033	7.86	53.008	-132.635	-	GSC
	14/03/30	30288.025	1.952	7.49	-	-	-	MF
	14/05/29	34695.100	1.290	5.08	-	-	-	MF
102	09/12/13	14554.000	1.433	5.53	52.877	-132.506	-	GSC
	09/12/13	27477.000	1.800	6.85	52.869	-132.514	-	GSC
	09/12/13	33198.725	1.320	5.17	-	-	-	MF
	09/12/21	35560.750	1.653	6.29	-	-	-	MF
103	09/12/13	12583.000	1.288	5.08	52.544	-131.972	-	GSC
	09/12/13	14890.000	1.382	5.36	52.541	-131.995	-	GSC
	09/12/13	17161.000	1.609	6.13	52.544	-131.987	-	GSC

Table 5: (continued)

Family ID	Date (YY/MM/DD)	Time (seconds)	Magnitude (M_w)	Slip (cm)	Latitude (dec. deg.)	Longitude (dec. deg.)	Depth (km)	Detection Method
104	09/12/17	16940.000	2.172	8.53	52.707	-132.431	-	GSC
	09/12/17	28933.000	2.013	7.77	52.710	-132.448	-	GSC
	09/12/17	63374.150	2.172	8.53	-	-	-	MF
	09/12/17	75367.000	2.013	7.77	-	-	-	MF
105	09/12/28	48377.000	1.881	7.19	53.113	-132.840	-	GSC
	09/12/28	49340.000	1.963	7.54	53.108	-132.830	-	GSC
106	05/06/26	27367.000	1.611	6.14	52.620	-132.119	-	GSC
	10/01/15	66627.000	1.948	7.48	52.611	-132.149	-	GSC
107	08/04/03	10778.000	1.905	7.29	53.528	-133.123	-	GSC
	10/02/09	76406.000	1.785	6.79	53.561	-132.991	-	GSC
108	10/02/22	36564.000	1.912	7.32	53.215	-132.995	-	GSC
	10/02/22	39608.000	1.608	6.12	53.243	-132.961	-	GSC
109	10/03/12	82203.000	2.397	9.73	52.583	-132.057	-	GSC
	12/12/03	67616.000	2.124	8.29	52.580	-132.068	16.2	GSC
	15/04/30	46945.675	1.740	6.62	-	-	-	MF
110	10/03/14	24499.000	2.263	9	52.500	-131.869	-	GSC
	10/03/14	24594.000	2.092	8.14	52.523	-131.838	-	GSC
111	10/02/19	42043.000	1.693	6.44	53.432	-132.894	-	GSC
	10/04/13	57305.000	2.058	7.98	53.480	-132.895	-	GSC
112	10/04/21	59327.000	2.078	8.07	52.855	-132.194	-	GSC
	10/04/21	77856.000	1.714	6.52	52.800	-132.312	-	GSC
113	08/02/07	69412.000	2.259	8.97	52.616	-132.104	-	GSC
	10/05/02	15856.000	2.160	8.47	52.673	-132.021	-	GSC
	10/05/21	78589.000	2.109	8.22	52.608	-132.127	-	GSC

Table 5: (continued)

Family ID	Date (YY/MM/DD)	Time (seconds)	Magnitude (M_w)	Slip (cm)	Latitude (dec. deg.)	Longitude (dec. deg.)	Depth (km)	Detection Method
114	10/06/05	17114.000	1.690	6.43	52.728	-132.309	-	GSC
	10/06/05	17199.000	2.446	10.02	52.727	-132.313	-	GSC
115	10/06/07	26048.000	1.671	6.36	52.826	-132.441	-	GSC
	10/09/21	36456.000	1.647	6.27	52.825	-132.443	-	GSC
116	10/06/09	12307.000	1.765	6.71	53.222	-132.786	-	GSC
	10/06/09	22799.000	1.340	5.23	53.229	-132.780	-	GSC
	10/06/10	18015.000	1.670	6.35	53.271	-132.594	-	GSC
117	08/10/21	17322.000	2.150	8.42	52.849	-132.408	-	GSC
	08/10/21	42347.775	2.150	8.42	-	-	-	MF
	10/06/22	21667.000	1.854	7.07	52.837	-132.445	-	GSC
118	10/07/21	30738.000	1.923	7.37	52.429	-131.750	-	GSC
	10/07/21	31047.000	1.836	7	52.414	-131.786	-	GSC
119	10/07/30	46938.000	1.773	6.75	52.459	-131.871	-	GSC
	10/07/30	50894.000	1.895	7.25	52.467	-131.871	-	GSC
	10/07/30	68192.000	1.516	5.8	52.473	-131.763	-	GSC
	10/07/30	86036.000	1.804	6.87	52.466	-131.856	-	GSC
	10/07/31	5607.000	1.952	7.5	52.463	-131.824	-	GSC
120	05/06/18	50326.800	1.061	4.44	-	-	-	MF
	10/08/15	7079.000	1.375	5.34	53.287	-133.016	-	GSC
	10/08/20	29039.025	1.022	4.34	-	-	-	MF
	11/04/21	13584.000	1.774	6.75	53.359	-132.989	-	GSC
121	07/09/18	52351.000	2.042	7.9	53.546	-133.108	-	GSC
	10/08/17	33675.000	2.079	8.07	53.449	-133.269	-	GSC
	13/10/24	77047.150	2.192	8.63	-	-	-	MF

Table 5: (continued)

Family ID	Date (YY/MM/DD)	Time (seconds)	Magnitude (M_w)	Slip (cm)	Latitude (dec. deg.)	Longitude (dec. deg.)	Depth (km)	Detection Method
122	10/06/17	83585.000	1.810	6.89	52.807	-132.071	-	GSC
	10/08/19	14092.000	1.881	7.19	52.732	-132.250	-	GSC
123	06/06/01	48500.000	2.148	8.41	52.931	-132.525	-	GSC
	07/07/28	32459.000	1.553	5.93	-	-	-	MF
	10/08/27	11571.000	2.330	9.36	52.904	-132.606	-	GSC
124	10/09/13	47777.000	2.931	13.31	52.844	-132.516	-	GSC
	10/09/13	48471.000	1.156	4.7	52.845	-132.513	-	GSC
125	10/09/14	12905.000	1.649	6.27	53.556	-133.153	-	GSC
	10/09/14	13152.000	1.546	5.91	53.569	-133.105	-	GSC
126	10/09/13	55428.000	1.300	5.11	53.082	-132.685	-	GSC
	10/09/14	48695.000	1.760	6.7	53.076	-132.684	-	GSC
	13/08/09	80857.775	1.133	4.63	-	-	-	MF
127	10/09/17	81295.000	1.141	4.66	53.075	-132.653	-	GSC
	13/06/27	6143.575	0.900	4.04	-	-	-	MF
	13/06/27	23483.575	0.900	4.04	-	-	-	MF
	13/07/10	43128.000	2.167	8.5	53.068	-132.673	22.4	GSC
	13/07/10	44286.150	1.005	4.3	-	-	-	MF
	13/07/13	67471.800	0.817	3.85	-	-	-	MF
	13/08/28	29042.425	1.777	6.76	-	-	-	MF
128	06/11/24	61655.000	2.196	8.65	53.874	-133.268	-	GSC
	10/09/20	28543.000	2.014	7.77	53.882	-133.449	-	GSC
	13/01/13	71200.800	1.475	5.66	-	-	-	MF
	14/06/08	81067.275	2.034	7.86	-	-	-	MF

Table 5: (continued)

Family ID	Date (YY/MM/DD)	Time (seconds)	Magnitude (M$_w$)	Slip (cm)	Latitude (dec. deg.)	Longitude (dec. deg.)	Depth (km)	Detection Method
129	10/09/20	73231.000	1.872	7.15	53.250	-133.055	-	GSC
	10/09/20	73759.000	1.817	6.92	53.248	-133.051	-	GSC
	10/09/21	38896.475	1.353	5.27	-	-	-	MF
130	10/09/22	14992.000	1.488	5.71	53.274	-132.843	-	GSC
	10/09/22	49092.000	1.530	5.85	53.284	-132.827	-	GSC
131	10/10/28	25319.000	1.867	7.13	52.604	-131.987	-	GSC
	10/10/28	40326.000	2.244	8.9	52.601	-132.000	-	GSC
132	10/12/02	65705.000	1.818	6.93	53.309	-132.720	-	GSC
	10/12/04	28107.000	1.718	6.53	53.265	-132.846	-	GSC
133	07/06/17	41414.000	1.999	7.71	52.642	-132.171	-	GSC
	11/01/25	44676.000	2.076	8.06	52.614	-132.147	-	GSC
134	09/08/09	75005.125	0.862	3.95	-	-	-	MF
	09/08/11	11672.300	0.956	4.18	-	-	-	MF
	09/08/13	18423.375	0.800	3.81	-	-	-	MF
	09/08/19	63343.600	1.356	5.28	-	-	-	MF
	09/08/21	78080.000	1.783	6.79	53.149	-132.634	-	GSC
	09/10/14	32586.725	1.705	6.48	-	-	-	MF
	09/11/25	39328.800	1.018	4.33	-	-	-	MF
	10/07/13	59248.725	1.302	5.12	-	-	-	MF
	10/07/27	79697.375	1.335	5.22	-	-	-	MF
	10/08/16	55482.600	0.988	4.26	-	-	-	MF
	10/08/26	84030.025	1.145	4.67	-	-	-	MF
	11/03/11	58716.000	1.812	6.9	53.179	-132.621	-	GSC
	11/03/14	962.000	1.821	6.94	53.185	-132.512	-	GSC

Table 5: (continued)

Family ID	Date (YY/MM/DD)	Time (seconds)	Magnitude (M_w)	Slip (cm)	Latitude (dec. deg.)	Longitude (dec. deg.)	Depth (km)	Detection Method
135	11/03/15	78185.000	2.516	10.44	53.335	-133.176	-	GSC
	11/03/15	80338.000	1.572	6	53.335	-133.186	-	GSC
136	11/03/29	82856.000	1.811	6.9	52.851	-132.569	-	GSC
	11/03/30	18494.000	1.890	7.23	52.849	-132.574	-	GSC
137	06/08/03	45850.275	1.172	4.74	-	-	-	MF
	11/03/30	69416.000	2.653	11.31	53.189	-132.987	-	GSC
	11/03/30	69617.000	1.569	5.99	53.196	-132.979	-	GSC
138	11/04/15	47426.000	1.490	5.71	53.123	-132.625	-	GSC
	11/04/21	67655.000	1.803	6.87	53.130	-132.599	-	GSC
	11/04/23	38537.175	1.529	5.85	-	-	-	MF
139	11/05/22	41069.000	1.754	6.67	52.904	-132.565	16.7	GSC
	11/05/23	50684.000	1.435	5.53	52.921	-132.552	-	GSC
	11/05/27	76679.000	1.530	5.85	52.915	-132.562	-	GSC
140	11/05/12	15040.750	1.085	4.5	-	-	-	MF
	11/05/12	60154.750	1.085	4.5	-	-	-	MF
	11/06/06	59318.000	1.271	5.02	53.167	-132.609	-	GSC
	11/06/07	53273.800	0.809	3.83	-	-	-	MF
	11/09/07	67313.000	2.306	9.23	53.155	-132.506	-	GSC
	11/09/08	73858.150	0.995	4.27	-	-	-	MF
141	11/06/09	42531.000	1.672	6.36	52.828	-132.378	-	GSC
	11/06/09	43116.000	1.711	6.51	52.819	-132.419	-	GSC
	13/10/23	61371.500	2.492	10.29	-	-	-	MF

Table 5: (continued)

Family ID	Date (YY/MM/DD)	Time (seconds)	Magnitude (M_w)	Slip (cm)	Latitude (dec. deg.)	Longitude (dec. deg.)	Depth (km)	Detection Method
142	11/06/09	42859.000	1.491	5.72	52.832	-132.401	-	GSC
	11/06/09	43371.000	1.343	5.24	52.820	-132.444	-	GSC
	11/06/09	43773.000	1.907	7.3	52.826	-132.409	-	GSC
	11/06/09	44026.000	1.560	5.95	52.842	-132.401	-	GSC
	11/06/09	44322.000	1.588	6.05	52.842	-132.390	-	GSC
	11/06/09	44538.000	1.724	6.56	52.821	-132.406	-	GSC
	11/06/09	45446.000	2.376	9.61	52.816	-132.417	-	GSC
	11/06/09	47002.000	1.540	5.88	52.820	-132.398	-	GSC
	11/06/09	47767.000	1.414	5.47	52.843	-132.393	-	GSC
	11/06/09	48094.000	1.360	5.3	52.833	-132.404	-	GSC
	11/06/09	53094.000	1.362	5.3	52.839	-132.405	-	GSC
	11/06/09	57714.000	2.001	7.71	52.834	-132.393	-	GSC
143	11/07/19	40277.000	2.043	7.91	53.250	-133.044	-	GSC
	11/07/19	41389.075	1.073	4.47	-	-	-	MF
	11/07/27	16169.000	1.642	6.25	53.258	-133.053	-	GSC
144	11/08/12	36880.000	1.770	6.73	53.532	-133.224	-	GSC
	11/08/12	39112.000	1.726	6.56	53.535	-133.167	-	GSC
145	11/08/24	27885.000	2.351	9.47	53.233	-133.058	-	GSC
	12/12/25	19292.000	2.999	13.86	53.241	-133.029	21.8	GSC
146	11/08/31	41248.000	1.782	6.78	52.595	-132.065	-	GSC
	11/08/31	47928.000	1.578	6.02	52.629	-131.997	-	GSC
147	06/07/12	81325.000	1.949	7.48	53.393	-133.240	-	GSC
	11/09/16	81465.000	1.869	7.14	53.526	-133.114	-	GSC

Table 5: (continued)

Family ID	Date (YY/MM/DD)	Time (seconds)	Magnitude (M_w)	Slip (cm)	Latitude (dec. deg.)	Longitude (dec. deg.)	Depth (km)	Detection Method
148	11/11/10	44205.000	3.198	15.58	53.112	-132.762	-	GSC
	11/11/11	57922.000	2.547	10.63	53.104	-132.798	-	GSC
	15/07/13	60803.225	1.929	7.39	-	-	-	MF
149	06/02/22	13686.000	1.958	7.52	52.712	-132.263	-	GSC
	11/12/21	30892.000	1.860	7.1	52.757	-132.238	-	GSC
150	12/01/10	59648.000	1.764	6.71	52.909	-132.495	-	GSC
	12/01/12	12015.175	1.839	7.02	-	-	-	MF
	12/01/12	36086.000	2.258	8.97	52.896	-132.540	-	GSC
151	12/08/08	14773.000	1.342	5.24	53.229	-132.797	-	GSC
	12/08/08	18997.400	1.206	4.84	-	-	-	MF
	12/08/08	28217.000	2.167	8.5	53.175	-132.733	-	GSC
	12/08/08	31126.350	1.179	4.76	-	-	-	MF
	12/08/08	62394.325	0.688	3.57	-	-	-	MF
	14/10/26	62916.250	0.888	4.01	-	-	-	MF
152	12/09/05	28934.000	2.028	7.84	53.337	-133.009	-	GSC
	12/09/05	29138.000	1.889	7.22	53.326	-132.971	-	GSC
	12/09/05	29268.250	1.513	5.79	-	-	-	MF
	12/09/05	30347.250	1.646	6.26	-	-	-	MF
153	12/10/21	3432.000	2.932	13.33	53.344	-132.258	-	GSC
	12/10/21	46082.000	2.362	9.53	53.262	-132.942	26.7	GSC
154	12/10/29	76631.000	3.434	17.9	52.564	-131.978	2.0	GSC
	13/01/12	27292.000	3.407	17.61	52.543	-131.917	10.2	GSC
155	12/10/31	26095.000	2.097	8.16	52.894	-132.433	20.0	GSC
	12/11/05	84316.175	2.437	9.96	-	-	-	MF

Table 5: (continued)

Family ID	Date (YY/MM/DD)	Time (seconds)	Magnitude (M_w)	Slip (cm)	Latitude (dec. deg.)	Longitude (dec. deg.)	Depth (km)	Detection Method
156	12/10/29	38138.775	2.069	8.03	-	-	-	MF
	12/10/31	82035.000	2.167	8.5	52.873	-132.480	15.0	GSC
	12/11/10	71620.075	2.193	8.63	-	-	-	MF
157	12/11/01	51168.000	2.726	11.81	52.478	-131.932	7.0	GSC
	12/11/04	85097.225	2.576	10.81	-	-	-	MF
	12/11/16	45273.000	2.595	10.93	52.529	-131.937	5.0	GSC
	12/12/06	42500.700	2.560	10.71	-	-	-	MF
158	12/11/11	65316.000	2.545	10.62	52.533	-131.910	7.7	GSC
	12/11/16	82755.000	2.346	9.44	52.513	-131.974	2.0	GSC
159	12/11/16	11102.000	2.345	9.44	52.587	-132.027	18.6	GSC
	13/10/05	45317.100	2.312	9.26	-	-	-	MF
	15/03/16	1097.000	2.401	9.75	52.577	-132.063	17.9	GSC
160	12/11/16	55238.000	2.645	11.26	52.545	-131.900	19.0	GSC
	12/12/12	29430.500	2.573	10.79	-	-	-	MF
	13/01/11	38249.650	2.360	9.52	-	-	-	MF
	14/02/13	41950.000	2.727	11.81	52.535	-131.912	11.5	GSC
161	12/11/11	65119.100	2.112	8.23	-	-	-	MF
	12/11/16	84939.000	2.141	8.38	52.628	-131.831	5.0	GSC
	12/11/23	1390.000	2.411	9.82	52.591	-131.832	4.2	GSC
	13/02/23	36117.200	2.605	11	-	-	-	MF
162	12/10/31	28469.000	2.439	9.97	52.868	-131.891	2.0	GSC
	12/11/17	26397.000	2.359	9.52	52.741	-132.302	1.0	GSC
163	12/11/21	12585.000	2.123	8.29	52.478	-131.932	6.0	GSC
	12/11/21	14243.000	2.093	8.14	52.545	-131.900	8.0	GSC

Table 5: (continued)

Family ID	Date (YY/MM/DD)	Time (seconds)	Magnitude (M$_w$)	Slip (cm)	Latitude (dec. deg.)	Longitude (dec. deg.)	Depth (km)	Detection Method
164	12/11/27	35447.000	2.310	9.25	53.115	-132.302	2.0	GSC
	12/11/27	36334.000	2.276	9.07	52.830	-132.465	1.0	GSC
165	12/11/28	71041.000	2.468	10.15	52.801	-132.256	19.4	GSC
	13/01/02	72427.325	2.508	10.39	-	-	-	MF
	13/02/20	86267.700	2.505	10.37	-	-	-	MF
	13/08/13	13334.000	2.574	10.8	52.790	-132.243	21.5	GSC
	15/02/14	15519.000	2.230	8.82	52.788	-132.249	20.0	GSC
166	12/11/30	18965.000	2.776	12.16	52.588	-132.020	5.2	GSC
	12/12/05	52698.000	2.835	12.59	52.581	-131.985	6.0	GSC
167	12/12/02	27255.000	2.405	9.78	52.631	-131.946	21.0	GSC
	13/06/23	35293.175	1.610	6.13	-	-	-	MF
	15/03/30	8004.000	2.213	8.74	52.582	-132.054	15.6	GSC
168	12/12/06	29565.000	2.179	8.57	52.731	-132.399	11.3	GSC
	12/12/07	3706.000	2.354	9.49	52.760	-132.381	30.0	GSC
169	12/11/02	46874.600	2.581	10.84	-	-	-	MF
	12/11/11	10458.900	1.732	6.59	-	-	-	MF
	12/11/17	321.000	2.404	9.78	52.846	-132.429	12.0	GSC
	12/12/08	79.000	2.254	8.95	52.997	-132.328	2.0	GSC
170	12/12/06	23761.000	2.507	10.38	52.865	-132.507	23.0	GSC
	12/12/08	668.000	2.132	8.33	52.881	-132.471	20.0	GSC
	13/10/18	37489.000	3.080	14.54	-	-	-	MF
	13/10/18	38668.775	1.962	7.54	-	-	-	MF
	15/12/15	24167.350	1.946	7.47	-	-	-	MF

Table 5: (continued)

Family ID	Date (YY/MM/DD)	Time (seconds)	Magnitude (M_w)	Slip (cm)	Latitude (dec. deg.)	Longitude (dec. deg.)	Depth (km)	Detection Method
171	12/12/19	13353.000	2.791	12.27	52.809	-132.320	22.1	GSC
	15/07/07	55909.000	2.155	8.44	52.776	-132.349	18.5	GSC
172	12/12/22	31396.000	2.159	8.47	52.847	-132.504	14.8	GSC
	12/12/22	35765.000	2.086	8.11	52.852	-132.471	14.5	GSC
	13/09/17	22878.825	1.680	6.39	-	-	-	MF
	14/03/03	12973.850	2.463	10.12	-	-	-	MF
173	12/11/26	17401.000	2.323	9.32	52.476	-131.893	0.0	GSC
	12/12/22	78338.000	2.366	9.56	52.498	-131.874	-	GSC
	13/01/23	25491.025	2.039	7.89	-	-	-	MF
	13/02/01	52885.675	1.892	7.23	-	-	-	MF
	13/08/12	65827.000	1.672	6.36	-	-	-	MF
	15/05/29	628.000	1.885	7.21	-	-	-	MF
174	12/11/27	22745.000	2.629	11.16	52.422	-131.858	0.1	GSC
	13/07/25	57865.000	2.612	11.04	52.468	-131.833	8.7	GSC
175	13/07/30	31694.000	2.713	11.72	52.768	-132.233	21.4	GSC
	14/09/18	49631.000	2.545	10.62	52.812	-132.150	23.3	GSC
176	13/04/18	6196.000	2.662	11.37	52.519	-131.939	9.1	GSC
	13/11/11	69951.000	2.796	12.3	52.502	-131.944	11.0	GSC
177	12/10/30	62753.000	2.787	12.23	52.596	-131.905	2.0	GSC
	12/11/13	38056.525	2.798	12.32	-	-	-	MF
	13/01/11	30432.825	2.793	12.28	-	-	-	MF
	14/02/13	15552.000	2.797	12.31	52.509	-131.911	8.5	GSC

Table 5: (continued)

Family ID	Date (YY/MM/DD)	Time (seconds)	Magnitude (M$_w$)	Slip (cm)	Latitude (dec. deg.)	Longitude (dec. deg.)	Depth (km)	Detection Method
178	12/12/23	40951.000	2.114	8.24	52.842	-132.390	20.0	GSC
	14/03/21	7524.000	2.258	8.97	52.854	-132.366	20.7	GSC
	14/05/02	6650.850	1.460	5.61	-	-	-	MF
	15/10/24	55417.100	1.788	6.81	-	-	-	MF
179	14/05/17	83126.425	2.064	8	-	-	-	MF
	14/05/17	83296.675	1.583	6.04	-	-	-	MF
	14/05/18	2114.000	2.237	8.86	53.288	-133.033	26.3	GSC
	15/12/30	8017.575	1.738	6.61	-	-	-	MF
	15/12/30	27717.000	3.100	14.7	53.290	-133.046	21.5	GSC
180	08/04/22	39459.000	2.024	7.82	53.828	-133.434	-	GSC
	14/07/02	38314.000	2.172	8.53	53.825	-133.397	-	GSC
181	13/07/31	38368.750	2.523	10.48	-	-	-	MF
	14/08/08	47183.000	1.971	7.58	52.895	-132.248	24.0	GSC
	15/02/10	10125.000	1.576	6.01	52.842	-132.377	15.1	GSC
182	13/05/17	27711.275	2.371	9.59	-	-	-	MF
	13/10/27	50162.725	2.031	7.85	-	-	-	MF
	14/08/13	63792.000	1.978	7.61	52.806	-132.181	22.9	GSC
	14/10/16	38503.050	1.639	6.24	-	-	-	MF
	15/09/30	45828.775	1.413	5.46	-	-	-	MF
	15/10/03	79413.000	2.013	7.77	52.769	-132.244	21.1	GSC

Table 5: (continued)

Family ID	Date (YY/MM/DD)	Time (seconds)	Magnitude (M_w)	Slip (cm)	Latitude (dec. deg.)	Longitude (dec. deg.)	Depth (km)	Detection Method
183	13/10/04	6723.050	2.894	13.03	-	-	-	MF
	14/08/20	66652.000	2.260	8.98	52.775	-132.238	22.4	GSC
	14/12/10	79843.525	2.121	8.27	-	-	-	MF
	15/01/21	250.525	2.570	10.77	-	-	-	MF
	15/12/11	15499.000	2.314	9.27	52.746	-132.303	15.7	GSC
184	09/04/15	45028.000	1.453	5.59	53.511	-133.185	-	GSC
	14/09/09	71996.000	2.187	8.6	53.516	-133.159	24.2	GSC
185	13/07/03	1073.150	1.879	7.18	-	-	-	MF
	14/09/23	15841.000	2.097	8.16	52.620	-132.017	20.1	GSC
186	13/02/27	84268.175	2.460	10.1	-	-	-	MF
	13/09/28	39994.475	1.864	7.12	-	-	-	MF
	14/04/16	16906.825	1.653	6.29	-	-	-	MF
	14/06/14	25774.900	1.361	5.3	-	-	-	MF
	14/10/19	21996.000	2.127	8.31	52.740	-132.312	16.0	GSC
	15/12/14	42974.000	1.647	6.27	52.739	-132.328	13.4	GSC
187	12/11/16	62449.000	2.448	10.03	52.776	-132.344	1.0	GSC
	14/12/17	14108.000	2.369	9.57	52.771	-132.293	22.0	GSC
188	13/03/13	32041.450	1.992	7.67	-	-	-	MF
	13/11/22	14121.000	2.253	8.94	52.680	-132.133	18.2	GSC
	15/01/23	3289.000	2.243	8.89	52.667	-132.143	18.2	GSC
189	14/10/05	12292.000	2.526	10.5	52.867	-132.469	16.8	GSC
	15/01/23	13348.000	2.349	9.46	52.849	-132.523	13.1	GSC

Table 5: (continued)

Family ID	Date (YY/MM/DD)	Time (seconds)	Magnitude (M_w)	Slip (cm)	Latitude (dec. deg.)	Longitude (dec. deg.)	Depth (km)	Detection Method
190	12/11/04	2100.575	2.533	10.54	-	-	-	MF
	12/11/11	74810.700	2.043	7.91	-	-	-	MF
	12/11/17	40356.100	2.581	10.85	-	-	-	MF
	12/12/25	27032.075	2.596	10.94	-	-	-	MF
	13/01/28	73757.525	2.432	9.94	-	-	-	MF
	15/01/15	29010.000	2.730	11.83	52.572	-131.962	10.7	GSC
	15/01/26	23913.000	2.486	10.25	52.582	-131.942	15.0	GSC
191	12/10/31	28153.000	2.915	13.19	52.599	-132.020	6.0	GSC
	13/01/11	22672.225	2.941	13.39	-	-	-	MF
	15/01/26	31057.000	2.914	13.18	52.576	-131.875	13.9	GSC
192	12/11/25	67580.000	2.536	10.56	52.660	-131.757	17.0	GSC
	13/04/12	78043.125	2.609	11.02	-	-	-	MF
	13/07/30	53000.525	2.244	8.89	-	-	-	MF
	14/02/12	23755.375	2.318	9.29	-	-	-	MF
	15/01/26	67245.000	2.405	9.78	52.546	-131.868	15.0	GSC
193	12/11/01	77207.000	2.628	11.15	52.564	-131.978	2.0	GSC
	13/01/11	20060.625	2.276	9.07	-	-	-	MF
	15/01/28	14422.000	2.698	11.61	52.569	-131.869	16.2	GSC
194	15/02/21	15986.000	1.722	6.55	53.094	-132.725	23.8	GSC
	15/02/21	49121.000	1.466	5.63	53.064	-132.740	17.8	GSC
	15/02/21	49354.000	2.044	7.91	53.098	-132.680	25.9	GSC
195	15/02/03	1800.000	1.552	5.92	52.818	-132.411	15.6	GSC
	15/02/24	27073.000	2.244	8.89	52.820	-132.378	22.2	GSC

Table 5: (continued)

Family ID	Date (YY/MM/DD)	Time (seconds)	Magnitude (M$_w$)	Slip (cm)	Latitude (dec. deg.)	Longitude (dec. deg.)	Depth (km)	Detection Method
196	09/05/06	47626.000	1.387	5.38	53.308	-133.065	-	GSC
	15/03/03	7936.000	2.047	7.93	53.320	-133.075	13.8	GSC
197	13/07/23	32677.975	1.274	5.03	-	-	-	MF
	13/09/01	10073.150	1.682	6.4	-	-	-	MF
	13/11/25	43723.550	1.450	5.58	-	-	-	MF
	13/11/25	44815.900	2.006	7.74	-	-	-	MF
	14/02/10	10074.675	1.182	4.77	-	-	-	MF
	14/06/17	25145.000	2.451	10.05	52.864	-132.450	21.8	GSC
	15/03/14	18582.000	1.719	6.54	52.861	-132.471	14.7	GSC
	15/11/10	39105.775	1.934	7.42	-	-	-	MF
198	09/12/05	39856.000	2.289	9.14	53.379	-133.153	-	GSC
	15/03/17	4584.000	2.082	8.09	53.376	-133.179	16.6	GSC
199	15/01/27	10139.275	1.631	6.21	-	-	-	MF
	15/03/13	11031.000	2.023	7.81	52.744	-132.285	13.3	GSC
	15/03/24	74446.000	2.088	8.12	52.751	-132.272	19.6	GSC
200	13/04/30	47537.550	1.897	7.26	-	-	-	MF
	13/10/10	4641.675	1.940	7.44	-	-	-	MF
	13/12/06	60003.475	2.162	8.48	-	-	-	MF
	14/06/27	31969.000	2.074	8.05	52.750	-132.281	16.9	GSC
	14/07/16	33893.150	2.003	7.72	-	-	-	MF
	14/07/16	36185.225	1.445	5.56	-	-	-	MF
	15/03/24	84700.000	1.990	7.67	52.742	-132.311	14.7	GSC
	15/11/02	38728.000	1.988	7.65	52.757	-132.263	20.6	GSC
	15/11/09	84785.350	1.362	5.3	-	-	-	MF

Table 5: (continued)

Family ID	Date (YY/MM/DD)	Time (seconds)	Magnitude (M_w)	Slip (cm)	Latitude (dec. deg.)	Longitude (dec. deg.)	Depth (km)	Detection Method
201	12/11/19	82753.000	1.927	7.39	52.775	-132.354	20.9	GSC
	15/04/04	51839.000	2.105	8.2	52.780	-132.336	19.2	GSC
202	15/04/05	69585.000	1.741	6.62	52.469	-131.858	15.3	GSC
	15/04/05	75294.000	2.654	11.32	52.473	-131.829	18.7	GSC
203	15/03/17	43881.000	1.970	7.57	52.962	-132.626	16.6	GSC
	15/04/16	51616.325	1.443	5.56	-	-	-	MF
	15/04/16	81145.000	2.116	8.25	52.965	-132.636	17.5	GSC
	15/04/16	81885.850	1.246	4.95	-	-	-	MF
	15/04/16	82399.650	1.375	5.34	-	-	-	MF
	15/04/16	84862.200	1.294	5.09	-	-	-	MF
	15/04/17	11242.000	2.247	8.91	52.988	-132.576	25.2	GSC
	15/04/17	37790.200	1.184	4.78	-	-	-	MF
	15/04/17	68526.550	1.016	4.33	-	-	-	MF
	15/04/19	4666.450	0.997	4.28	-	-	-	MF
	15/04/20	6200.225	1.256	4.98	-	-	-	MF
	15/04/20	27594.000	1.207	4.84	-	-	-	MF
	15/04/20	59155.600	1.653	6.29	-	-	-	MF
	15/04/22	46860.900	0.935	4.13	-	-	-	MF
	15/05/12	22550.375	0.876	3.98	-	-	-	MF
204	15/05/23	42477.000	1.759	6.69	52.705	-132.327	13.7	GSC
	15/06/22	28103.000	1.727	6.57	52.714	-132.281	21.5	GSC
	15/07/02	5277.025	1.100	4.54	-	-	-	MF
	15/08/09	61967.000	1.815	6.92	52.715	-132.301	18.7	GSC

Table 5: (continued)

Family ID	Date (YY/MM/DD)	Time (seconds)	Magnitude (M$_w$)	Slip (cm)	Latitude (dec. deg.)	Longitude (dec. deg.)	Depth (km)	Detection Method
205	14/04/04	77222.000	2.028	7.84	52.776	-132.246	21.5	GSC
	15/05/24	71018.000	1.406	5.44	-	-	-	MF
	15/06/08	79245.000	1.750	6.66	52.752	-132.286	17.2	GSC
206	14/08/04	30712.000	1.920	7.35	52.812	-132.259	23.1	GSC
	15/06/22	79783.000	2.046	7.92	52.767	-132.339	16.9	GSC
207	13/07/16	45174.700	2.183	8.58	-	-	-	MF
	13/09/19	31817.000	2.279	9.08	52.785	-132.316	16.4	GSC
	15/06/26	56470.000	2.058	7.98	52.791	-132.312	17.7	GSC
208	13/06/06	33949.825	1.969	7.57	-	-	-	MF
	13/06/19	39716.050	1.365	5.31	-	-	-	MF
	13/11/07	75968.475	2.048	7.93	-	-	-	MF
	14/09/03	3868.975	1.635	6.22	-	-	-	MF
	15/07/10	59602.000	1.584	6.04	52.479	-131.933	15.8	GSC
	15/07/23	34530.000	1.781	6.78	52.507	-131.862	19.5	GSC
	15/07/23	34882.675	1.281	5.05	-	-	-	MF
209	15/07/12	2939.000	2.027	7.83	52.473	-131.825	13.9	GSC
	15/07/12	5111.575	1.594	6.07	-	-	-	MF
	15/07/12	11822.100	1.574	6	-	-	-	MF
	15/07/12	12290.000	2.086	8.11	52.483	-131.823	14.2	GSC
210	15/08/01	13779.000	2.446	10.02	52.692	-132.292	25.9	GSC
	15/08/03	64999.000	1.696	6.45	52.705	-132.286	15.8	GSC
211	05/06/19	29605.000	1.537	5.87	53.280	-133.154	-	GSC
	15/08/06	6102.000	2.038	7.88	53.293	-133.141	18.9	GSC

Table 5: (continued)

Family ID	Date (YY/MM/DD)	Time (seconds)	Magnitude (M_w)	Slip (cm)	Latitude (dec. deg.)	Longitude (dec. deg.)	Depth (km)	Detection Method
212	15/07/14	17323.000	2.054	7.96	52.519	-131.902	10.5	GSC
	15/08/14	15911.000	1.993	7.68	52.600	-131.793	13.4	GSC
	15/09/06	61717.075	1.644	6.26	-	-	-	MF
213	10/01/24	41380.000	1.955	7.51	52.747	-132.276	-	GSC
	13/01/17	6863.475	2.020	7.8	-	-	-	MF
	13/10/10	54376.925	1.775	6.76	-	-	-	MF
	15/09/14	3391.000	2.068	8.02	52.739	-132.300	16.3	GSC
214	08/07/22	711.000	2.443	10	53.499	-133.227	-	GSC
	15/09/15	24402.000	1.992	7.67	53.520	-133.210	10.7	GSC
215	13/06/11	19567.050	1.867	7.13	-	-	-	MF
	15/09/18	7259.000	2.145	8.4	52.594	-132.012	6.9	GSC
	15/09/18	7630.000	2.018	7.79	52.614	-131.963	10.5	GSC
216	15/09/15	11164.000	1.651	6.28	52.573	-131.986	7.2	GSC
	15/09/18	51721.000	2.186	8.6	52.561	-132.021	7.8	GSC
217	15/11/18	47603.000	2.237	8.86	52.749	-132.297	18.1	GSC
	15/11/19	65640.000	2.461	10.11	52.751	-132.299	21.1	GSC
218	12/11/27	1783.000	1.969	7.57	52.739	-132.270	19.2	GSC
	12/12/01	59142.275	1.968	7.57	-	-	-	MF
	13/04/21	55768.150	1.745	6.64	-	-	-	MF
	15/12/22	44894.000	2.391	9.7	52.772	-132.161	23.4	GSC
219	15/12/25	37622.000	2.439	9.97	53.176	-132.805	21.8	GSC
	15/12/25	37767.000	2.145	8.39	53.153	-132.845	18.6	GSC

Table 5: (continued)

Family ID	Date (YY/MM/DD)	Time (seconds)	Magnitude (M_w)	Slip (cm)	Latitude (dec. deg.)	Longitude (dec. deg.)	Depth (km)	Detection Method
220	15/12/28	74094.000	2.218	8.76	53.068	-132.740	24.0	GSC
	15/12/29	17614.000	1.863	7.11	53.051	-132.824	15.9	GSC
	15/12/29	19531.000	1.779	6.77	53.047	-132.787	14.2	GSC
221	15/12/29	41033.000	2.279	9.08	53.253	-133.135	10.9	GSC
	15/12/29	51744.000	2.352	9.48	53.289	-133.087	18.7	GSC
	15/12/30	8659.500	1.884	7.2	-	-	-	MF
222	15/12/30	4878.425	2.465	10.13	-	-	-	MF
	15/12/30	5093.000	2.454	10.07	53.272	-133.073	25.1	GSC
	15/12/30	7377.000	2.261	8.99	53.284	-133.078	20.3	GSC
	15/12/30	13420.000	2.599	10.96	53.282	-133.083	20.1	GSC
223	14/05/18	6438.175	1.931	7.4	-	-	-	MF
	14/05/18	14768.525	2.206	8.7	-	-	-	MF
	14/05/18	15699.000	1.442	5.56	-	-	-	MF
	14/05/18	15810.650	1.823	6.95	-	-	-	MF
	14/05/18	16291.200	1.782	6.78	-	-	-	MF
	15/12/30	7762.300	1.758	6.69	-	-	-	MF
	15/12/30	12490.625	1.845	7.04	-	-	-	MF
	15/12/30	16165.000	2.155	8.45	53.271	-133.062	22.2	GSC
	15/12/30	20171.000	2.242	8.89	53.267	-133.083	18.1	GSC
	15/12/30	29911.275	1.869	7.14	-	-	-	MF
	15/12/31	55520.725	1.894	7.24	-	-	-	MF
224	15/12/30	23759.000	1.806	6.88	53.258	-133.098	17.8	GSC
	15/12/30	24389.000	2.051	7.94	53.338	-132.879	28.1	GSC
	15/12/30	28964.000	3.100	14.71	53.254	-133.119	22.8	GSC

Appendix B

Constraining Repeating Earthquake Magnitudes

In Section 3.1.2, we show how to arrive at a system of equations that honours all relative M_0 weights between repeating earthquakes in a given family. For a family with n earthquakes, the system is written as

$$
\begin{bmatrix}
1 & -w_{12} & 0 & 0 & \cdots & 0 \\
1 & 0 & -w_{13} & 0 & \cdots & 0 \\
\vdots & \vdots & \vdots & \vdots & \ddots & \vdots \\
1 & 0 & 0 & 0 & \cdots & -w_{1n}
\end{bmatrix}
\begin{bmatrix}
M_{01} \\
M_{02} \\
M_{03} \\
\vdots \\
M_{0n}
\end{bmatrix}
=
\begin{bmatrix}
0 \\
0 \\
\vdots \\
0
\end{bmatrix},
\tag{16}
$$

where M_{0i} is the absolute M_0 of event i, and w_{1i} is the M_0 ratio of event 1 relative to event i. This system (16) enforces precise relative M_0 between all members of a repeating earthquake family.

To constrain absolute M_0, we employ the original M_W and M_0 estimates from Section 3.1.1. Consider a three-earthquake family (A, B, and C) with catalogued absolute moment estimates M_{0A}^{cat}, M_{0B}^{cat}, and M_{0C}^{cat}. Initially, we consider the following system that utilizes the initial M_0^{cat} estimates, :

$$
\begin{bmatrix}
1 & 0 & 0 \\
0 & 1 & 0 \\
0 & 0 & 1
\end{bmatrix}
\begin{bmatrix}
M_{0A} \\
M_{0B} \\
M_{0C}
\end{bmatrix}
=
\begin{bmatrix}
M_{0A}^{cat} \\
M_{0B}^{cat} \\
M_{0C}^{cat}
\end{bmatrix}.
\tag{17}
$$

This system can be rearranged to resemble that of (16) through decomposition into its relative and absolute M_0 information:

$$
\begin{bmatrix}
1 & -w_{AB} & 0 \\
1 & 0 & -w_{AC} \\
w_{AB}w_{AC} & w_{AC} & w_{AB}
\end{bmatrix}
\begin{bmatrix}
M_{0A} \\
M_{0B} \\
M_{0C}
\end{bmatrix}
=
\begin{bmatrix}
0 \\
0 \\
w_{AB}w_{AC}M_{0A}^{cat} + w_{AC}M_{0B}^{cat} + w_{AB}M_{0C}^{cat}
\end{bmatrix},
\qquad (18)
$$

which can be written generally for a family with n earthquakes as

$$
\begin{bmatrix}
1 & -w_{12} & 0 & 0 & \cdots & 0 \\
1 & 0 & -w_{13} & 0 & \cdots & 0 \\
\vdots & \vdots & \vdots & \vdots & \ddots & \vdots \\
1 & 0 & 0 & 0 & \cdots & -w_{1n} \\
\prod_{j\neq1} w_{1j} & \prod_{j\neq2} w_{1j} & \prod_{j\neq3} w_{1j} & \prod_{j\neq4} w_{1j} & \cdots & \prod_{j\neq n} w_{1j}
\end{bmatrix}
\begin{bmatrix}
M_{01} \\
M_{02} \\
M_{03} \\
\vdots \\
M_{0n}
\end{bmatrix}
=
\begin{bmatrix}
0 \\
0 \\
\vdots \\
0 \\
\sum_i \left(M_{0i}^{cat} \prod_{j\neq i} w_{1j} \right)
\end{bmatrix},
\qquad (19)
$$

$$
\mathbf{Gm = d}. \qquad (20)
$$

Note that $w_{11} = 1$, and that the weights w_{ij} in (19) will not generally be the same as those in (16) because the absolute M_0^{cat} information will not be completely consistent with the relative M_0 information supplied through the SVD analysis. Because we expect the the relative information from the SVD analysis to be more robust than that from the catalogue, we adopt the weight equations from (16), and discard those from (19). In (19,20), $\mathbf{G}$ has size $[n \times n]$ and rank n, which allows us to solve for the true moments ($\mathbf{m}$) directly:

$$
\mathbf{m = G}^{-1}\mathbf{d}. \qquad (21)
$$

We confirm that (21) produces stable and accurate results for $\mathbf{m}$ by checking that the condition number of $\mathbf{G}$ is sufficiently low for all repeating earthquake families.

The equation we use to constrain absolute M_0 (n^{th} row of $\mathbf{G}$) is not the only available option. The simplest option is to consider a single M_{0i}^{cat} (e.g., the largest) and define all absolute M_0 within the family based on this one value and the weights in (16). This simple method relies strongly on a single M_{0i}^{cat} value, discards other useful M_{0j}^{cat} estimates, and is therefore prone to errors in measurement. A

better method, which utilizes all M_{0i}^{cat} values, is to constrain the sum of M_0 in the solution to be equal to the sum of M_{0i}^{cat}. If using this method, the nth row of the system in (19) is defined as

$$
\begin{bmatrix} 1 & 1 & \cdots & 1 \end{bmatrix} \begin{bmatrix} M_{01} \\ M_{02} \\ \vdots \\ M_{0n} \end{bmatrix} = \begin{bmatrix} \sum_i M_{0i}^{cat} \end{bmatrix}. \tag{22}
$$

We test the accuracy and robustness of replacing the final equation in (19) with (22) versus the original system. A synthetic family of 10 earthquakes is generated with the M_W of each event assigned randomly from a uniform distribution in the range $1.0 \leq M_W \leq 2.5$ and M_0 weights, w_{ij}, calculated as in (16). Then, a randomly selected earthquake from the list has its M_W changed by ± 1.0, which represents the case when an original recorded M_W is overestimated/underestimated by standard detection methods. Following this perturbation, we solve for $\mathbf{m}$ from (19, 21) and measure the ℓ_2-norm of the error between actual M_0 for all earthquakes in the family (i.e., before perturbation) and those produced from solving the system. We then solve (21) again, but substitute (22) for the nth row of the system. This process is repeated 100,000 times for a magnitude perturbation of +1.0 (Figure 16a), and an additional 100,000 times for a magnitude perturbation of -1.0 (Figure 16b). When using (19) the error ($\|\text{error}_\perp\|$ in Figure 16) is lower 83% of the time, compared to the error when substituting (22) for the nth row ($\|\text{error}_\Sigma\|$ in Figure 16). Upon inspection, the large negative outliers in Figure 16 are due to trials where both forms of the solution are very inaccurate, and thus neither result is desirable in these small number of cases. Overall, the system in (19) appears to be more accurate and robust than if a simple sum of moments is used as the constraint, as in (22).

Additional inspection of (19) reveals that the first $(n-1)$ rows are identical to those in (16), and the nth row is orthogonal to all other rows. In the present study, $\mathbf{G}$ has size $[n \times n]$ and rank n, and thus can be solved exactly by (21). In this case, orthogonality of the nth row with respect to the rest of the system is not necessary, because all equations are satisfied exactly by the solution. However, future applications may involve additional stations and/or separate M_0 ratio measurements for individual components. In these situations, $\mathbf{G}$ would be a "tall" matrix (i.e., more equations than unknowns), and the system would be overdetermined. It is desirable to have the absolute M_0 constraint orthogonal to the

rest of the system for the overdetermined problem, because it allows for the absolute M_0 constraint to be satisfied without affecting the relative moment weights that are recovered independently. Because of this orthogonality, as well as the robustness/accuracy demonstrated above, we choose (19) as the system to solve. As such, we satisfy all relative M_0 information from the SVD analysis in the first $(n-1)$ rows, and constrain all absolute M_0 information with a single, orthogonal equation in the nth row.
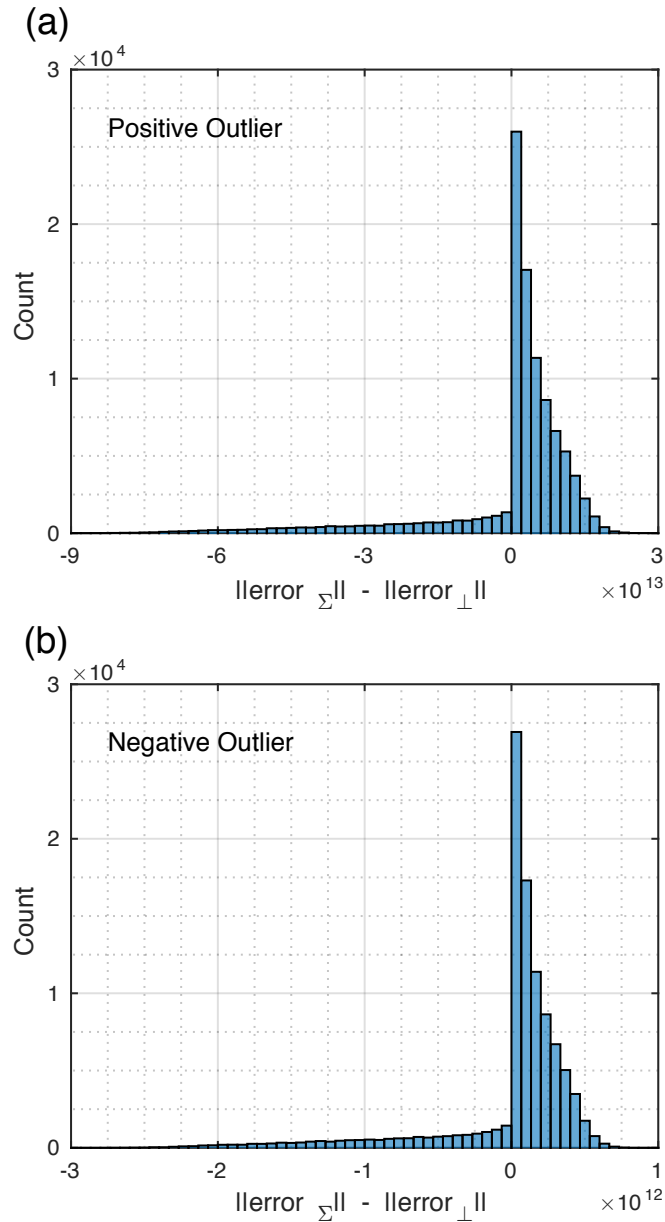
Figure 16: Histograms of error differences in measured M_0, relating to the tests of robustness and accuracy for (19) and (22). (a) A random event is given a positive M_0 perturbation, and (b) a negative M_0 perturbation. Both (a) and (b) result from 100,000 individual trials. The ℓ_2-norm of the error in M_0 (measured in Nm) when using the orthogonal absolute M_0 constraint in (19) is given by $\|\text{error}_\perp\|$, and the same error measurement but when using the sum of M_0 equation in (22) is given by $\|\text{error}_\Sigma\|$. The orthogonal equation is demonstrated to be more resistant to outliers, performing better than the simple sum of M_0 equation in 83% of trials. See text for full methodology of this test.

Appendix C

Repeating Earthquake Groups

In Section 3.4 we explain how repeating earthquake families are divided into groups based on their assigned focal mechanisms and locations along the Queen Charlotte plate boundary. Figure 17 provides a cross-section for each repeating earthquake group. Note that plots for 3Q and 1S are empty as there are no families in these groups. For other groups, not all families are visible within the plots because families without depth estimates cannot be plotted. Table 6 provides details for each group.
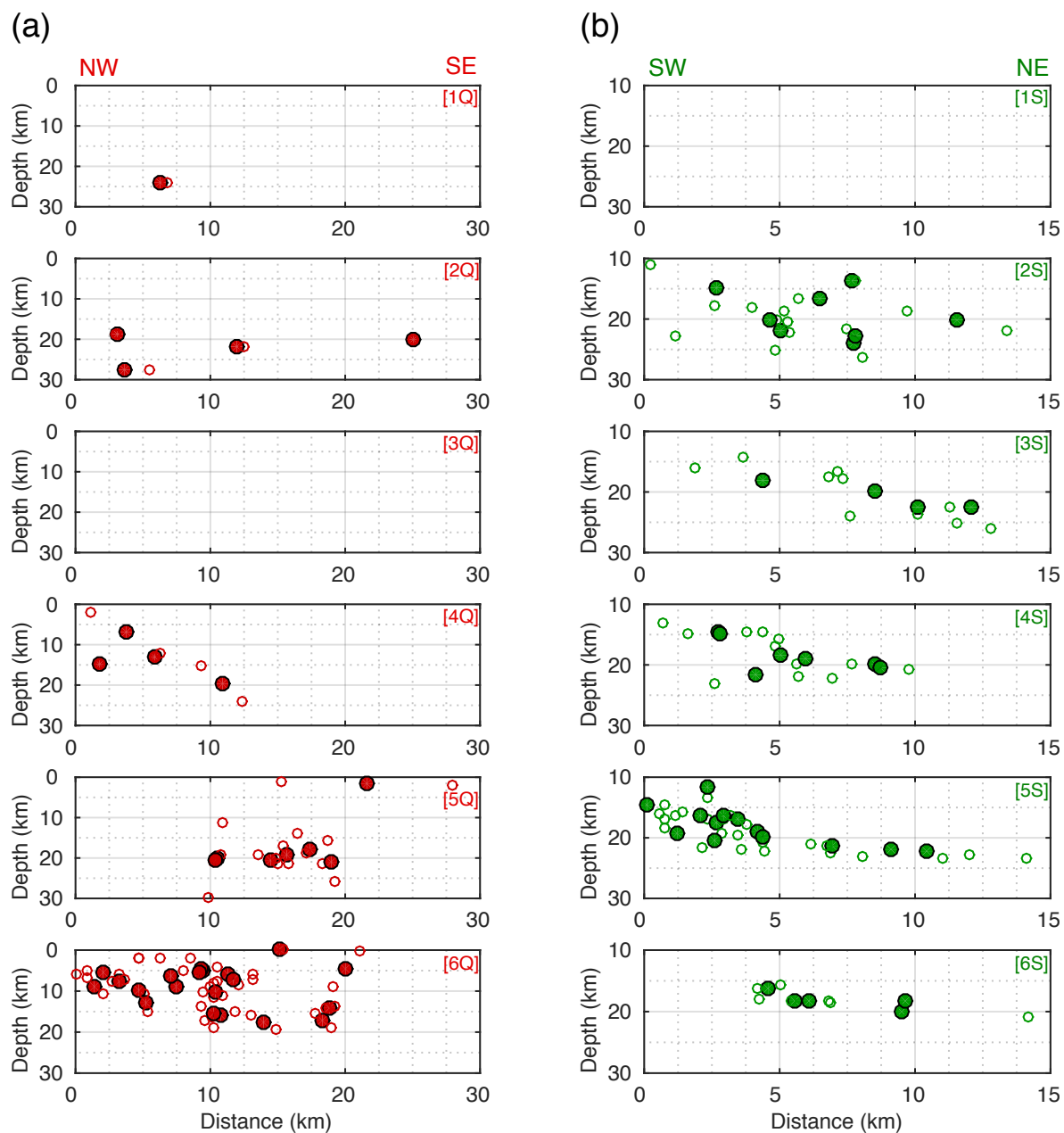
Figure 17: Cross-sections of all (a) QCF-related repeating earthquake groups, with profiles taken parallel to the surface trace of the QCF and horizontal exaggeration of 3.3, and (b) subduction-related repeating earthquake groups, with profiles taken perpendicular to the surface trace of the QCF (i.e., parallel to plate subduction) and horizontal exaggeration of 4.4. Group names are given in brackets in the top-right corner of each plot. Filled circles are family average locations, and empty circles are individual repeating earthquake locations. Note that some families do not have depth estimates, and are absent from the cross-sections. Also note that horizontal distance reference points are arbitrarily chosen for each profile, and do not relate between different plots.

Table 6: Details of the groupings of repeating earthquake families used in the present study. Strike-slip groups are those assumed to account for dextral strike-slip motion along the QCF, subduction groups are those assumed to exhibit thrust motion on the subduction interface, and unclear groups are those whose slip-types cannot be determined (see Section 3.4). For details of specific repeating earthquake families, see Table 5.

Group Name	Slip Type	Center Location	Number of Families	Number of Earthquakes	List of Families
1Q	Strike-slip	53.7°N, 133.2°W	11	24	001 035 039 043 057 073 080 111 121 147 184
2Q	Strike-slip	53.3°N, 132.9°W	18	63	005 006 007 008 017 032 034 037 054 089 090 091 116 130 132 145 152 211
3Q	Strike-slip	53.1°N, 132.65°W	0	0	
4Q	Strike-slip	52.9°N, 132.4°W	9	35	070 071 117 124 141 142 156 169 181
5Q	Strike-slip	52.75°N, 132.25°W	10	26	112 114 122 162 165 168 201 204 205 210
6Q	Strike-slip	52.5°N, 131.9°W	28	92	002 004 018 055 072 077 103 113 154 157 158 160 161 163 166 173 174 176 177 190 191 192 193 202 208 209 215 216

Table 6: (continued)

Group Name	Slip Type	Center Location	Number of Families	Number of Earthquakes	List of Families
1S	Subduction	53.7°N, 133.2°W	0	0	
2S	Subduction	53.3°N, 132.9°W	32	112	022 023 030 036 041 042 047 053 059 061 066 067 068 074 078 088 097 100 108 120 135 137 143 151 179 196 198 219 221 222 223 224
3S	Subduction	53.1°N, 132.65°W	14	74	016 027 028 099 105 126 127 134 138 140 148 194 203 220
4S	Subduction	52.9°N, 132.4°W	12	40	086 093 094 115 123 155 170 172 178 189 195 197
5S	Subduction	52.75°N, 132.25°W	16	62	040 048 069 075 171 175 182 183 186 187 199 200 206 207 213 218
6S	Subduction	52.5°N, 131.9°W	13	32	020 025 044 049 081 084 106 109 133 159 167 185 188

Table 6: (continued)

Group Name	Slip Type	Center Location	Number of Families	Number of Earthquakes	List of Families
1U	Unclear	53.7°N, 133.2°W	9	22	011 012 076 107 125 128 144 180 214
2U	Unclear	53.3°N, 132.9°W	9	28	010 014 026 050 051 052 056 129 153
3U	Unclear	53.1°N, 132.65°W	5	22	021 024 046 095 101
4U	Unclear	52.9°N, 132.4°W	16	45	015 031 058 060 063 064 065 079 085 087 096 102 136 139 150 164
5U	Unclear	52.75°N, 132.25°W	7	17	029 045 082 098 104 149 217
6U	Unclear	52.5°N, 131.9°W	15	36	003 009 013 019 033 038 062 083 092 110 118 119 131 146 212